Stony Brook University

Structural and Functional Studies of Negative Regulators of TCR signaling

A Dissertation Presented

By

Yunting Chen

to

The Graduate School

in Partial fulfillment of the

Requirements

for the Degree of

Doctor of Philosophy

in

Biochemistry and Structural Biology

Stony Brook University

December 2007

Stony Brook University

The Graduate School

Yunting Chen

We, the dissertation committee for the above candidate for the

Doctor of Philosophy degree,

Hereby recommend acceptance of this dissertation

Nicolas Nassar, Assistant Professor
Department of Physiology and Biophysics
Dissertation Advisor

W. Todd Miller, Professor
Department of Physiology and Biophysics
Chairperson of Defense

Suzane Scarlata, Professor
Department of Physiology and Biophysics

Wali Karzai, Associate Professor
Department of Biochemistry and Cell Biology

Nicholas Carpino, Assistant Professor
Department of Molecular Genetics and Microbiology

This Dissertation is accepted by the Graduate School

Lawrence Martin
Dean of the Graduate School

Abstract of the Dissertation

Structural and Functional Studies of Negative Regulators of TCR signaling

By

Yunting Chen

Doctor of Philosophy

in

Biochemistry and Structural Biology

Stony Brook University

2007

Nicolas Nassar

Recognition of foreign pathogens by T cell receptor (TCR) activates complex signaling cascades to generate an immune response. To ensure that T cells respond appropriately to antigenic stimuli, TCR signaling is subjected to multiple levels of regulation. While the positive regulation of TCR stimulation is well studied, little is known about its negative regulation. Two proteins, Sts-1 and Sts-2, were recently found to negatively regulate signaling pathways downstream of TCR. In an effort to shed light on the role of these proteins, we solved the crystal structures of the C-terminal domains of the Sts proteins. These structures reveal homology to members of the phosphoglycerate mutase/ acid phosphatase (PGM/AcP) family enzymes, with residues known to be important for catalytic activity conserved in sequence and position in the active site. To further ascertain the location of the active site, structures of the complexes with phosphate and tungstate were solved showing the residues involved in catalysis.

Biochemical data show that Sts-1 functions as a phosphatase that can target several tyrosyl-phosphorylated proteins, including the kinase ZAP-70. We further investigated the importance of the conserved active site residues by site-directed mutagenesis and kinetic analysis. Using *p*NPP as a model substrate, analysis of pH effect

on the k_{cat}/K_m profiles of Sts-1_{PGM} demonstrated that at least one ionizable group is required for the activity. The dramatic reduction of k_{cat} addressed the importance of H565 and R462 in assisting phosphatase activity by Sts-1_{PGM}. Furthermore, E490Q and E490A mutants exhibited a loss of pH dependency in the k_{cat}/K_m profile, indicating that in the native enzyme Glu490 serves as general acid and must be protonated for activity. Using mass spectroscopy, we showed that His380, the nucleophilic residue is transiently phosphorylated during hydrolysis.

To understand the cause of weaker catalytic activity of Sts-2_{PGM}, we mutated residues outside of the signature motif to the corresponding residues in Sts-1_{PGM}. The generated mutants have enhanced *in vitro* phosphatase activity, suggesting that Sts-2_{PGM} may have substrate(s) that is/are different from that of Sts-1_{PGM} and the mutated residues may play a role in substrate selection.

Since the substrates of both Sts-1 and Sts-2 are still unknown, we focused on a newly identified silkworm enzyme, ecdysteroid-phosphate phosphatase (EPPase), which shares ~ 40% sequence identity to Sts-1 with known substrate, as a model to understand the mode of action of Sts proteins. The crystal structure of EPPase was determined and showed homology to PGM family members. The presented structural, biochemical, and kinetic data provide an initial characterization of a new family of protein tyrosine phosphatase.

TABLE OF CONTENTS

LIST OF FIGURES

Chapter 1

Chapter 2

Chapter 3

Chapter 4

LIST OF TABLES

Chapter 1

Chapter 2

Chapter 3

Chapter 4

INTRODUCTION

1.1 The immune system

A great variety of infectious microbes exist in the environment we live in. To combat infectious agents, our immune system has evolved complex mechanisms to protect us. The components involved in immune responses include a variety of cells, and the soluble molecules they secrete. The specific recognition of pathogens is mediated by lymphocytes, which are B cells and T cells. Usually, B cells recognize intake antigen and make antibodies, while T cells are responsible for the destruction of intracellular pathogens and infected host cells. T cells recognize antigens only when they are presented on the surface of the cells with major histocompatibility complex (MHC) molecules by the T-cell antigen receptor (TCR) (Figure 1). The T-cell receptor comprises a disulphide-linked heterodimer of either αβ or γδ chains that enables T cells to recognize a diverse array of antigens. Both forms of TCR associate with a series of polypeptides, collectively called CD3, to form the T-cell receptor complex. Recognition of an antigen-MHC complex by the TCR initiates the signaling events that activate a variety of tyrosine kinases and downstream effectors to regulate cellular responses, inducing the production of cytokines (i.e. interleukin-2 (IL-2)) to trigger the activation of secondary messenger systems for T cell division and proliferation (Figure 2).

Undoubtedly, the immune system is highly regulated and deficiencies in any part of the system lead to a great probability of infection from foreign pathogens. Moreover, there are occasions such as inappropriate reaction to self-antigens, known as autoimmunity; ineffective immune response, known as immunodeficiency; and

overactive immune response, known as hypersensitivity are caused by immune system deficiencies. (Roit *et al*.2001)

1.2 T cell receptor signaling

Recognition of foreign antigens by the T cell receptor (TCR) complex leads to the activation of an effective immune response. The TCR subunits do not have intrinsic tyrosine kinase or phosphatase activity. To induce signal transduction of antigen receptors, the TCR appears to recruit and activate protein tyrosine kinases (PTKs). Engagement of TCR initiates a transient increase in phosphotyrosine in a number of intracellular proteins, which ultimately leads to enhanced gene transcription, cell proliferation and differentiation (Weiss and Littman, 1994). The earliest event in this pathway appears to be tyrosine phosphorylation on immunoreceptor tyrosine-based activation motifs (ITAM) of TCR signal-transducing subunits (CD3 and TCRζ) by two members of the Src family of PTK expressed in T cells, Lyk and Fyn (Zhang *et a*l., 1998). These modifications on ITAM serve as binding sites and direct the recruitment of ZAP-70, a Syk-family PTK, to the TCR via its tandem Src-homology 2 domains. Once ZAP-70 is recruited, it is then phosphorylated and activated by Lck and Fyn (see Figure 2).

The activated ZAP-70 phosphorylates several substrates, including LAT (linker for activation of T cells) and SLP-76 (SH2 domain-containing leukocyte phosphoprotein of 76 kDa) adapter proteins which plays a crucial role in the nucleation of signaling complexes that promote activation of many pathways, including the Ras/MAPK and the phospholipase C/Ca^{2+} signaling pathways (Zhang *et al*., 1998; Yamasaki *et al.*, 2001;

Clements *et al*., 1999; Koretzky and Myung, 2001). To maintain appropriate T cell response and immune equilibrium, T cells possess mechanisms to limit the intensity and duration of signals generated by TCR. One mode of negative regulation involves the internalization of receptor complex into subcellular location, thereby reducing the pool of available TCR for stimulation (Koretzky and Myung, 2001). Alternatively, negative regulators are recruited to interfere with the TCR downstream signaling pathways (see proposed signaling pathway in Figure 3).

1.3 Discovery of the Suppressor of TCR signaling

I. Identification of Jak2-interacting protein, p70.

Sts-1 was originally identified in a screen for proteins that specifically binds to a tyrosine phosphorylated peptide derived from Jak2 and designated as p70 (70 kDa) (Carpino *et al*., 2002). Jak2 belongs to the janus kinase family that regulates cellular processes such as cell growth, differentiation and transformation through their association with cytokine receptors. Jak2 contains a central Src 2 homology (SH2) domain and two C-terminal JAK homology domains (JH1 and JH2) and is activated in response to several growth factors and cytokines such as IL-3, GM-CSF and erythropoietin (Watanabe *et al*., 1997; Witthuhn *et al*., 1993). The activation of Jak2 initially requires transphosphorylation of a critical tyrosine (Tyr1007) within its activation loop resulting in tyrosine phosphorylation of multiple sites on the cytokine receptors chains and subsequent recruitment of a variety of proteins to the receptor complex (Feng *et al*., 1997). Following activation of kinase activity, there are a number of additional tyrosine

residues that are phosphorylated. One of the major sites of autophosphorylation with murine Jak2 is Tyr966, which is specifically required for a number of signaling proteins to bind. Using a large-scale affinity purification approach, Carpino and colleagues identified a 70 kDa protein that was recruited to phosphorylated Tyr966 (Carpino *et al.*, 2002).

II. Identification of UBASH3A.

A second family member of p70 was identified based on sequence homology (~ 45% homologous). Initially, in a study using genomic sequence and expressed sequence tags to identify candidate genes for Down syndrome phenotypes, a critical region (DFNB10 locus) was mapped within human chromosome 21 (21q22.3) (Bonne-Tamir *et al*., 1996). Within refined DFNB10 region, a novel cDNA was isolated (Wattenhofer *et al*., 2001). Because it contains homologies to ubiquitin-association (UBA), Src-homology 3 (SH3), and a novel domain, the gene was named UBASH3A. UBASH3A is expressed in several tissues belonging to immune system, including spleen, bone marrow, and peripheral blood leukocytes (PBLs). Both p70 and UBASH3A are involved in negative regulation of TCR signaling, therefore designated suppressor of TCR signaling, Sts-1 and Sts-2 (Carpino *et al*., 2004).

III. Roles of Sts family in TCR signaling.

The suppressor of TCR signaling family of proteins, Sts-1 and Sts-2, were found to play a role in negatively regulating signaling pathways downstream of TCR (Figure 3). T cells from mice lacking Sts-1 and Sts-2 are hypersensitive to TCR stimulation and

show increased phosphorylation on ubiquitinated ZAP-70 (Carpino *et al*., 2004), a key component of the TCR signaling machinery. ZAP-70 deficient mice displays a phenotype with no mature CD4+ and CD8+ T cells, while ZAP-70 mutations in humans lead to severe developmental and functional defects within the T cell compartment (Negishi *et al*., 1995; Elder, 1998). How Sts proteins negatively regulate the TCR signaling is unclear and the nature of their substrates is also unknown.

IV. Cbl-interacting proteins.

Recently, Sts-1 and Sts-2 (formerly designated as p70 and UBASH3A) were identified as two novel Cbl-interacting proteins that inhibit endocytosis of epidermal growth factor receptor (EGFR) and platelet-derived growth factor receptor (PGFR) (Kowanetz *et al*., 2004). Degradation of growth factor-activated receptor tyrosine kinase (RTK) represents one of the main mechanisms for the negative regulation of cell signaling and normal cellular homeostasis (Dikic *et al*., 2003). Removal of RTKs from cell surface is controlled by protein ubiquitination, an evolutionarily conserved modification where ubiquitin is covalently attached to lysine residue of the target protein (Pickart, 2001). The multiple-ubiquitin ligase, casitas B-lineage lymphoma (Cbl), plays a prominent role in mediating ligand-dependent down-regulation of RTKs (Thien and Langdon, 2001). With the use of antibodies cross-reacting with Sts-1 and Sts-2, Kowanetz *et al*. demonstrated that Cbl readily associates with endogenous Sts-1/Sts-2 in HeLa cells. In addition, a mutant form of Sts-2 containing non-functional SH3 domain (W279A) was unable to bind either to Cbl or EGFR, confirming that the binding of SH3 domain to Cbl is critical for association of Sts-1/Sts-2 to EGFR.

1.4 Functional roles of Sts proteins in regulating TCR signaling

High levels of Sts-1 and Sts-2 were detected in bone marrow, spleen, and thymus suggesting a role for the Sts protein in cells of the hematopoietic system. In splenic lymphocytes, Sts-1 is expressed in both B and T cells, while Sts-2 is expressed in T cells. The roles Sts-1 and Sts-2 play in the regulation of TCR signaling have been demonstrated by studying the phenotype of mice lacking Sts proteins (Carpino *et al*., 2004). Sts-1/-2$^{-/-}$ double knockout (dKO) mice were viable and overtly normal with no significant differences in the numbers of red cells, hemoglobin levels, or hematocrits (Carpino *et al.*, 2004). However, the total number of splenocytes recovered from the dKO mice was greater than from wild type mice. Nevertheless, thymocytes and T cells from the dKO mice were hyperproliferated relative to wild type in response to TCR stimulation. Additionally, following receptor engagement in Sts-1/-2$^{-/-}$ dKO T cells, an increased level of tyrosine phosphorylation of ZAP-70 was observed. Two substrates of ZAP-70, LAT and SLP-76, were also found to have enhanced tyrosine phosphorylation. These results demonstrated that Sts-1 and Sts-2 play critical roles in negatively regulating the signal transduction downstream in response to TCR stimulation.

1.5 Domain structure of the Sts family members

Sts-1 and Sts-2 share approximately 40% amino acid sequence identity. Sts-1 is ubiquitously expressed, whereas Sts-2 is preferentially expressed in hematopoietic cells and tissues (Wattenhofer *et al*., 2001). Both proteins are characterized by a unique multi-domain structure, with an N-terminal UBA domain and a SH3 domain (Figure 5). Both UBA and SH3 domains are protein-protein interaction domains. The UBA domain is a

short conserved region that is found in many proteins that can interact directly with monoubiquitin, polyubiquitin and/or a ubiquilyted protein (Di Fiore *et al*., 2003). The presence of a UBA domain in a protein indicates that it is involved in ubiquitylation or deubiquitylation that can alter protein location or activity to regulate many biological processes (Hicke *et al*., 2005). The SH3 domain, the central regions in Sts-1 (residues 259 – 316) and Sts-2 (residues 245 – 302), are found in many proteins involved in tyrosine kinase signaling (Pawson, 1995). It has been shown that SH3 domains mediate protein-protein interactions by binding to proline-rich regions (PXXP) in ligand proteins (Sparks *et al*., 1996). In addition, the C-terminus has resemblance to the phosphoglycerate mutase (PGM) family of enzymes (Crowhurst *et al*., 1999; Jedrzejas, 2000; Bond *et al*., 2002). PGM is an evolutionarily conserved enzyme that plays critical role in glycolysis. PGM family members including fructose-2,6-bisphosphatase, yeast *S. cerevisiae* PGM, and *E. coli* dPGM act as phosphatases and/or phosphotransferases (Jedrzejas, 2000; Mikhailik *et al*., 2007).

Phosphoglycerate mutase (PGM) is widely distributed in mammalian tissues where it reversibly catalyzes the reaction for the metabolism of glucose and/or 2,3-phosphoglycerate (Fothergill-Gillmore and Watson, 1989). Monophosphoglycerate mutase (mPGM) catalyzes transfer of phospho-group from 3-phosphoglycerate (3-PGA) to 2-phosphoglycerate (2-PGA) in glycolysis and gluconeogenesis pathways (Chen *et al.*, 1974), while bisphosphoglycerate mutase (bPGM) converts 1,3-phosphoglycerate (13PGA) to 23PGA (Forthergill-Gilmore and Watson, 1989). The mPGM enzymes can be divided into two groups, the ones dependent on 23PGA as cofactor are “dPGM”, otherwise are “iPGM” (Jedrzejas 2000). The dPGMs are ~ 27 kDa and exist as

monomers, dimers or tetramers. In contrast, the iPGMs are ~ 50 kDa and are mostly monomers.

Several structures of PGM enzymes have been solved (Crowhurst *et al*., 1999; Jedrzejas *et al*., 2000; Bond *et al*., 2002). The PGM monomer has an α/β fold consisting of a β-sheet core with α-helices flanked on both sides (Figure 4). There is one active site per monomer located at the C-terminal end of β-sheet. The active site is consisting of several conserved key residues, two histidines, two arginines, and a glutamic acid (Winn *et al.* 1981). Site-directed mutagenesis of these active site residues has revealed the catalytic mechanism of the active site (Jedrzejas, 2000). Importantly, in the case of dPGM, His8 is involved in forming a phosphohistidine-enzyme intermediate (Winn *et al.*, 1981; Fothergill-Gillmore and Watson, 1989; Rose, 1970, 1971; Nairn *et al.*, 1995). The amino acid sequence Arg-His-Gly-Glu (RHGE) has been identified as a signature motif in the PGM family, which is also present in the acid phosphatase (AcP) family as Arg-His-Gly/Asn (RHG/N) (Vicent *et al.*, 1992). This signature pattern of ^{379}RHGE^{382} is also present within the C-terminal region of Sts-1, suggesting that this region of Sts-1 is evolutionarily related to PGM/AcP superfamily (Mikhailik *et al.*, 2007).

1.6 Structure of Sts-1$_{PGM}$

Our lab has solved the crystal structure of Sts-1$_{PGM}$ by X-ray crystallography (Mikhailik *et al*., 2007). The final model consists of three identical molecules of Sts-1$_{PGM}$ in the asymmetric unit. Two molecules form a dimer and the third forms a dimer with the molecule in the neighboring asymmetric unit, which is consistent with the fact that Sts-1$_{PGM}$ dimerizes in solution (Kleinman *et al*., 2006). The Sts-1$_{PGM}$ monomer forms an α/β

type fold similar to that adopted by all members of the PGM superfamily enzymes (Jedrzejas, 2000). The core of the molecule is formed by a central 7-stranded β sheet and is surrounded by 8 α-helices (α1 – α8). The C-terminal β-strand (β7) located outside the protein core makes a strong interaction with a neighboring molecule, contributing to the dimer interface. The ^{379}RHGE^{382} signature pattern is located at the carboxyl end of the central β sheet (Figure 6). Based on structural (Figure 7) and sequence homology (Figure 8) to the PGM/AcP enzymes, this cavity is likely the Sts-1_{PGM} catalytic pocket (Mikhailik *et al*., 2007).

1.7 Phosphatase activity associated with Sts-1.

An intrinsic phosphatase activity associated with the C-terminal PGM-like domain of Sts-1 (residues 369 – 638) was identified using the phosphatase substrate analog para-nitrophenyl phosphate, *p*NPP (Mikhailik *et al*., 2007). The K_m value for *p*NPP hydrolysis of Sts-1_{PGM} was determined to be approximately 1 mM at pH 7.5 (Mikhailik *et al*., 2007). In comparison, the K_m of bacterial PGM (***B. stearothermophilus***) is 3 mM and human prostatic acid phosphatase is 0.7 mM (Rigden *et al*., 2001; Kilsheimer and Axelrod, 1957). In addition, Sts-1_{PGM} enzyme activity was observed irrespective of the presence or absence of a variety of metal ions, suggesting that a metal ion cofactor is not required for the reaction, which is a common property to all PGM/AcP family members (Vicent *et al*., 1992; Mikhailik *et al*., 2007). Since the Sts proteins have been implicated in negative regulation in TCR signaling (Carpino *et al*., 2004), the ability of Sts-1 to dephosphorylate key signaling proteins downstream of the TCR was investigated. Sts-1_{PGM} was able to dephosphorylate Zap-70 and a wide range of proteins

that become tyrosine phosphorylated following TCR stimulation (Mikhailik *et al*., 2007). Furthermore, the role of Sts-1 catalytic activity in regulating TCR signaling was examined. In a reconstitution assay, Sts-1/-2$^{-/-}$-activated T cells are hyperresponsive to TCR stimulation, and reconstitution of mutant T cells with Sts-1 cDNA significantly reduces the proliferative response (Mikhailik *et al*., 2007). In addition, it was shown that a Sts-1$_{PGM}$ mutant lacking catalytic His380 and His565 at the active site displayed no phosphatase activity towards Src-pTyr (Mikhailik *et al*., 2007). These results suggest that Sts-1 phosphatase activity plays a role in the negative regulation of TCR signaling and indicate that Sts proteins may function as protein tyrosine phosphatases.

1.8 Protein tyrosine phosphatases

Tyrosine phosphorylation is the major signaling mechanism for signal transduction to regulate many cellular events, including cell proliferation and differentiation, activation of gene transcription, and cell motility and morphology. Cells of the immune system express more genes encoding PTKs and protein tyrosine phosphatases (PTPs) to carry out high level of tyrosine phosphorylation than other cell types (Mustelin *et al*., 2005). Signaling proteins are phosphorylated on conserved tyrosine residues by PTKs and dephosphorylated by PTPs. Both PTKs and PTPs can promote activation or inhibition effects of the signaling pathways that are required for cell responses. To control the tyrosine phosphorylation state in the cell, PTKs and PTPs function together to regulate the activity of effectors.

In the human genome, there are 107 genes that encode PTPs, 90 genes for PTKs; T cells express at least 45 different PTPs (Table 1) (Mustelin *et al*., 2005). Each PTP has

a catalytic domain for specific substrates, and at least a protein-protein or protein-lipid interaction motif to target itself to specific locations. The important feature of dephosphorylation ability of PTPs is that a catalytic cysteine residue in the active site is phosphorylated during substrate hydrolysis. The formation of this cysteinyl-phosphate intermediate was examined by generating a Q262A mutant of PTP1B to trap the intermediate within a PTP1B crystal (Pannifer *et al*., 1998).

PTP1B is the first PTPase to be purified and characterized and is found in a wide variety of human tissues (Tonks *et al*., 1988; Sarmiento *et al*., 2000). It is capable of dephosphorylating a number of receptor tyrosine kinases, including insulin receptor and the EGF receptor (Sarmiento *et al*., 2000). Because PTP1B negatively regulates insulin signaling, it has becoming the major target related to type II diabetes and obesity (Ahmad *et al*., 1995). In fact, the discoveries of alterations in PTPs to cause immune dysfunction and diseases are increasing. The crucial roles of many PTPs found in immune cells, such as which signaling pathways they are involved in and which substrates they recognize, are still far from being clear. Understanding the regulation mechanisms of PTPs in the immune system will undoubtedly help us develop more effective treatment against allergic and autoimmune diseases in the future.

1.9 Novel relationship to ecdysteroid phosphate phosphatase

A previously identified enzyme from the eggs of the silkworm *Bombyx mori*, ecdysteroid-phosphate phosphatase (EPPase), was shown to bear sequence similarity to Sts-1 and Sts-2 (Yamada and Sonobe, 2003; Davies *et al*., 2007). Davies and colleagues showed that the conserved catalytic arginine and histidine residues are conserved in these

proteins. Remarkably, a long form of the EPPase homologue in *Drosophila* has been described (751 residues). It is similar to the domain architecture of Sts-1, contains a N-terminal UBA domain, followed by an SH3 domain, and a PGM domain at the carboxyl end. Therefore, EPPase was characterized as a member of the histidine phosphatase superfamily. All enzymes in this superfamily (including dPGM, PhoE, SixA, CobC, and FBPase-2s) have a histidine residue in the active site that becomes phosphorylated during the catalytic cycle. Moreover, Sts-1 and EPPases from *B. mori* and *Drosophila* all carry activity that can hydrolyze ecdysteroid-phosphate, with a preference for ecdysteroids with a 22-phosphate (Davies *et al*., 2007).

EPPase and Sts proteins share sequence homology, including the residues known to be important for catalytic activity. Studies on how EPPase interacts with its substrates can lead to an understanding of the interactions of Sts proteins with their potential ligands, including steroid-like substrate(s). Steroid hormones have been shown to have profound influence on the immune system, including apoptosis of immature thymocytes and mature T cells (Winoto and Littman, 2002). T cell development (thymocytes) undergoes stages of selection. To survive the differentiation of T cell antigen receptor in the thymus and be exported to peripheral lymphoid organs, TCR engage appropriate interaction with MHC, called positive selection, to rescue thymocytes from programmed cell death. Thymocytes carrying TCR with high affinity to self-antigens are hazardous auto-reactive T cells and will be prevented from maturation and eliminated (i.e. apoptosis), by a process called negative selection (Jameson *et al*., 1995). Recent studies on one of the steroid hormones, corticosteroids, which bind to the nuclear hormone glucocorticoid receptor (GR), play a key role in the selection of T cells during their development in

thymus (Ashwell *et al*., 2000; Winoto and Littman, 2002). This observation led to the development of therapeutic cortisone and other synthetic steroids in treatment of inflammation and malignancy. Since Sts proteins suppress TCR signaling and T cell proliferation, they may have hormone-like substrates that are involved in selection of T cells during differentiation.

1.10 Open questions and goals of the dissertation

How are Sts-1 and Sts-2 involved in TCR regulation? At the beginning of this work, little was known about the Sts proteins: how they function, the nature of their substrate(s), and how they antagonize TCR signaling. Little information has been published concerning the molecular function of the Sts proteins PGM domains. We have previously shown that the PGM domain of Sts-1 carries phosphatase activity that is important in negatively regulating TCR signaling (Mikhailik *et al*., 2007). However, no studies have attempted to elucidate the structural and functional differences between Sts-1 and Sts-2. We used structural and biochemical approaches to address these questions using the weak homology to PGM family members as a guiding hypothesis. The objective of the present study was to determine and compare the crystal structures of Sts-1, Sts-2 and EPPase alone or in complex with tungstate and phosphate. We showed that the structures of these three proteins share strong homology, with the residues known to be important for the phosphatase activity lining the active site. Comparison of these structures led to questions of substrate specificity. In addition, we used a kinetics approach to understand the catalytic roles of the active site residues and thereby establish the catalytic mechanism for the phosphatase activity.

Figure 1. Recognition of MHC-peptide on the antigen-presenting cell (APC) by T cell receptor. After aggregation of MHC-peptide on the T cell receptor, either CD4 or CD8 can join the complex and recruit tyrosine kinases, such as Lck, to CD4 or CD8 to phosphorylate the immunoreceptor tyrosine-based activation motifs (ITAM) on the CD3 γγ dimer. The phosphorylation event on the ITAM motifs is the first step of T cell activation. (Figure taken from Roit *et al*., 2001)

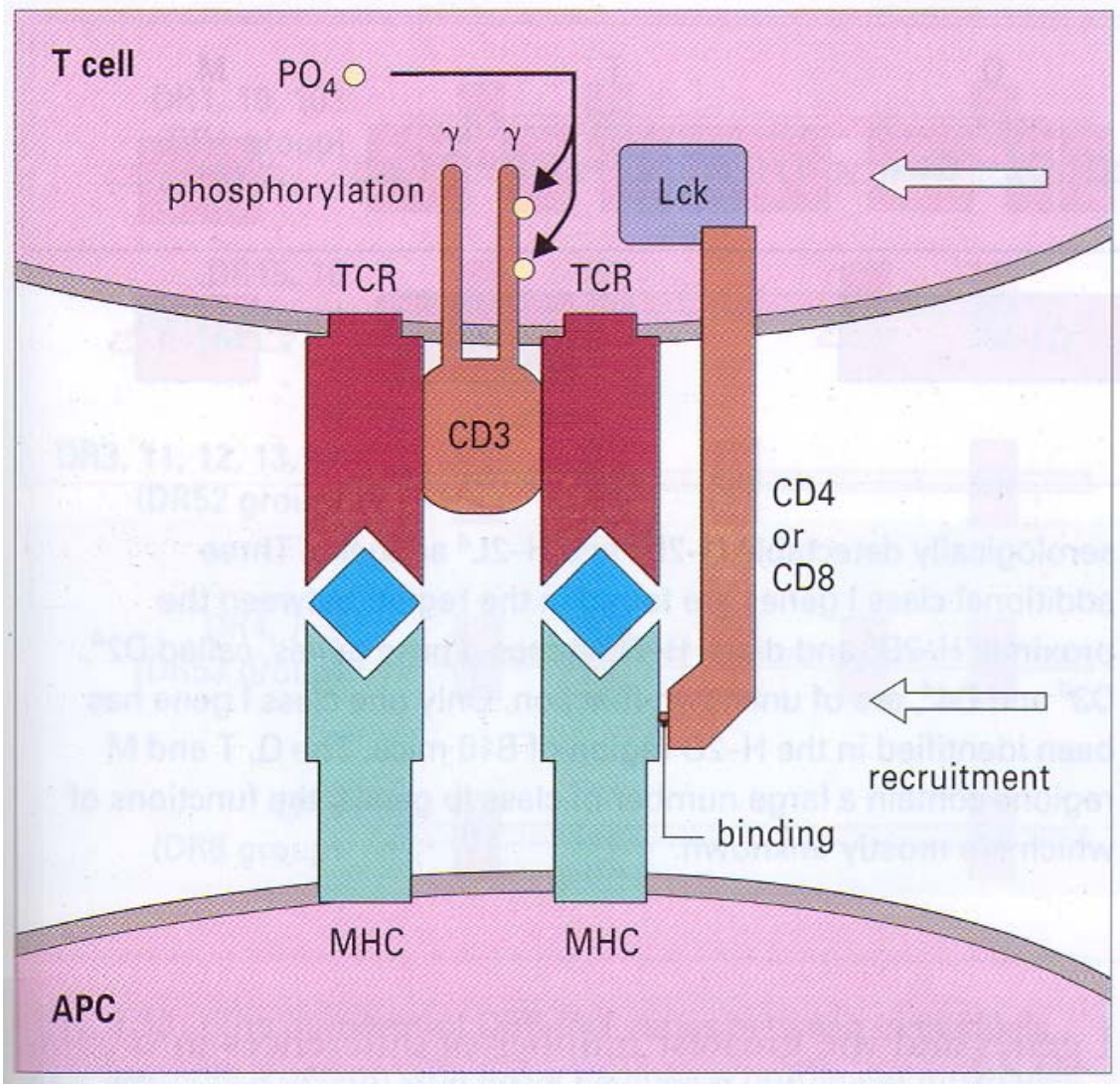

Figure 2. Signal transduction pathways involved in T cell activation. Engagement of surface receptors such as CD4, CD28, and CD45 with the TCR complex results in the activation of the tyrosine kinases Fyn and Lck, which allows association of ZAP-70. ZAP-70, Fyn and PI-3 kinase integrate kinase cascades that activate specific transcription factors. Activation of phospholipase C (PLC-γ) by Fyn leads to activation of two pathways by the cleavage of PIP2 into IP3 and DAG. IP3 releases Ca2+ from the ER to activate calcineurin, which dephosphorylates the transcription factor NF-AT and causes its translocation to the nucleus. DAG activates PKC, which translocates NF-κB to the nucleus. The transcription factors activate genes including *fos* and *jun* to induce cell division. (Figure taken from Roit *et al*., 2001)

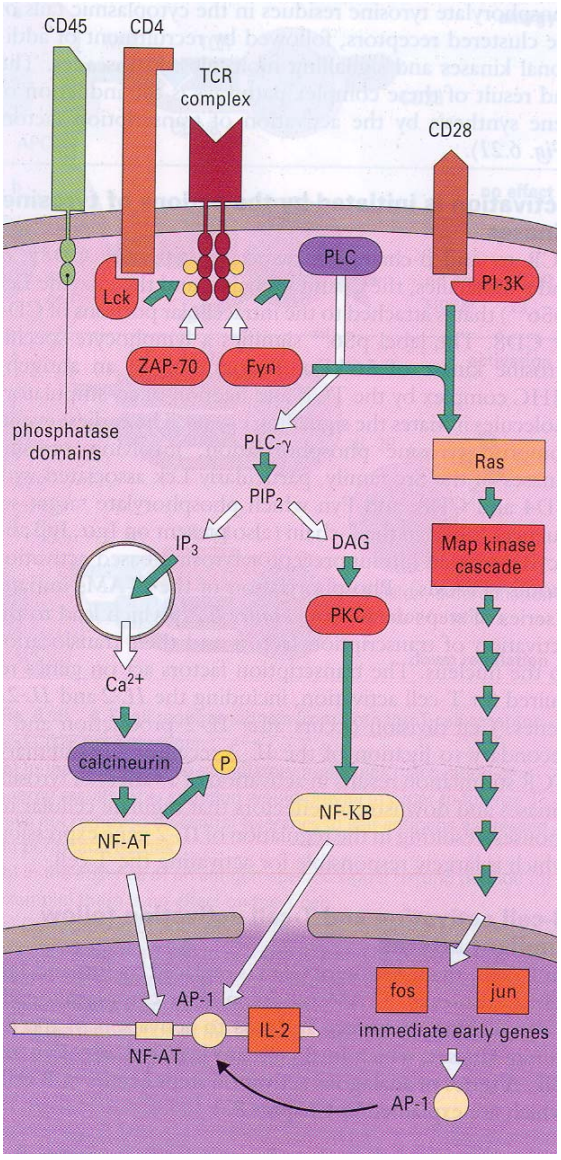

Figure 3. Sts proteins and T-cell receptor signaling. How Sts proteins negatively regulate TCR signaling is still unknown. One possibility is that they inhibit the activation of Zap70. Another possibility is that they dephosphorylate an unknown substrate. Therefore, the possible routes that Sts proteins could be involved in TCR signaling are labeled with question mark.

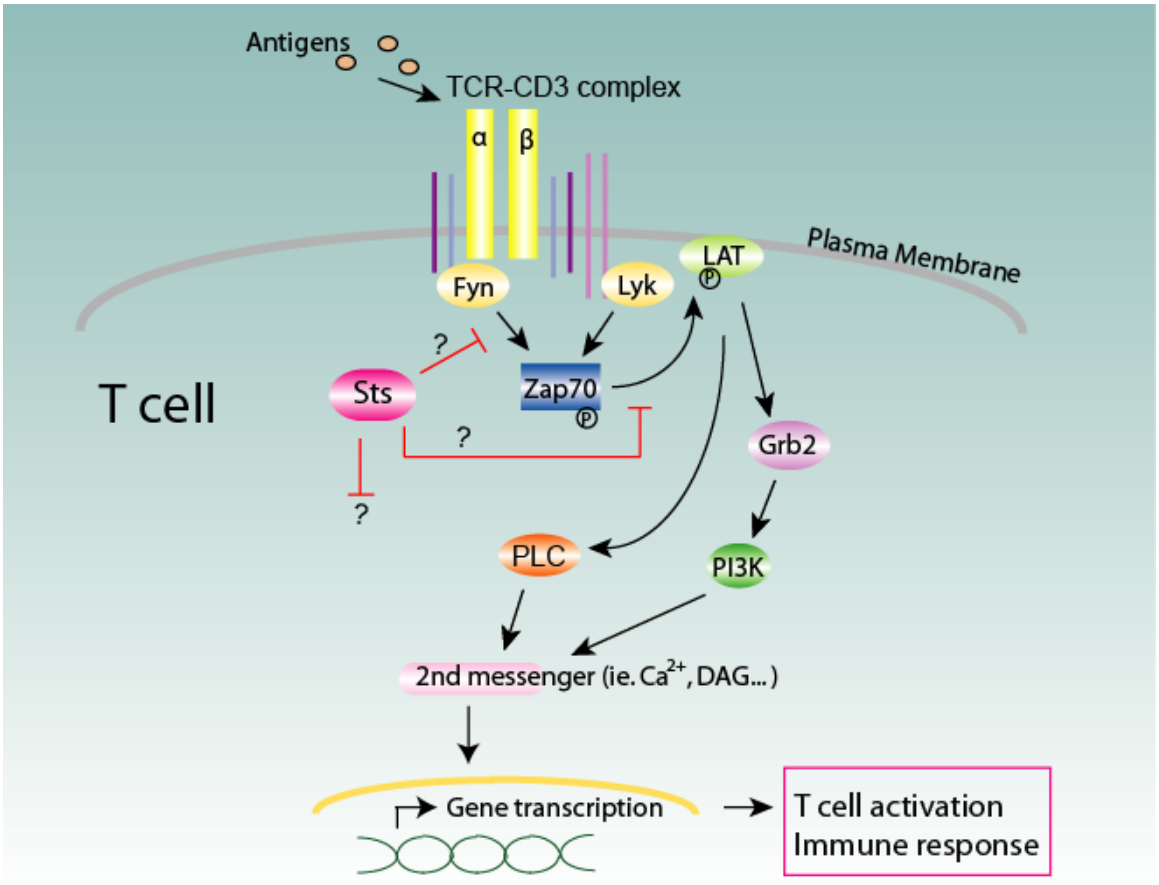

Fyn: a member of the Src family of tyrosine kinases.

Lyk: Leukocyte-specific protein tyrosine kinase, a member of the Src family of tyrosine kinases.

Zap-70: Zeta-chain-associated protein kinase of 70 kDa.

LAT: Linker of activated T cells, a transmembrane adaptor protein.

Grb2: Growth receptor bound protein 2, an adaptor protein.

PI3K: Phosphoinositide 3-kinase.

PLC: Phospholipase C.

DAG: Diacylglycerol, a second messenger signaling lipid made by PLC.

Figure 4. Ribbon diagram of *S. cerevisiae* dPGM (Crowhurst *et al*., 1999). The N- and C-termini are indicated. This α/β-fold is structurally conserved in PGM family. Structure generated with PyMol. 3PGA: 3-phosphoglyceric acid (in color). Protein data bank ID: 1QHF.

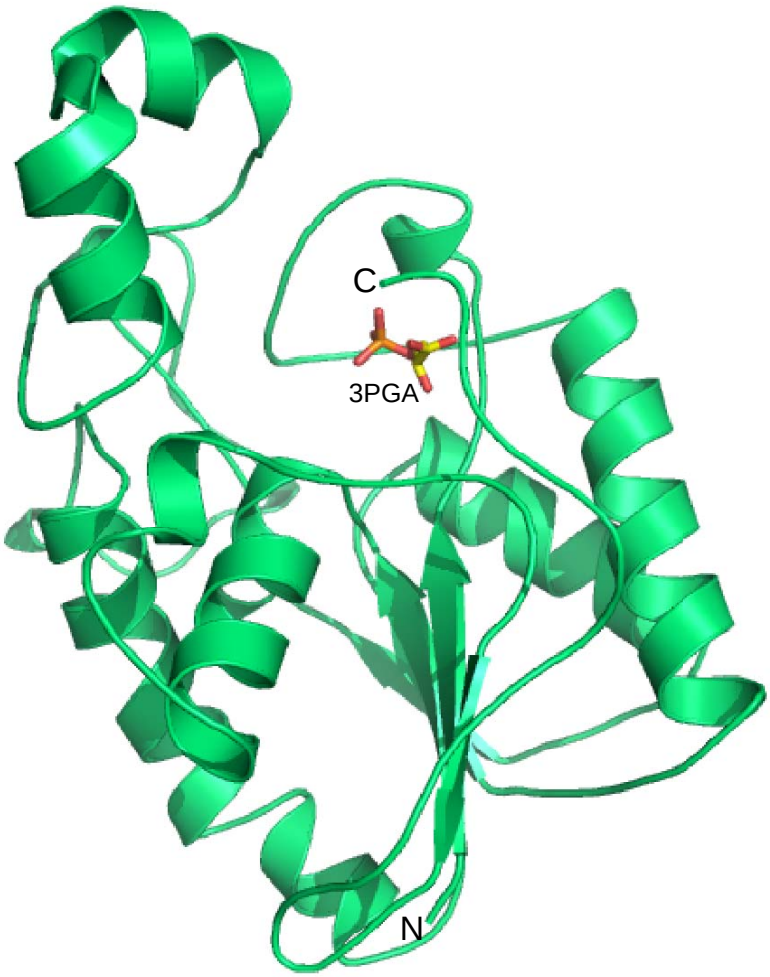

Figure 5. Domain structures of Sts-1, Sts-2 and EPPase. UBA: ubiquitin-association domain (blue), SH3: Src-homology 3 domain (yellow), PGM: phosphoglycerate mutase homology region (pink).

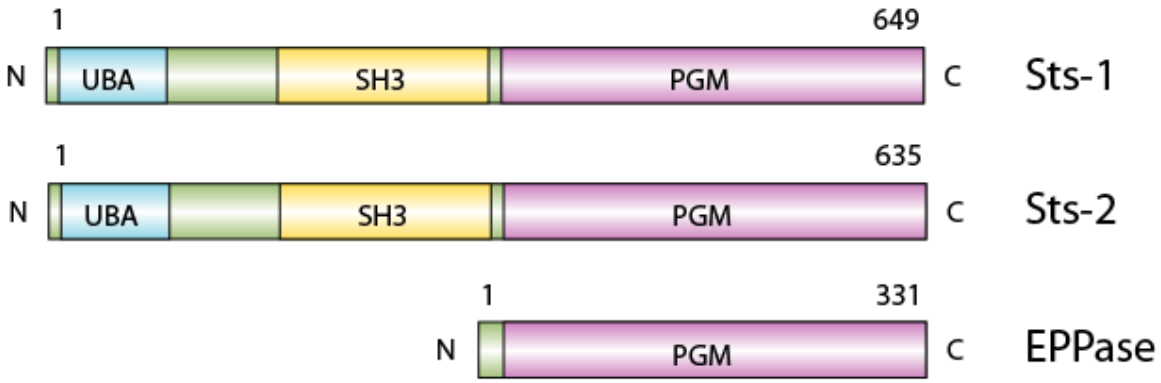

Figure 6. Ribbon diagram of the Sts-1_{PGM} dimer; monomers colored in yellow or blue. The top view has the 2-fold axis of the dimer perpendicular to the page. In the bottom view, the 2-fold axis is parallel to the page. The side chains of His-380 and His-565 are shown as ball-and-stick representations to indicate the location of the active site. (Mikhailik *et al*., 2007)

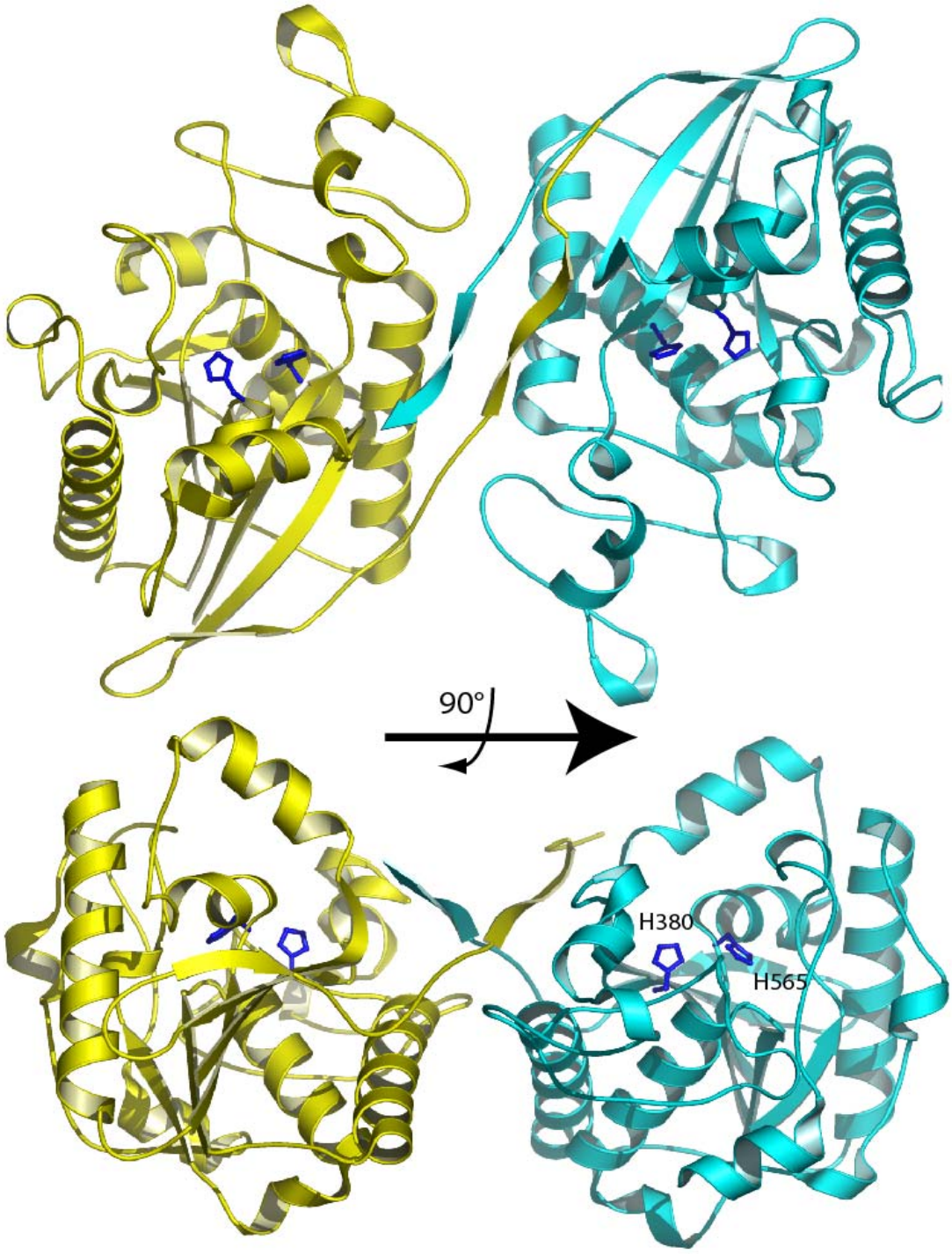

Figure 7. Structural comparison of Sts-1_{PGM} and *E. coli* PGM (ecPGM). Critical catalytic residues of ecPGM, and the homologous residues of Sts-1_{PGM}, are shown in gold ball-and-stick representation. The two regions that deviate between the two structures, inserts 1 and 2 (Sts-1 residues 399 – 436 and 505 – 535) are in red and blue, respectively. The C-termini are shown in green. (Mikhailik *et al*., 2007)

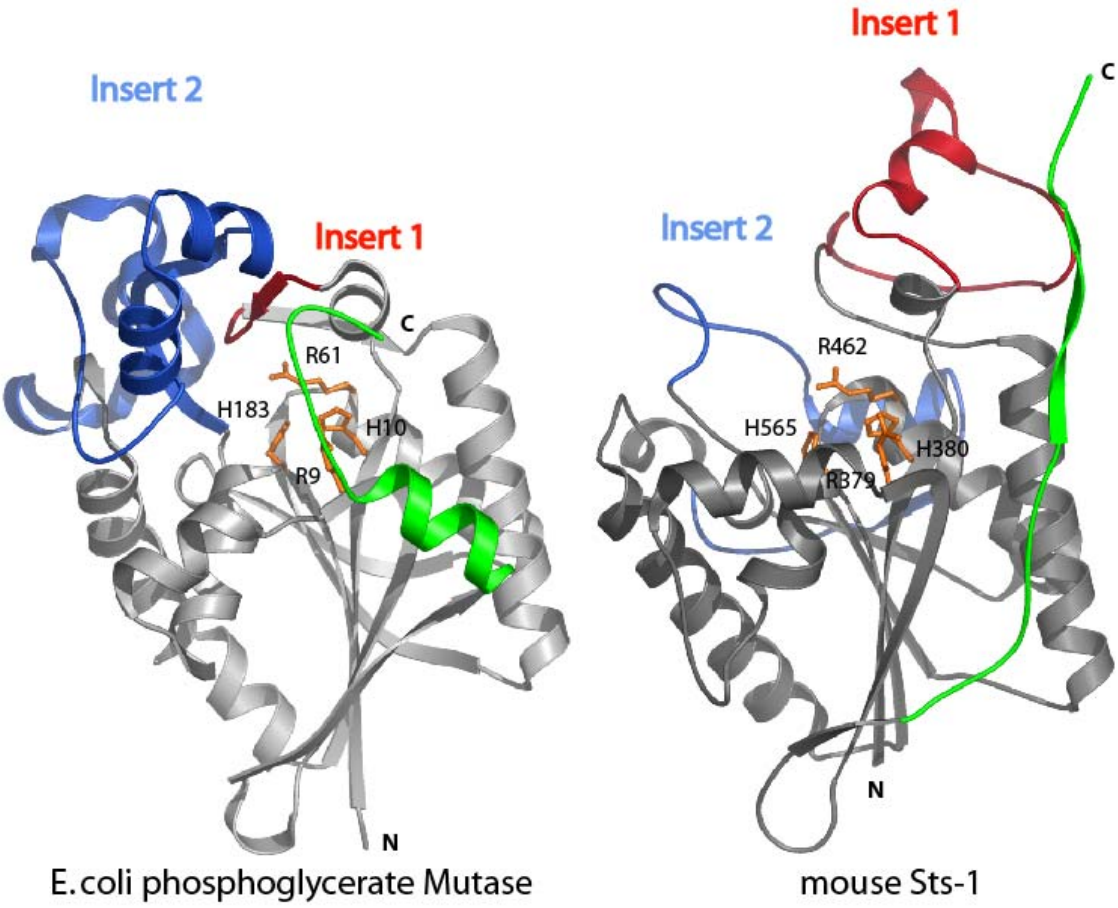

Figure 8. Structure based sequence alignment of mouse Sts-1 and *E. coli* PGM. Identical residues are in red. Inserts 1 and 2 are shaded in gray.

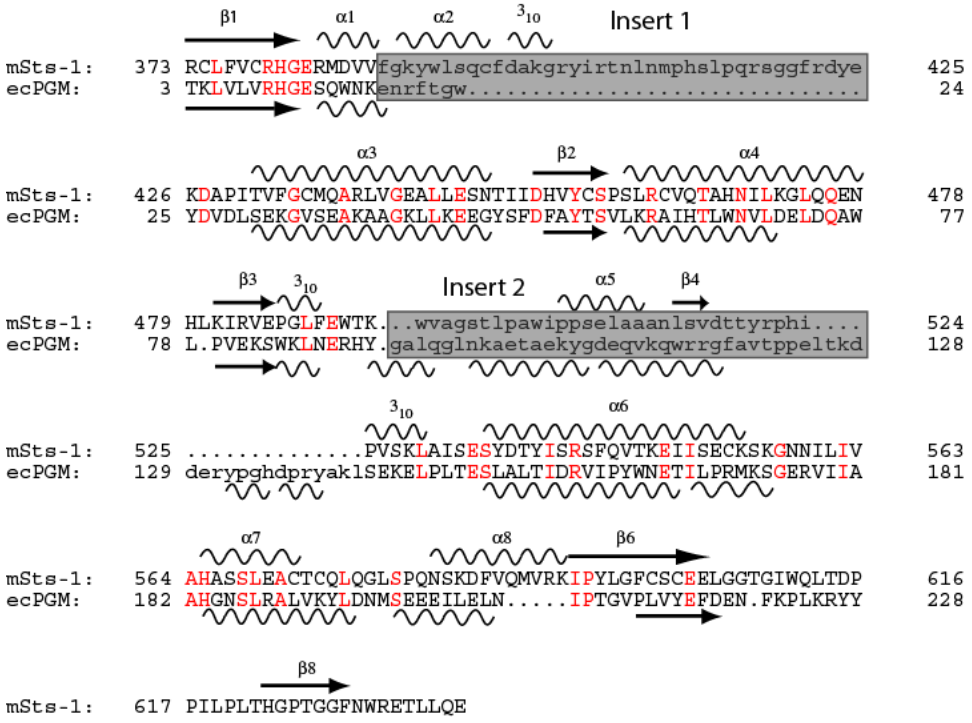

Table 1. Protein tyrosine phosphatases (PTPs) expressed by T cells and their main functions (Mustelin *et al*., 2005).

Class	PTP*	Role in lymphocyte activation	Mechanism, function and substrates
Receptor-like PTPs (Class I)	CD45	Positive	Positively regulates LCK and FYN
	RPTP-ε	ND	Unknown, might regulate SRC-family PTKs
	CD148	Negative	Might dephosphorylate LAT, PLC-γ and other substrates
Non-receptor, classical PTPs (Class I)	HEPTP	Negative	Regulates ERK and p38 in cytosol
	PTP1B	None	Regulates insulin receptor and other receptor PTKs
	TCPTP	Negative	Dephosphorylates STAT1 in nucleus
	PTPH1	Negative	Inhibitory, dephosphorylates ITAMs and VCP
	PTP-MEG1	Negative	ND
	PTP-MEG2	None	Regulates secretion, no effect on early TCR-signalling events
	PEZ	ND	ND
	PTP-BAS	None	Binds CD95 (FAS)
	LYP (PEP)‡	Negative	Dephosphorylates activation loops of LCK, FYN and ZAP70
	PTP-PEST	Negative	Binds CSK, dephosphorylates CAS, SHC, PYK2 and FAK
	PTP-HSCF	ND	Binds CSK and ITK
	SHP1	Negative	Mediates inhibition through ITIM-containing receptors, dephosphorylates ZAP70 and SYK
	SHP2	Positive	Augments ERK activation, crucial for lymphoid development
	HDPTP	ND	ND
Other class I PTPs	PAC1	Negative	Dephosphorylates ERK in nucleus
	MKP1	Negative	Dephosphorylates MAPKs in nucleus
	MKP3	Negative	Dephosphorylates ERK in cytosol
	MKP5	Negative	Dephosphorylates JNK in nucleus
	MKP6	Negative	Associates with CD28
	VHR	Negative	Activated by ZAP70, dephosphorylates ERK, JNK and STAT5
	VHX	Negative	ND
	VHZ	ND	ND
	RNGTT	None	Processes mRNA
	PRL1, -3	ND	ND
	CDC14	None	Regulates exit from mitosis
	PTEN	Negative	Counteracts PI3K, reduces survival
	MTM1	ND	Presumably regulates intracellular-vesicle traffic
	MTMR1, -2, -3, -4, -14	ND	Presumably regulate intracellular-vesicle traffic
	MTMR5	ND	Catalytically inactive, regulates MTM1 and MTMR2
	MTMR10	ND	Catalytically inactive, regulates MTMR2
	MTMR11	ND	Catalytically inactive
Class II PTPs	LMPTP	Positive	Dephosphorylates ZAP70 on the tyrosine residue at position 292
Class III PTPs	CDC25A, -B, -C	None	Activates CDKs
Aspartic-acid-based PTPs	EYA3, -4	ND	Regulate transcription

2. A CATALYTIC MECHANISM FOR THE Sts-1 PGM DOMAIN

PARTIALLY ADAPTED FROM:

Mikhailik A, Ford B, Keller J, Chen Y, Nassar N, and Carpino N. A phosphatase activity of Sts-1 contributes to the suppression of TCR signaling. *Molecular Cell* 27, 486 – 497, August 3, 2007.

ABSTRACT

Signaling pathways mediated by kinases downstream of the T cell receptor (TCR) play a crucial role for a proper immune response. To ensure that T cells response appropriately, TCR signaling pathways are subjected to multi-step regulatory checkpoints. We previously demonstrated that Sts-1, suppressor of TCR signaling, has phosphatase activity targeting the tyrosine kinase Zap-70 and therefore negatively regulates signaling pathways of the TCR. Furthermore, the X-ray structure of Sts-1 C-terminus reveals that it has homology to all members of the phosphoglycerate mutase/acid phosphatase (PGM/AcP) family of enzymes, with residues known to be important for PGM/AcP catalytic activity position in Sts-1. The structure of the phosphate bound Sts-1_{PGM} at 2.6 Å resolution shows that the phosphate ion is located at a shallow cavity surrounding by these residues (Arg379, His380, Arg462, Glu490, and His565), indicating this cavity is likely the active site of Sts-1_{PGM}. The catalytic mechanism for Sts-1_{PGM} was investigated using *para*-nitrophenyl phosphate as a model substrate. Using 1D ^{31}P NMR and MALDI-TOF, the transient phospho-histidine intermediate was observed when Sts-1_{PGM} H565A mutant was treated with *p*NPP. The pH dependence of the kinetic parameters k_{cat}/K_m exhibits a slope of ~ –1 descending in basic pH range, indicating that at least one group must be protonated for activity. Mutations of the conserved active site residues and examined the pH effect on the k_{cat}/K_m profile for these mutants shows a significant decrease in k_{cat} values of R462A, H565A, and H380A indicating the important roles of these residues in substrate binding. However, the k_{cat}/K_m profiles of these residues are pH-dependent (with a slope of ~ –1). The k_{cat}/K_m profile is

pH-independent when the conserved acidic residue, Glu490, was changed to Ala or Gln, suggesting that Glu490 acts as general acid and is responsible for the phospho-intermediate formation. Glu490 may also serve as general base by utilizing a proton from a water molecule in the hydrolysis of intermediate.

INTRODUCTION

2.2.1 Phosphatase activity of Sts-1_{PGM}

Two members of the Suppressor of T cell receptor (TCR) signaling family of proteins (Sts-1/Sts-2) were recently shown to be involved in negative regulation downstream of TCR signaling (Carpino *et al*., 2004). Sts-1 was originally discovered in a screen for proteins that bind to a specific tyrosine kinase Jak2 (Carpino *et al*., 2002). Sts-1 and Jak2 were subsequently shown to interact, although the role of Sts-1 in Jak2 signaling has not been established. The Sts proteins were also identified by virtue of their ability to bind to the ubiquitin ligase Cbl (Kowanetz *et al*., 2004; Feshchenko *et al*., 2004).

The realization that Sts-1 and Sts-2 have roles in regulating signaling pathways downstream of the TCR emerged from an analysis of T cells derived from mice genetically engineered to lack the two proteins (Carpino *et al*., 2004). In particular, native Sts-$1/2^{-/-}$ T cells are hypersensitive to TCR stimulation, exhibiting a pronounced increase in TCR-induced proliferation relative to wild-type cells. This phenotype is accompanied by a marked increase in cytokine production by Sts-$1/2^{-/-}$ T cells and significantly increased susceptibility of double knockout mice to autoimmunity in a mouse model of multiple sclerosis. In addition, Sts-$1/2^{-/-}$ native T cells display enhanced phosphorylation and activation of Zap-70, a tyrosine kinase that plays an important role in relaying signals from the TCR (Mikhailik *et al*., 2007). This later finding suggests that the Sts proteins control the level of Zap-70 activation during TCR engagement. However, while these

studies identified a role for the Sts proteins in regulating signaling pathways downstream of the TCR, they did not address their intracellular targets or mechanisms of action.

Both Sts proteins are characterized as a multidomain structure consisting of an N-terminal ubiquitin-association (UBA) domain and a central Src-homology 3 (SH3) domain. The Sts C-terminus has passing resemblance to members of the phosphoglycerate mutase (PGM) family of enzymes (Carpino *et al*., 2002). PGM, an evolutionarily conserved enzyme that plays a critical role in glycolysis, lends its name to a family of enzymes that share a common structural fold and the ability to act as phosphatases and/or phosphotransferases. PGM family members also share a clear biochemical and structural relationship to members of the acid phosphatase (AcP) family of enzymes (Jedrzejas, 2000).

2.2.2 Relationship between kinases and phosphatases

Phosphorylation and dephosphorylation of proteins mediate signal transduction that controls critical cellular events, such as cell proliferation, division, and apoptosis. Protein kinases phosphorylate substrates by transferring phosphate group from ATP onto serine, threonine, or tyrosine side chains. This action usually leads to activation of signaling proteins to further activate or inhibit biological processes. The phosphate group is eventually removed by a phosphatase to maintain a balance of phosphorylation. Without proper regulation of the phosphorylation level, the phosphorylated protein would be in a constant state of being activated or inhibited. Many cancers show a mutation or deletion of a protein tyrosine phosphatase (PTP) gene, which leads to abnormal proliferation (e.g. PTEN) (Siminovitch *et al*., 1999; Fraser *et al*., 2004).

2.2.3 Families of protein tyrosine phosphatases.

Two types of PTPs, conserved in sequence and structure, can be functionally distinguished. The classical PTPs, which are specific to tyrosine residues, and the dual-specificity phosphatases (DSPs), which additionally dephosphorylate serine and threonine residues. Both types are included in receptor and nonreceptor tyrosine phosphatase classes (Figure 1 on page 46). Members of the PTP family contain a signature motif, (I/V)HCXAGXXR(S/T)G, a highly conserved active site sequence with the Cys and Arg residues essential for their enzymatic functions (Barford *et al*., 1996; Fauman and Saper, 1996).

Hydrolysis of the phosphate monoester by *Yersinia* PTP suggested the active site residues Cys403 as the nucleophilic group. Glu290 and Asp356 were identified as general base and general acid by investigating the pH effect on the k_{cat} and k_{cat}/K_m values for the wild type and mutants (Zhang *et al*., 1994). Moreover, Pannifer *et al*. (1998) identified the conserved Cys215 as the nucleophilic group by determining the structure of PTP1B cysteinyl-phosphate intermediate (Figure 2). Collectively, the reactions catalyzed by PTPs involve a dephosphorylation of phosphotyrosine residues via the formation of a transient cysteinyl-phosphate intermediate.

2.2.4 Mechanisms of phosphatase catalytic activity

The important role of this essential cysteine as a nucleophile to form a thio-phosphate intermediate during hydrolysis is reported in the literature. Denu *et al*. (1996) observe a covalent phosphoenzyme intermediate using phosphorus ^{31}P NMR for the dual-specific vaccinia H1-related phosphatase (VHR). The trapping of the intermediate was

done by site-directed mutation of two critical catalytic residues in VHR, D92N/S131A. VHR Asp92 was previously shown to act as a general acid by protonating the leaving group phenolic oxygen (Denu *et al*., 1995), while the S131A mutation shifted the rate-limiting step from intermediate formation to intermediate hydrolysis (Denu and Dixon, 1995).

2.2.5 Aim of the proposed work

The aim of the present study is to elucidate the mechanism in the Sts-1_{PGM}-catalyzed reaction. We investigate the contribution of the ionization of the PGM domain of Sts-1 by studying the pH effects on the enzyme kinetics. By examining the pH effect on wild type and active site mutants, we demonstrate the important roles of conserved residues at the active site. We show that Glu490 plays the role of the general acid and also a role in the breakdown of the phosphoenzyme intermediate.

MATERIALS AND METHODS

2.2.1 Reagents

All of the reagents were of the purest grade commercially available. Sodium chloride, trypton, yeast extract for Lurie-Bertani (LB) medium preparation were purchased from VWR, EMD, and EM. Isopropyl-β-thiogalactopyranoside (IPTG) was from Calbiochem, and ampicillin was from Shelton scientific. Acrylamide and molecular weight maker for sodium dodecyl sulfate polyacrylamide gel electrophoresis (SDS-PAGE) analysis were from BioRad and Sigma. Sts-1_{PGM} Protein assay reagent was purchased from Pierce. *para*-nitrophenol phosphate (*p*NPP) was purchased from Sigma. Potassium phosphate (dibasic) and sodium hydroxide were from EMD and Fisher. Solutions for initial crystallization screen were from Hampton research or Sigma. Polyethylene glycol was purchased from Fluka or Sigma. Magnesium acetate, sodium tungstate and sodium orthovanadate were from Fisher, Matheson, and Alfa Aesar; Tris and Hepes were from Mallickrodt Baker and EMD, respectively.

2.2.2 Cell strains, expression vectors, and site-directed mutagenesis.

The wild type and mutants of the recombinant Sts-1_{PGM} domain (residues 369 – 638) was cloned in the pProEX-HTb vector (Life Technologies) as a N-terminally his-tagged protein and expressed in *Escherichia coli* BL21-CodonPlus (DE3) strain (Stratagene), as described previously (Kleinmen, 2006). Site-directed mutagenesis was carried out using the QuikChange XL Site-directed Mutagenesis Kit. Cells were grown in

Lurie-Bertani (LB) medium at 37ºC and induced with 0.35 mM IPTG at 18ºC and overnight.

2.2.3 Protein purification and crystallization.

The wild type and mutant proteins were purified on a Ni-NTA column (Qiagen) followed by removal of the His-tag by the action of tobacco Etch virus (rTEV) protease followed by gel filtration chromatography on a Superdex 200 column (GE Healthcare) as described in Kleinman *et al*., 2006. Initial crystals were grown at 20ºC, using the hanging drop vapor diffusion method, by mixing equal amount of 20 mg/ml Sts-1 $_{PGM}$ (in 20 mM Hepes, 150 mM NaCl, pH 7.5, and 10 mM DTT) with a solution consisting of 11-14% (w/v) polyethylene glycol 8000 (PEG 8000, Fluka), 0.2 M $MgCl_2$ or MgAc, and 0.1 M Hepes, pH 7.5. The drops were equilibrated against 1 ml reservoirs of the same solution. The crystals belong to space group C2 with unit cell dimensions of a = 116.2 Å, b = 74.3 Å, c = 100.1 Å, β = 101.5°.

2.2.4 Sts-1$_{PGM}$ Structure determination

For the Sts-1$_{PGM}$/phosphate complex, one crystal was soaked overnight in a solution containing 18% (w/v) polyethylene glycol 8000 (PEG 8000, Fluka), 0.2 M $MgCl_2$ or MgAc, 0.1 M Hepes, pH 7.5, and 200 mM Na/K phosphate and equilibrated against 1 ml reservoirs of the same solution. Data to 2.6 Å resolution were collected at beamline X26C and the structure was refined in the program REFMAC5.0. An extra density too large for a water molecule but large enough to accommodate a phosphate ion

was found in the vicinity of His-380 in each monomer (Figure 3C, peak height 7.3 σ, 6.2 σ, and 4.5 σ in chain A, B, and C respectively).

2.2.5 MALDI-TOF mass spectroscopy analysis

To investigate the phosphorylation transition event in Sts-1PGM active site, we treated wildtype and mutant H565A with 5 mM pNPP at 37ºC for 10 minutes. The reaction was stopped by the addition of 0.1 M NaOH and chilled on ice. The *p*NPP-treated sample and a *p*NPP-free sample were analyzed by MALDI-TOF (matrix-assisted laser desorption ionization/time-of-flight) mass spectroscopy. The protein was in a solution containing 20 mM Hepes, pH 7.5, 150 mM NaCl, and 5 mM BME.

2.2.6 Phosphorus NMR

Purified Sts-1_{PGM} wild type and mutants R462A, H565A and Q372V/S586Y were used to detect phosphorylated intermediate. Each sample protein (~ 1 mM) was mixed with 5 mM pNPP in a solution containing 0.15 M NaCl, 20 mM Hepes, pH 7.5 and 10% D_2O in a 5-mm NMR tube at 4ºC. 1D-^{31}P NMR spectra were measured on a Bruker Avance 700 MHz NMR spectrometer using a 5 mm TXI probe. Chemical shifts were reported in ppm relative to 5 mM inorganic H_3PO_4 buffered at pH 7.5. The spectra were obtained with 250 ms delay between pulses. The 1 min spectra were acquired in 88 scans. The chemical shifts were assigned by obtaining spectra for each separately.

2.2.7 Pull down assays

Wild type Sts-1 is able to dephosphorylate the peptide "NH_2-SVYESP-pY-SDPEE" (ANASPEC). We coupled this peptide to Affi-Gel 15 beads (Bio-Rad) in binding buffer (5 mM EDTA, 50 mM Hepes, 100 mM NaCl, 0.1 % Trition X-100, 1 mM DTT, pH 7.5) at 4ºC overnight according to the manufacturer's guidelines. The coupled peptide was used to pull down possible candidate Sts-1 mutants. The reactions were initiated by mixing peptide-bound Affi-gel with proteins in binding buffer and incubated at room temperature for 30 minutes. The Affi-gel was then washed with binding buffer at least three times to remove unbound proteins. The binding results were visualized by SDS-PAGE.

2.2.8 Phosphatase assay

Activity of the wild type and mutants of the Sts-1_{PGM} domain was measured using para-nitrophenol phosphate (*p*NPP) (Sigma) as a substrate. The reaction mixture was prepared with diluent containing 100 mM TAB (25 mM Tris, 50 mM acetic acid, 25 mM bis-Tris), 150 mM NaCl, 0.1 mM EDTA, and 1 mM dithiothreitol (DTT). The TAB buffer used maintains a constant ionic strength of 0.1 M through out the entire pH range used in this study (Ellis and Morrison, 1982; Denu *et al.*, 1995). The reaction was initiated by adding the protein at the indicated concentrations to the reaction mixture, which was pre-incubated at 37ºC. The reaction was stopped by adding 13% K_2HPO_4 or 0.5 M NaOH and chilled on ice. The amount of para-nitrophenol (*p*NP) converted from *p*NPP was quantified by measurement at 405 nm and carried out using the following relationship:

$OD_{405} = a \cdot b \cdot c$ ($a = 1.78 \times 10^4\ M^{-1} \cdot cm^{-1}$; b = light path (cm); c = [*p*NP])

Formation of *p*NP was measured at various substrate concentrations. Initial velocity (*v*) of the *p*NP formation was determined over the linear range function of time. To determine the kinetic parameters k_{cat} and K_m, the initial velocities were measured at various substrate concentrations (S) and the data were fitted to equation 1 using the program SigmaPlot 5.05 (SPSS Science Inc., Chicago).

$$v = \frac{k_{cat} \bullet S}{(S + K_m)} \qquad [1]$$

2.2.9 Inhibition test

Inhibition of $Sts\text{-}1_{PGM}$ phosphatase activity by tungstate, phosphate, and vanadate were determined as follow. Boiling sodium orthovanadate till its color turned clear was required to activate vanadate. The reaction mixture containing sodium tungstate/sodium potassium phosphate/sodium orthovanadate was pre-incubated before adding the protein. At various fixed concentrations of inhibitors (0, 0.1, 0.5, 1, 2.5, and 5 mM), the initial rate at 1 mM *p*NPP was measured as described for phosphatase assay. The data were fit to the equation 2 to obtain the inhibition constant.

$$\nu = V_{max} / (1 + K_i\,[I]) \qquad [2]$$

RESULTS

2.3.1 Phosphatase activity of Sts-1_{PGM}

In eukaryotes, protein phosphorylation and dephosphorylation are among the most important regulatory events in cells. The relative rate of tyrosine phosphorylation compared with phosphotyrosine dephosphorylation is an important regulatory mechanism in the growth control of normal and transformed cells (Lin and Clinton, 1986). Members of the phosphoglycerate mutase (PGM) families play critical roles as regulators in many signaling pathways. The amino acid sequence Arg-His-Gly-Glu, "RHGE", has been identified as a signature pattern that correlates with membership in the PGM family, while the related sequence Arg-His-Gly/Asn ("RHG/N") correlates with membership in the family of acid phosphatase (AcP) (Bazan *et al*., 1989). The presence of the amino acid sequence "R-H-G-E" within the C-terminal domain of Sts-1 and Sts-2 suggests that this region is related to PGM/AcP enzymes. To investigate this possibility, we tested whether the Sts proteins had enzymatic activity. Sts-1_{PGM} (residues Gly369 – Glu638) was expressed in *E. coli*, purified to homogeneity, and tested for the ability to hydrolyze the phosphatase substrate, *p*NPP. The time course of Sts-1_{PGM} and other phosphatases (25 nM)-catalyzed *p*NPP hydrolysis is illustrated in figure 3. The activity of Sts-1_{PGM} reaches to steady state after ~ 2,000 seconds. PTP1B (purified protein provided by Dr. Carpino) was used as a control since it has been heavily studied using *p*NPP as substrate. EPPase is recently identified from the silkworm *B. mori* that shares sequence homology with Sts proteins. In figure 4, a saturation curve for an Sts-1-catalyzed reaction shows the relation between the concentration of substrate, *p*NPP and hydrolysis rate. These results show that

recombinant Sts-1_{PGM} is able to dephosphorylate *p*NPP with kinetics that resemble a Michaelis-Menten enzyme-catalyzed reaction, suggesting that Sts-1_{PGM} has an intrinsic phosphatase activity. As shown in figure 3, the Sts-1 phosphatase activity is comparable to, if not better than that of PTP-1B. In addition, Sts-1 was shown to hydrolyze a pTyr containing peptide, but not the peptides containing pSer or pThr (Mikhailik *et al*., 2007)

2.3.2 Structure of Sts-1 PGM domain in complex with phosphate

The wild-type structure of Sts-1_{PGM} monomer was previously determined in our lab (Mikhailik *et al*., 2007) and revealed a structure similar to that adapted by all members of the PGM superfamily (Jedrzejas, 2000). The Sts-1 C-terminus folds into an α/β type structure that consists of a central seven-stranded β sheet flanked by eight α helices (α1 to α8) on both sides, with a C-terminal β strand extending outside the protein core that strongly interacts with neighboring molecules (see figure 6 on page 19). All β-strands are parallel, with the exception of β6. The ^{379}RHGE^{382} signature pattern is located at the carboxyl end of the central β sheet structure, and the two arginines and two histidines of Sts-1 that are homologous to PGM/AcP catalytic residues extend into a semi-barrel-shaped depression (17 Å in length by 8 Å in diameter) present at this location on the surface of Sts-1_{PGM}. Based on overall structural homology to PGM/AcP enzymes, this cavity is likely to be the Sts-1_{PGM} catalytic pocket.

The structural similarity between Sts-1_{PGM} and ecPGM at the active site residues within the catalytic pocket has been previously described (Mikhailik *et al*., 2007). In ecPGM, His10 has been identified as the nucleophile during the ecPGM-catalyzed reaction, and four other residues (Arg9, Arg61, Glu88 and His183) are all thought to help

stabilize the negatively charged phosphate that is being hydrolyzed (Bond *et al*., 2001). The proximate residues within Sts-1 (Arg379, His380, Arg462, Glu490, and His565) adopt an identical configuration (Figure 5), suggesting that they are involved in the dephosphorylation reaction. To ascertain whether the shallow cavity surrounding these residues is the active site of Sts-1_{PGM}, I soaked the Sts-1_{PGM} crystal in a buffer containing 200 mM buffer and determined the structure of the complex at 2.6 Å resolution (Table 1). A clear density in which a phosphate molecule was built was evident in the difference Fourier electron density map. As shown in figure 6, the side chains of Arg379, His380, Arg462, Glu490, His565, and the main amino group of Ala566 all stabilize the phosphate moiety. The phosphate molecule replaces three water molecules that were found close to His380 in the phosphate-free structure (Figure 7) without disturbing the overall structure of the cavity. In addition, there is no phosphate molecules bound to the protein at any site other than this cavity. Thus, this solvent-exposed cavity can stabilize a phosphate group and is likely to be the active site of Sts-1_{PGM}.

2.3.3 Proposed catalytic mechanism

Based on the sequence and structural homology between Sts-1 and ecPGM, we propose two mechanisms for the phosphatase activity of Sts-1. Fig 8 illustrates a mechanism involving reversible binding of substrate (k_1 and k_2), formation of intermediate (k_3), and intermediate hydrolysis (k_5) (Denu and Dixon, 1995). The k_{cat}/K_m parameter provides information on substrate binding (k_1 and k_2) and intermediate formation (k_3), whereas k_{cat} provides information on the formation (k_3) and breakdown of the intermediate (k_5). The crystal structure of Sts-1_{PGM} suggests that upon binding of a

phosphorylated substrate, the phosphate is stabilized by hydrogen bonds made with Arg379, Arg383, Arg462, Glu490, and His565 in the active site. It has been reported that phosphatases of the PGM/AcP family contain a conserved histidine residue that is required as a nucleophile for activity (Jedrzejas 2000). We have argued that His380 in Sts-1 is deprotonated due to its interaction with the Arg379 carbonyl main chain and serves an important role for nucleophilic attack on the phosphate leading to a transient phospho-His380 intermediate (Figure 7, Mikhailik *et al*., 2007).

We propose two alternative mechanisms for the release of substrate. In the first mechanism (Figure 9A), His565 is the general acid. After the oxygen linked between phosphate and substrate is cleaved, His565 activates a water molecule to hydrolyze phospho-His380. Once the phosphate is released, the active site is available for the next substrate. The second mechanism is similar, except the general acid residue that is responsible for hydrolyzing the intermediate is Glu490 (Figure 9B). Other conserved active site residues, Arg379, Arg383, and Arg462, are unlikely to act as general acid/base, because their high pKa values do not allow them to be protonated with a pH range below 9. Their role is to stabilize the structure of the transient state.

2.3.4 Capture of enzyme-phosphate intermediate state

I. MALDI-TOF experiment.

To investigate whether the hydrolysis of substrate goes through a transient phospho-His380 intermediate, as described in figure 9 (A or B), we proposed that mutating His565 to Ala should slow down the release of phosphate from phospho-His380. To test this hypothesis, we used the MALDI-TOF to monitor the mass change of

H565A incubated with and without 5 mM *p*NPP at 37ºC for 10 minutes. Figure 10 shows that when compared to untreated H565A protein (peak at 30,585 Da), the *p*NPP incubated protein shows a second species with molecular weight of 30,661 Da, which corresponds to, within the precision of mass spectroscopy, the molecular weight of one attached phosphate group (76 Da). This result is consistent with the fact that the hydrolysis reaction goes through a phosphorylated intermediate that was stabilized by the H565A mutant. The MALDI-TOF data does not show where the phosphate is covalently attached and further investigations are needed to answer this question.

II. ^{31}P NMR detection of the phospho-Sts-1$_{PGM}$ intermediate.

To gain more insight into the formation of the phospho-intermediate, we used ^{31}P solution NMR to track the phosphatase reaction. ^{31}P NMR is another powerful tool to detect the formation of the phosphoenzyme intermediate during turnover. This technique was used in the study of the dual-specific vaccinia H1-related phosphatase (VHR). In this phosphatase, changing the conserved Ser131 to alanine in the active site (HCXXGXXRS) shifted the rate-limiting step from intermediate formation to intermediate hydrolysis. The covalent thiol-phosphate intermediate was observed using phosphorous ^{31}P NMR (Denu *et al*., 1996). To detect the transient phospho-histidine intermediate by ^{31}P NMR, 1 mM Sts-1$_{PGM}$ wild type or mutant H565A was rapidly mixed with 5 mM *p*NPP in a 5 mm NMR tube. The entire reaction was followed by monitoring the resonance of the conversion of the substrate, *p*NPP (- 2 ppm), to the product free phosphate (0 ppm), and the appearance of an intermediate. At 4°C, *p*NPP was fully hydrolyzed by wild-type Sts-1$_{PGM}$ right after mixing and before we were able to collect any spectra. In contrast, no signals other than *p*NPP were detected from the sample containing H565A and the

intensity of *p*NPP remained stable at 4°C for up to 60 minutes, we therefore increased the temperature to 37°C. At this temperature, *p*NPP was slowly hydrolyzed and a signal appeared at 0.6 ppm (Figure 11). The intensity of this signal increases while the intensity of the *p*NPP peak decreases demonstrating the hydrolysis of *p*NPP. Interestingly, the peak at 0.6 ppm (t = t1: ~ 10 minutes after the mixing of *p*NPP) shifts during the hydrolysis of *p*NPP to 0.3 ppm (t = 60': *p*NPP is all hydrolyzed at 60 minutes). No signal corresponding to free phosphate (0 ppm) was detected. We interpreted the data with the possible existence of five phosphate-species. These are free *p*NPP, *p*NPP bound to the protein, phosphate covalently bound to the protein, phosphate non-covalently bound to the protein, and free phosphate. The signal of "free *p*NPP" should appear nearby the signal of "*p*NPP bound to the protein", which is not seen during the whole experiment. Therefore the species of "*p*NPP bound to the protein" is negligible. At the end of the experiment (t = 60'), the signal at 0.3 ppm reached an intensity similar to that of *p*NPP at t = t1, suggesting that all 5 mM *p*NPP was hydrolyzed by H565A mutant indicating that this peak is that of free phosphate in the presence of Sts-1_{PGM} H565A. The final chemical shift of this signal is different from the default signal of inorganic phosphate (0 ppm). This might be caused by the high viscosity of the sample mixture due to high protein concentration changes the chemical shift of the free phosphate. Presumably, the small peak (0.6 ppm) at t = t1 is that of "the phosphate covalently bound to the protein" or that of the phospho-intermediate. The intensity of this peak should not be higher than 1 mM (the concentration of H565A mutant used) since the K_m of H565A mutant is ~ 1.5 mM. The phosphate must be released and accumulation of the free phosphate leads to an increase in the signal that eventually emerges with the small peak (0.6 ppm) of "the

phosphate bound to the protein". This interpretation explains the cause of the shift. An experiment of H565A mixed with inorganic phosphate is required to answer this question.

2.3.5 The pH-dependence of the phosphatase activity of Sts-1

It is a common feature in enzyme catalysis that one or more active site residue(s) functions as a general acid or base. To establish the existence of acid/base catalysis of Sts-1_{PGM} phosphatase activity, we measured the phosphatase activity using *p*NPP as the substrate at various pHs. This technique has been successfully used to investigate the basis for phosphatase activity of *Yersinia* PTP and VHR (Zhang *et al*., 1994; Denu and Dixon, 1995; for a review see Fersht, 1985). For each pH value, a linear rate of product formation was measured for six or more *p*NPP concentrations and fitted to a Michaelis-Menten equation to obtain the rate constants K_m and k_{cat}. The profile of k_{cat}/K_m versus the pH should reflect the presence of general acids and bases (Denu *et al*., 1995). To ensure that the enzyme was saturated, we used a *p*NPP concentration as high as 20 mM. The velocity measured at high *p*NPP concentrations reached a steady state within a short time (usually less than a minute). For these high *p*NPP concentrations, I ensured that I had at least three data points in the first minute to determine the initial velocity. Since this is lower than what I usually use to determine the initial velocity, the measurement error for these data points is probably higher than for the lower *p*NPP concentrations. The plot of K_m versus the pH is shown in figure 12. Increase in the pH results in an increase in the K_m for pH values higher than 6.5, indicating that the binding of *p*NPP to Sts-1_{PGM} is less favorable at high pHs. The plot of the turnover number, k_{cat}, against the pH displays a bell

curve and the limb in the basic pH range (pH 8.0 – 9.0) descends linearly with a slope of – 0.42. The k_{cat} plot suggests that the maximal rate is around pH 7.0 (Figure 13).

2.3.6 Enzyme kinetics analysis – identification of critical ionized groups

The profile of the log k_{cat}/K_m against the pH reflects the critical ionizations for Sts-1-catalyzed *p*NPP hydrolysis. The plot displays a plateau at pH 4.5 – 5.75, and descends linearly after that with a slope of –0.7 (close to –1), indicating that at least one ionizable group must be protonated for activity (Figure 14). Because of the difficulty in obtaining kinetic data at a pH lower than 4.5 (protein starts to precipitate), we cannot rule out the existence of a group with a pKa lower than 4.5.

To identify the amino acid(s) responsible for the pH dependency in the k_{cat}/K_m profile, we mutated several conserved residues in Sts-1. Each residue was altered to alanine and glutamate 490 was also mutated to glutamine in order to minimize potential structural alterations. The kinetic parameters for the wild type and mutants H380A, R462A, E490A, E490Q, and H565A were determined at pH 7.5 (Table 2). Among all the signature residues in the active site of the Sts-1 PGM domain, Glu490 is the only acidic residue. All the mutants yielded k_{cat} values between 0.02 and 0.4 s^{-1} and the k_{cat}/Km values ranged from 0.6 to 790 $M^{-1}s^{-1}$. E490A exhibited a 35-fold reduction in k_{cat} (1.9 s^{-1}) and a 14-fold decrease in k_{cat}/K_m value (96.5×10^2 $M^{-1}\cdot s^{-1}$). Interestingly, the E490Q mutant has a 7-fold decrease of k_{cat} (10.32 s^{-1}) and a 7-fold decrease in the K_m so that its k_{cat}/K_m value remains similar to that of the wild type Sts-1_{PGM}. R462A and H565A mutations significantly decrease the rate of activity. Their k_{cat}/K_m values (0.6×10^1 $M^{-1}\cdot s^{-1}$ and 0.2×10^2 $M^{-1}\cdot s^{-1}$) are decreased 20,000-fold and 6,000-fold respectively when

compared to wild type. The mutation of the nucleophile, His380, also shows a 200-fold decrease in k_{cat}/K_m values.

2.3.7 Analysis of the conserved residue, histidine 565 and glutamate 490

Whether protonation or deprotonation of an active site residue is required for the reaction, a mutation to Ala, or a corresponding amide, would significantly perturb the catalytic rate constants when plotted function of the pH. We established the pH profile of the k_{cat}/K_m values of H380A, E490A, E490Q, and H565A mutants to identify the group that is responsible for the ionization observed in wild type Sts-1. The profile of the k_{cat}/K_m versus pH for the H565A mutant is identical to that of wild type protein, except that the H565A mutant has a 6,000-fold drop in activity at all pH values (Figure 14). Both curves retain a plateau at acidic pHs and descend linearly; the slope of the wild type is close to –1 while the slope of H565A mutant is –0.4, indicating that one group is protonated in both wild type and H565A for activity.

Unlike other mutants that have a limb descending at basic pHs, the k_{cat}/K_m profile of both E490A and E490Q displays a dramatic difference from the k_{cat}/K_m pH profile for the wild type Sts-1. Both E490A and E490Q show a pH-independent k_{cat}/K_m. This piece of data strongly suggests that Glu490 is the general acid (see figure 9B). In addition, the pH profile of k_{cat} of E490Q (Figure 15) is flat throughout the pH range 5.5 to 9.0 (E490Q precipitates at pHs lower than 5.0). Since the k_{cat} value reflects the second half of the reaction illustrated in figure 8, it is likely that Glu490 is also involved in the breakdown of the phosphorylated intermediate. Taken together, our proposed mechanism in figure 9B is more likely to describe the phosphatase mechanism of Sts-1.

2.3.8 Inhibition of Sts-1_{PGM} phosphatase activity

It has been reported that tetrahedral tungstate is a competitive inhibitor of tyrosine phosphatase and is isosteric with the substrate and product of the catalyzed reaction (Fauman *et al*., 1996). Phosphate and PO_3-like moieties (i.e. tungstate, nitrate, tartrate, and vanadate) are commonly used to study the interactions between phosphatases and phosphorylated ligands. We checked the inhibition ability of phosphate, nitrate, tungstate, and vanadate on Sts-1_{PGM} for *p*NPP hydrolysis. The assays were carried out by incubating the enzyme with a fixed concentration of *p*NPP (1 mM) in the presence of various concentrations of phosphate or phosphate-like moieties. The phosphatase activity of Sts-1_{PGM} decreases by 50% in the presence of 0.08 mM of WO_4^{2-}, which is about 132 times more effective than PO_4^{3-} (10.56 mM at pH 7.5) (Figure 16). Sts-1_{PGM} is also weakly inhibited by vanadate (1 mM), but not inhibited by nitrate or tartrate with concentrations as high as 200 mM. Besides phosphate-like moieties, we also tested several *p*NPP analogs (4-nitrophenyl sulfate, p-nitrocatechol sulfate, benzylphosphonic acid, b-naphthyl sulfate and disodium pyrophosphate) for their ability to inhibit Sts-1_{PGM}. Only 4-nitrophenyl sulfate and p-nitrocatechol sulfate showed weak inhibition on Sts-1_{PGM}, the rest of the *p*NPP analogs (concentration as high as up to 10 mM) showed no detectable effect on Sts-1_{PGM} activity (Table 3).

2.3.9 Binding of Sts-1_{PGM} H565A to a tyrosyl-phosphorylated peptide

Given that Sts-1_{PGM} was able to dephosphorylate peptides containing pTyr, but not pSer and pThr (Mikhailik *et al*., 2007), we investigated whether any Sts-1_{PGM} mutants can bind to a pTyr-peptide. This assay should determine which mutant to use to

determine the crystal structure of the Sts-1_{PGM}/peptide complex. I coupled a synthesized Zap70-like peptide containing phosphorylated tyrosine (SVYESP-pY-SDPEE) to Affi-Gel 15 (Bio-Rad) according to the manufacture's protocol. The beads with covalently bound pTyr-peptide were incubated with the Sts-1_{PGM} mutants (R462A, E490A and H565A) at room temperature for 30 minutes. Sts-1_{PGM} wild type served as the negative control since it dephosphorylates the substrate with a rate too high to detect binding. The binding result was analyzed by SDS-PAGE. Except for the H565A mutant, wild type and other Sts-1_{PGM} mutants (R462A and E490A) show no detectable binding to the peptide (Figure 17). Because there is no positive control for this assay or a way to quantify the amount of peptide on the beads, this is only a qualitative assay. More detail tests are required to quantify the binding between H565A mutant and pTyr-peptide. Previously, the observation from NMR data suggests that H565A slows the rate-limiting step of the breakdown of the phospho-intermediate. In this pull down assay, H565A mutation seems to slow down the cleavage of peptide, suggesting that the binding of pTyr-peptide to the H565A mutant is different from the binding between *p*NPP and the H565A mutant. Moreover, the fact that H565A was the only mutant that shows binding to pTyr-peptide, it can be used as a bait to pull down its *in vivo* substrate(s) in the future research.

DISCUSSION

Several studies have suggested that members of the PTP family of enzymes employ similar catalytic mechanisms to hydrolyze their phosphorylated substrates. Using mutational approaches, the catalytic roles of the active site residues have been demonstrated. The critical feature of these phosphatases is that they utilize a nucleophilic residue to form a phospho-intermediate. For example, PTP-1B, VHR and Cdc25 utilize a cysteine as a nucleophile so that the reaction mechanism goes through a transient phosphorylated cysteine (Zhou *et al*., 1994; Denu *et al*., 1996; Pannifer *et al*., 1998; McCain *et al*., 2002). In addition to the nucleophilic residue, the catalytic mechanism usually utilizes a general acid that activates a water molecule to hydrolyze the phospho-intermediate. For example, Asp356 in the *Yersinia* PTP, Asp92 in VHR and Asp129 in the bovine liver low molecular weight acid phosphatase were shown to serve as general acids in the catalytic mechanism (Zhang *et al*., 1994; Denu *et al*., 1995; Taddei *et al*., 1994). However, little experimental data is available to characterize the general acid and base shared by members of the PGM family of proteins.

In this work, we determined the crystal structure of Sts-1_{PGM} in complex with phosphate and revealed that the conserved residues that are important for the activity of PGM proteins. The phosphate ion is in the cavity at the carboxyl end of the β-sheet that we predicted to be the active site. We have observed a transient phospho-intermediate in MALDI-TOF and ^{31}P NMR experiments with the Sts-1_{PGM} H565A mutant. Because these experiments do not directly show that the conserved nucleophile His380 is phosphorylated, more experiments are required to show which residue is phosphorylated

during hydrolysis. However, based on the sequence homology with ecPGM, which was found to be phosphorylated at His12 (the equivalent of His380 in Sts-1) (Bond *et al*., 2001), it is very likely that His380 is phosphorylated during hydrolysis.

To identify the catalytic roles of the active site residues, we investigated the pH effect on two kinetic parameters, k_{cat} and k_{cat}/K_m to characterize the reaction mechanism. The pH profile of k_{cat} values for Sts-1_{PGM} suggests that one group is ionized in the turnover of the enzyme-substrate complex (see figure 8). In addition, the pH profile of the k_{cat}/K_m values of Sts-1_{PGM} wild type indicates that at least one group is protonated during the formation of the enzyme-substrate complex. Compared to the wild type, the activity of H565A is 10,000-times decreased in k_{cat}/K_m, and > 100-fold decreased in k_{cat}, indicating that His565 is important for stabilization of the substrate. Another conserved residue, Arg462, also shows a significant decrease on both k_{cat} and K_m parameters (> 300- and 6-fold, respectively), suggesting that it plays an important role in stabilizing the substrate.

Unlike the mutants H380A, R462A and H565A that had a large effect on kinetic parameters, the E490A and E490Q mutants exhibited less than a 30-fold decrease in k_{cat} when compared to wild type. Most importantly, the pH profile of the k_{cat}/K_m values of E490A and E490Q displays a loss in pH dependency. This is strong evidence that Glu490 must be protonated and act as the general acid to donate a proton to release the substrate. This step leads to the formation of a covalent phospho-intermediate. The deprotonated Glu490 then can substrate a hydrogen from a water molecule which will attack and remove the phosphorus atoms from the active site. This observation indicates that the mechanism we proposed in figure 9B describes accurately to the real catalytic reaction.

The mechanism in figure 9B is similar to that has been reported in literature based on the k_{cat}/K_m pH profile for *Yersinia* PTPase, human VHR, and low-molecular weight acid phosphatase in the enzyme-catalyzed hydrolysis of *p*NPP (Zhang *et al*., 1994; Denu and Dixon, 1995; Taddei *et al*., 1994). These proteins all hydrolyze substrates utilizing an aspartic acid and the reaction goes through a phospho-intermediate. Moreover, many enzymes use an aspartic acid or a glutamic acid as proton donor, and function optimally at around pH 7 (Nielsen and McCammon, 2003). Interestingly, Sts-1 and the proteins of the PTP family share either no sequence homology, but appear to employ an aspartic acid or glutamic acid as a general acid independently of the nature of the phosphorylated residue.

Our data are consistent with Sts-1 being a PTP and a member of the PGM family. Yet when we tested the inhibition with known PGM-inhibitors (e.g. ammonium arsenate, phosphate, selenate, tungstate and vanadate) for Sts-1 $_{PGM}$, it was strongly inhibited by tungstate but not other phosphate-like moieties, indicating that the substrate recognition in the Sts-1_{PGM} active site is different from that in members of the PGM family. Besides, the potent inhibitor ([1,1-difluoro-1-(2-naphthalenyl)-methyl] phosphonic acid (6)) for PTP1B did not show any inhibition on Sts-1_{PGM}, suggesting that the substrate selectivity in Sts-1_{PGM} is different from that in the PTP family. These inhibition data provoke a possibility that Sts proteins can be classified as a new family in the category of the phosphatase superfamily.

Figure 1. Domain structures of protein tyrosine phosphatases. All members form both nontransmembrane PTP subtypes and receptor-like PTP subtypes bear at least one conserved PTP domain that carries phosphatase activity. (Figure taken from Anderson *et al*., 2001)

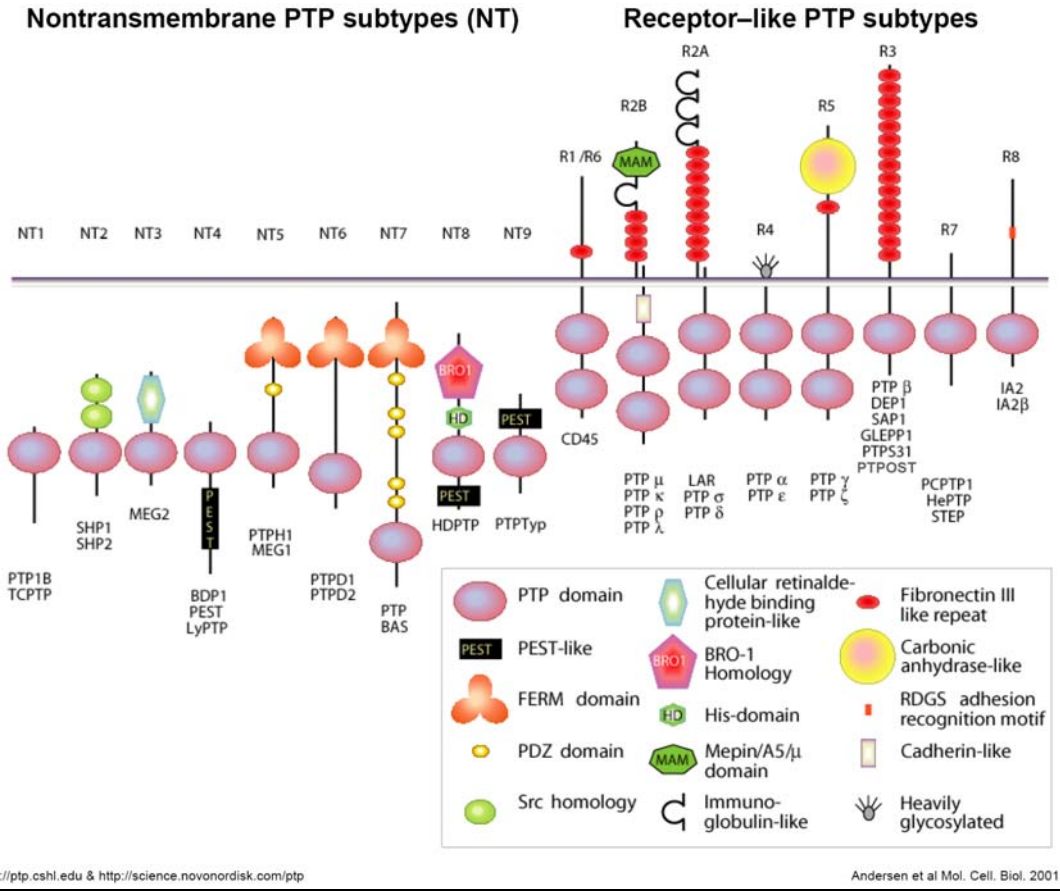

Figure 2. The active site of the PTP1B Q262A-cysteinyl-phosphate intermediate (Pannifer *et al*., 1998). Gln262 is an important residue that can activate water molecules to hydrolyze phospho-intermediate. Cys215 is the nucleophilic group that is transiently phosphorylated during hydrolysis of pTyr. Structure generated with the program PyMol. Protein data bank ID: 1A5Y.

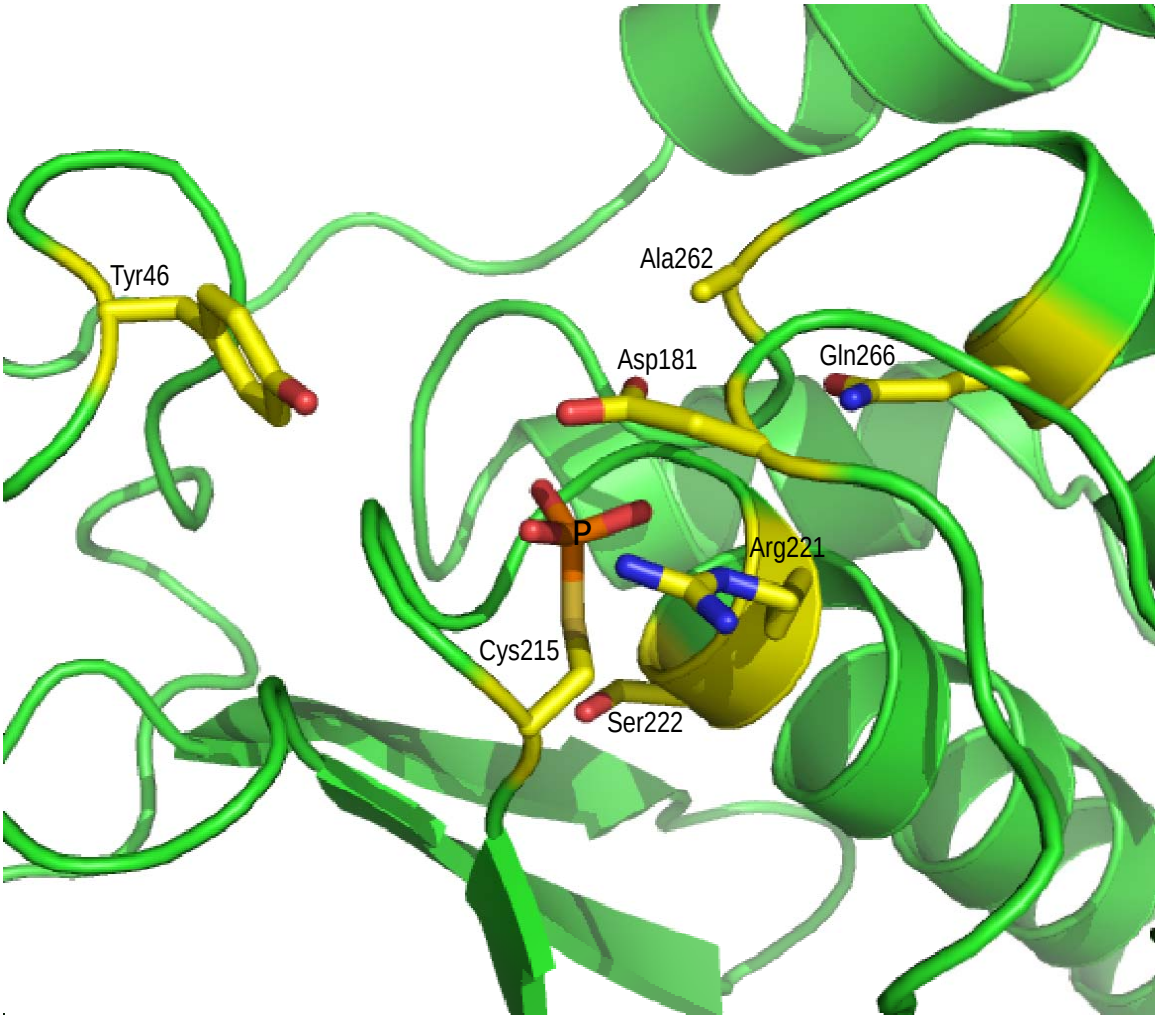

Figure 3. Phosphatase activity of Sts-1_{PGM} and other phosphatases. Each data set was obtained from experiments performed under the same condition (pH 7.5), 25 nM of protein and 1 mM *p*NPP incubated at 37ºC. The formation of the hydrolysis product, *p*NP was measured at 405 nm.

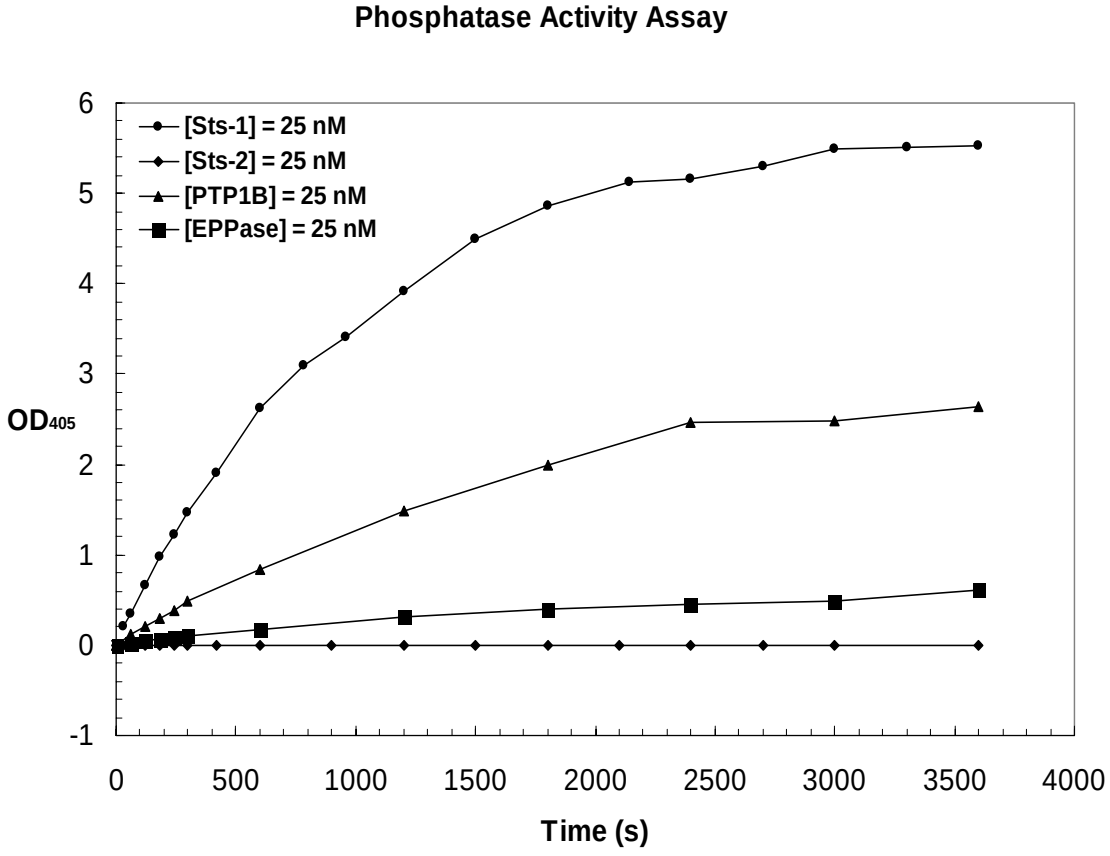

Figure 4. Saturation curve of Sts-1-catalyzed pNPP hydrolysis. The data were determined with 25 nM of Sts-1 at pH 7.0. The data were fitted to eq [1] to generate the curve.

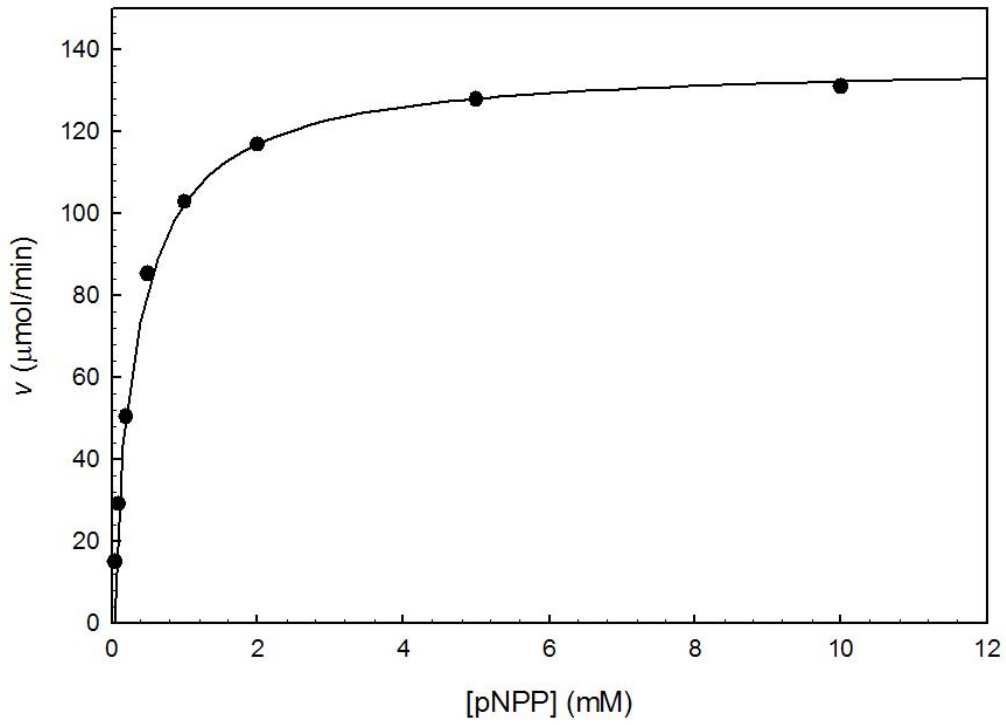

Figure 5. Active site residues. Superposition of the known active site residues of ecPGM (cyan) with the homologous residues of Sts-1_{PGM}.

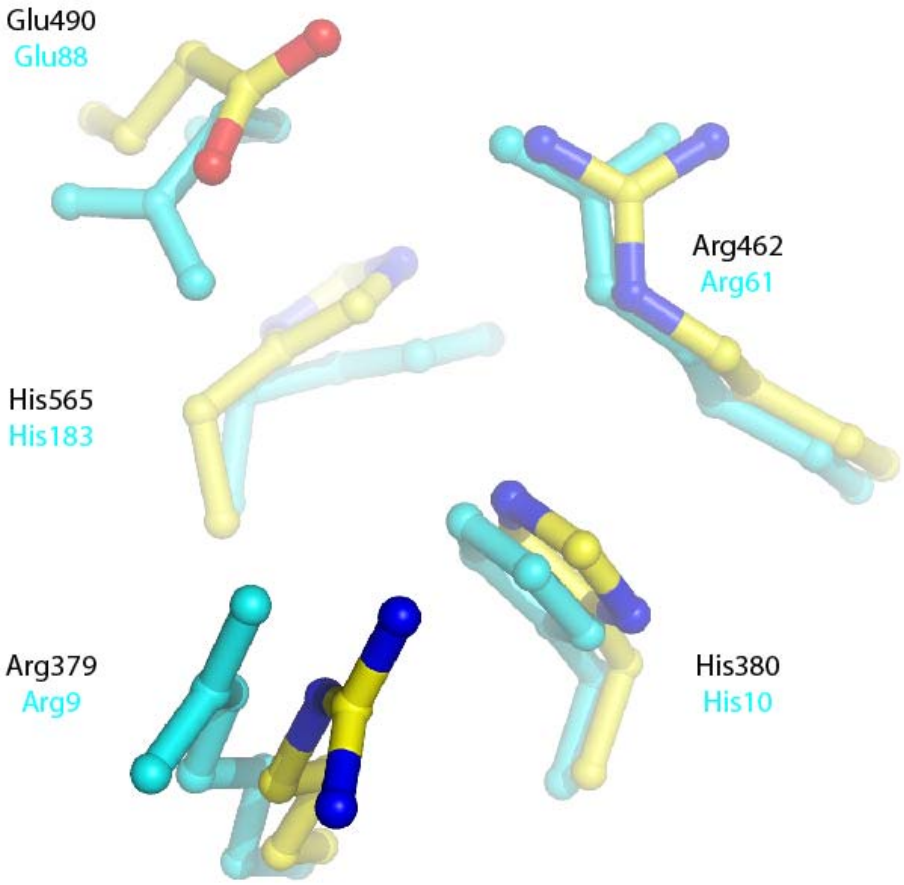

Figure 6. Interactions made by Sts-1_{PGM} active site residues with a phosphate ion. The Sts-1_{PGM} active site residues interacting with the phosphate molecules are shown in ball-and-stick representation. Dotted lines represent hydrogen bond interactions. Secondary structure elements are displayed in green.

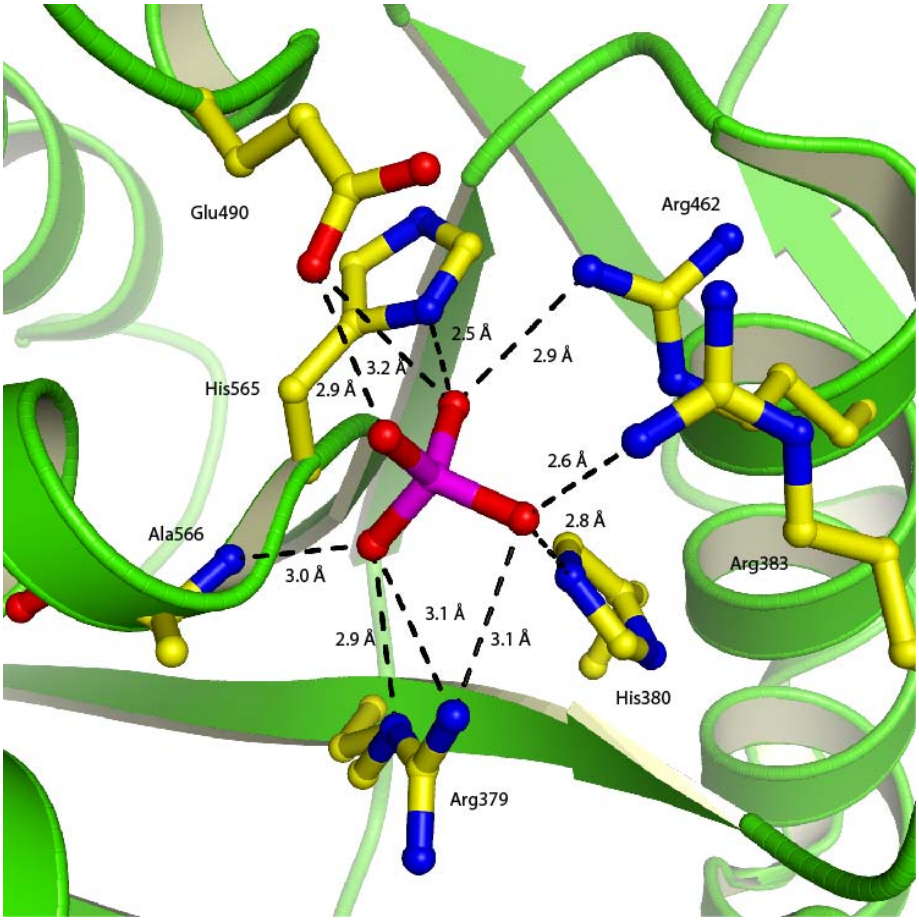

Figure 7. Residues lining the active site. As described in the text, the Sts-1PGM site has the shape of an open semi-barrel, 17 Å in length and 8 Å in diameter. A portion of the barrel is lined extensively with positive charge contributed by basic residues Arg-379, Arg-383, Lys-390, Lys-426, Arg-462, and Arg-592. However, an array of hydrophobic residues (Phe-489, Trp-494, Val-390, Lys-426, Pro-501, and Trp-503) and two acidic residues Asp-427 and Glu-490 complete the wall of the active site. The presence of eight basic residues and only two acidic residues gives the active site in Sts-1_{PGM} a strong positive potential that is consistent with the stabilization of negative charges such as those of a phosphate group.

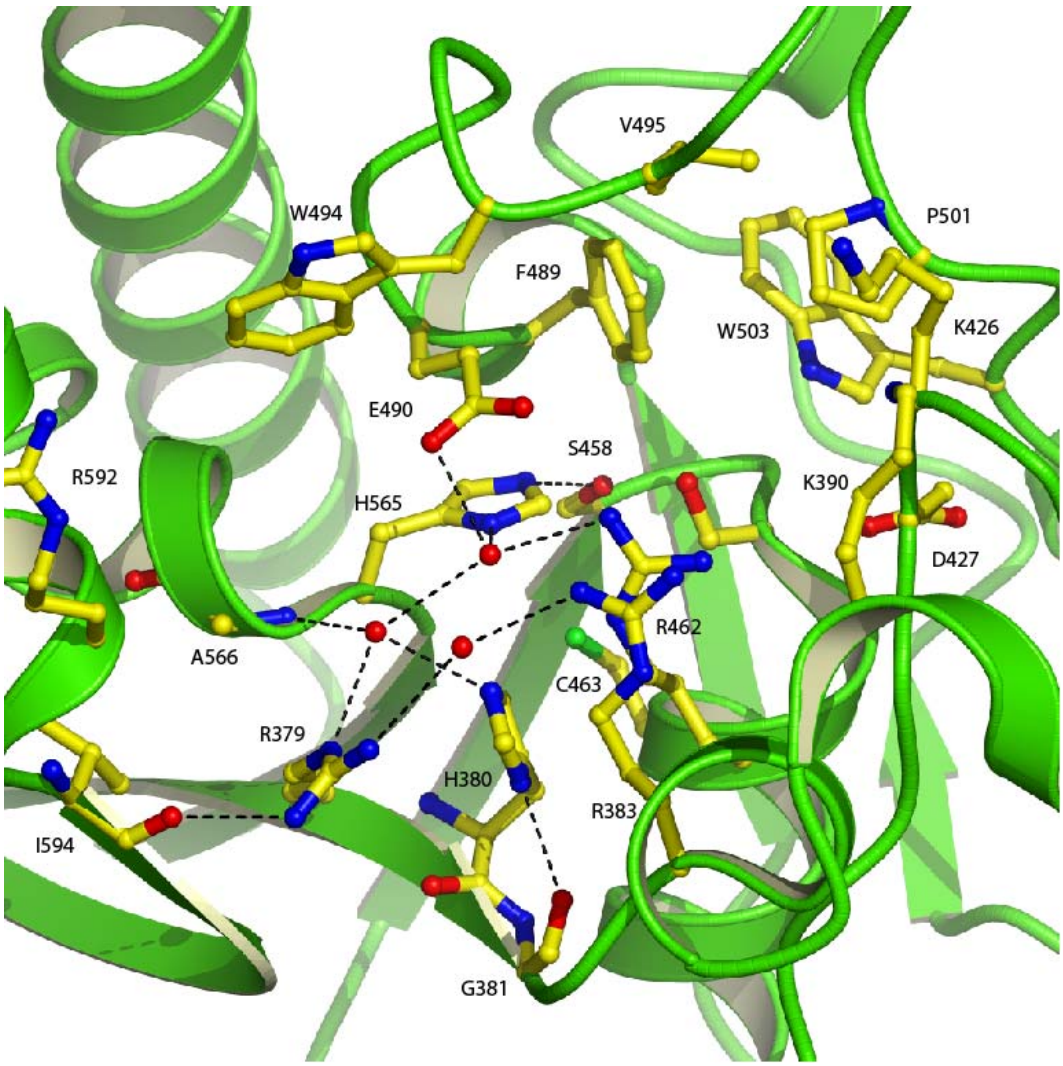

Figure 8. Kinetic mechanism for Sts-1. k_1 is the constant of the formation of enzyme-substrate (ES). k_2 and k_3 are the dissociation constants of the ES complex. k_5 is the hydrolysis rate of the phosph-enzyme intermediate (E--P) to free enzyme (E) and phosphate (P).

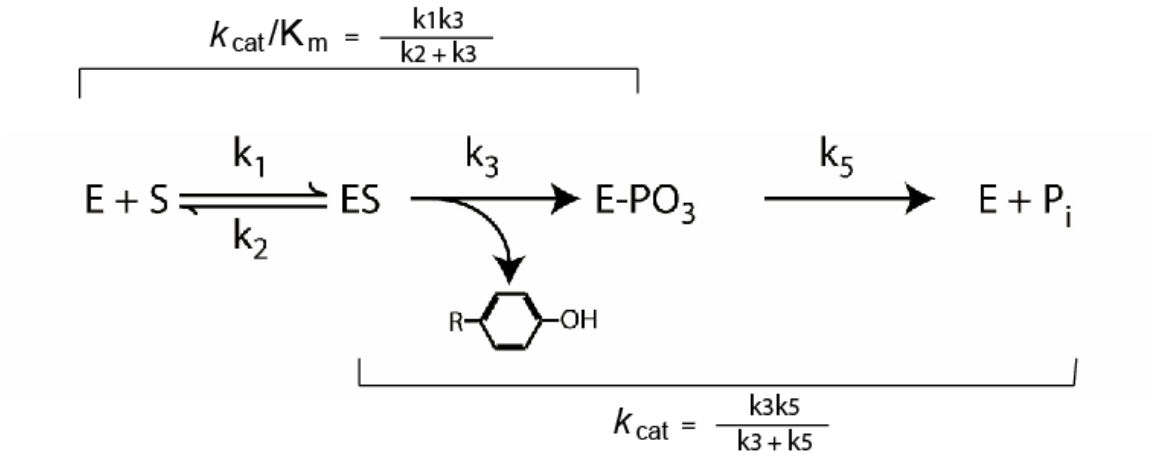

Figure 9. Proposed catalytic mechanism A of Sts-1_{PGM}. The reaction is initiated (from top-left, clockwise) by binding of phospho-tyrosine (in red) in the active site of Sts-1_{PGM}. The conserved residues Arg379, Arg462, Glu490, and His565 play an important role in stabilizing the bound substrate. As it is shown in this figure, His565 is the general acid to cleave the bound substrate at the oxygen link.

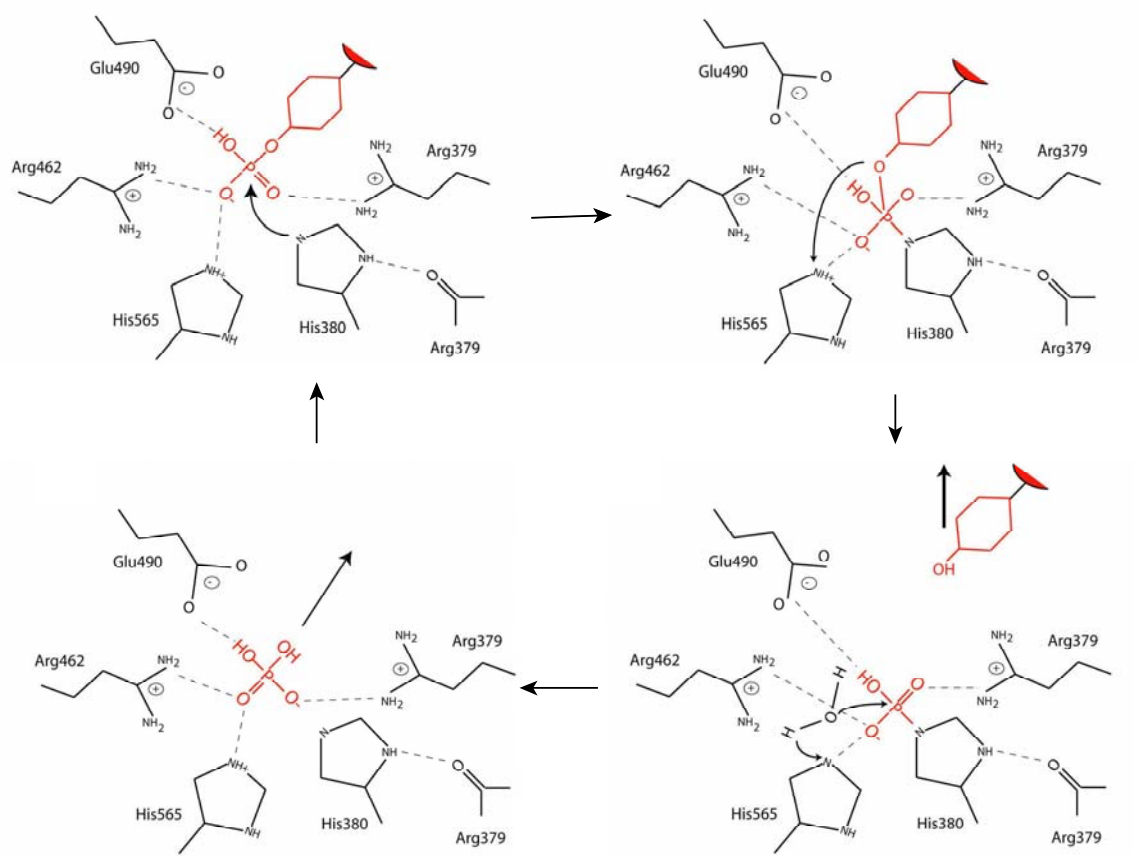

Figure 9 (Continued). Proposed catalytic mechanism B of Sts-1_{PGM}. The reaction steps are similar to that described for mechanism A, except Glu490 is the general acid to cleave the bound substrate at the oxygen link.

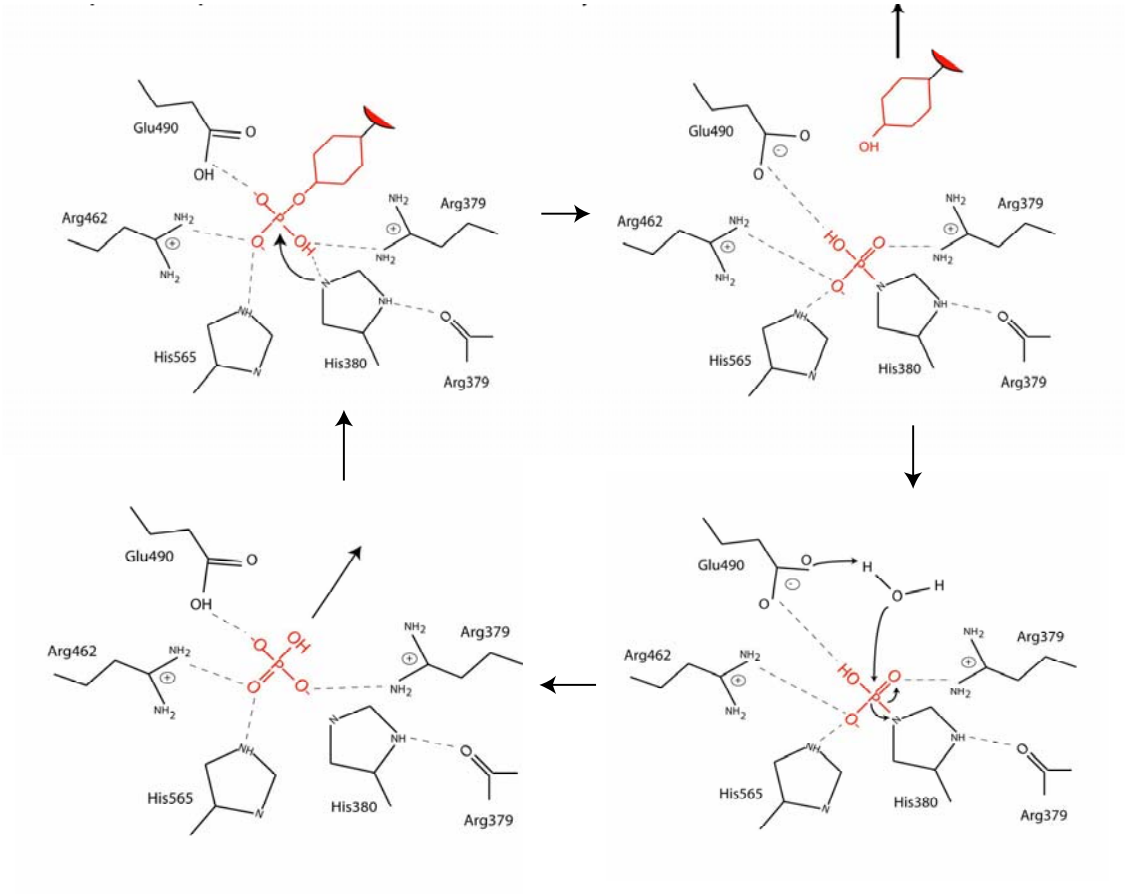

Figure 10. MALDI-TOF result of Sts-1_{PGM} H565A treated with *p*NPP. Two species were obtained from the MALDI-TOF result. The first peak corresponds to the mass of Sts-1_{PGM} H565A (30,585 Da) and the second peak corresponds to the mass of phosphorylated Sts-1_{PGM} H565A intermediate (30,661 Da).

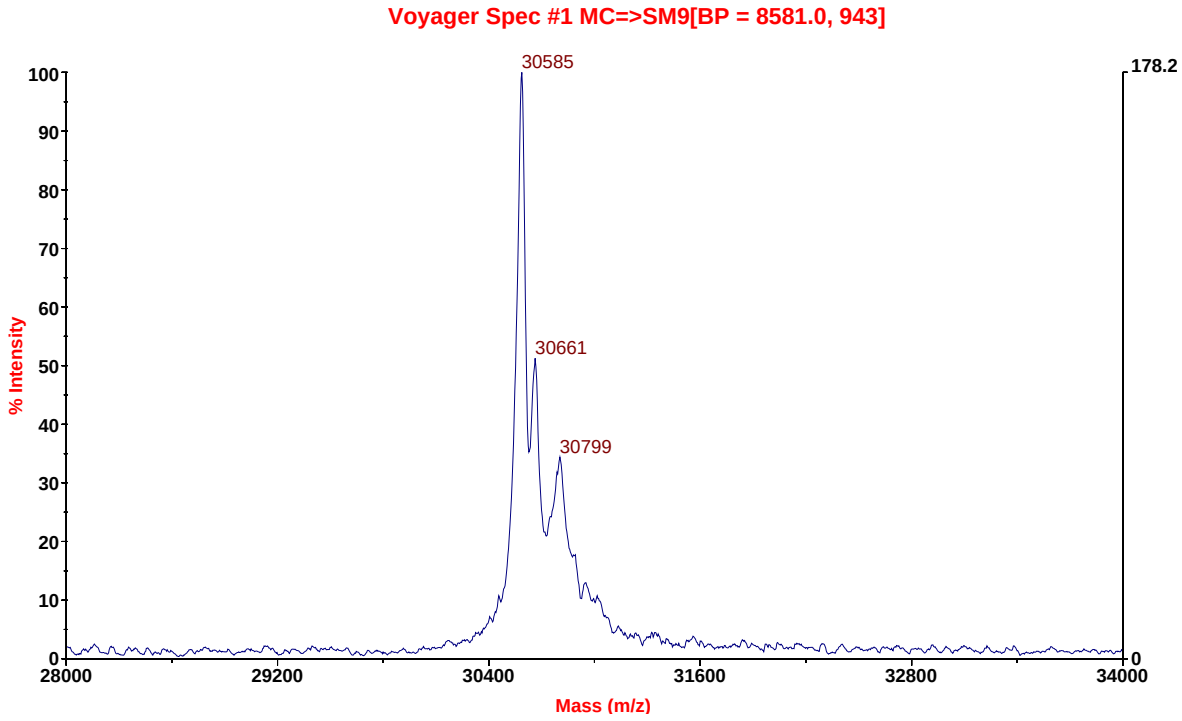

Figure 11. ^{31}P-NMR of the Sts-1$_{PGM}$ H565A during catalytic turnover. Two resonances were observed. The resonance at - 2 ppm corresponds to *p*NPP, the resonance at 0 ppm corresponds to free phosphate, and the resonance at 0.4 ppm corresponds to intermediate.

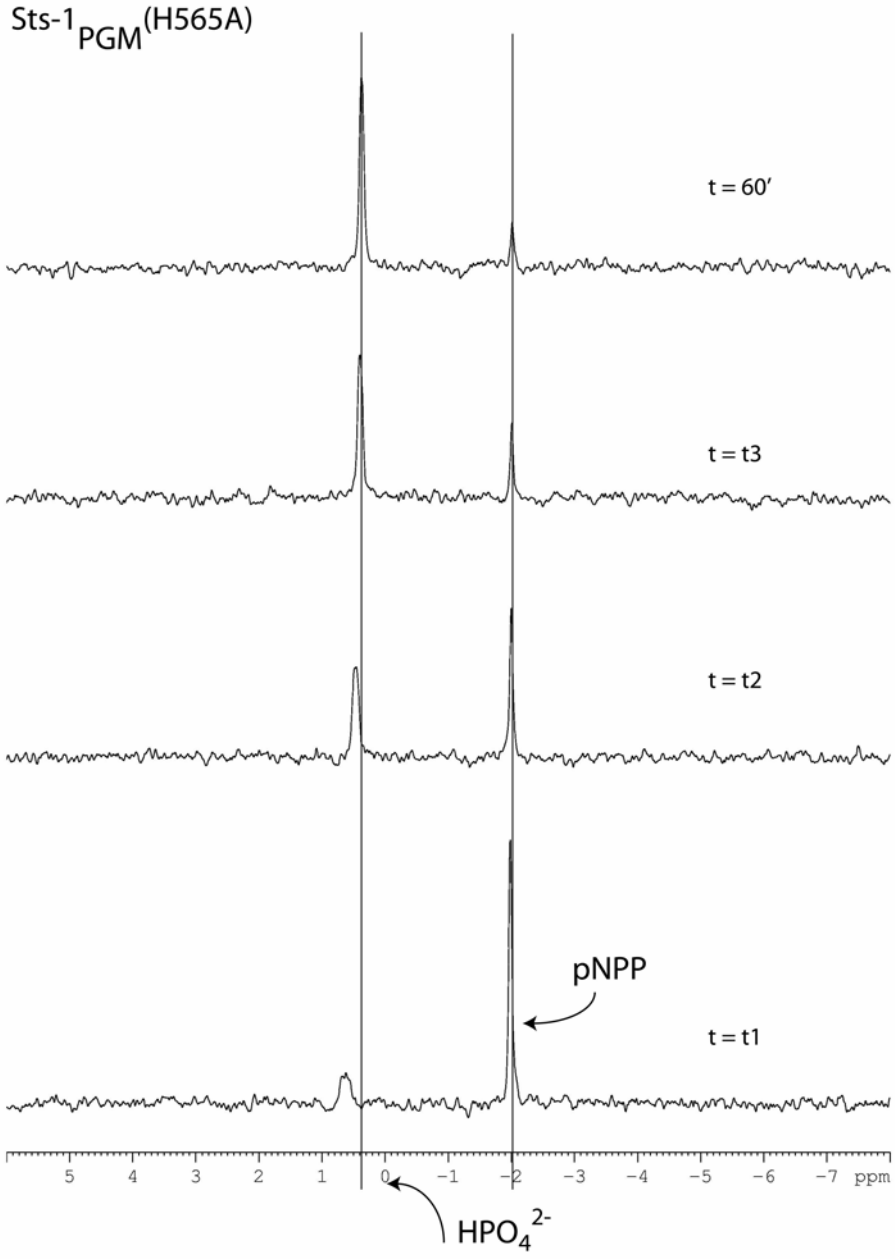

Figure 12. pH dependency of the Michaelis constant (K_m) of Sts-1_{PGM}. Each data set was measured using *p*NPP as the model substrate and fitted to eq [1] (see Materials and Methods, 2.2.8) to obtain K_m values.

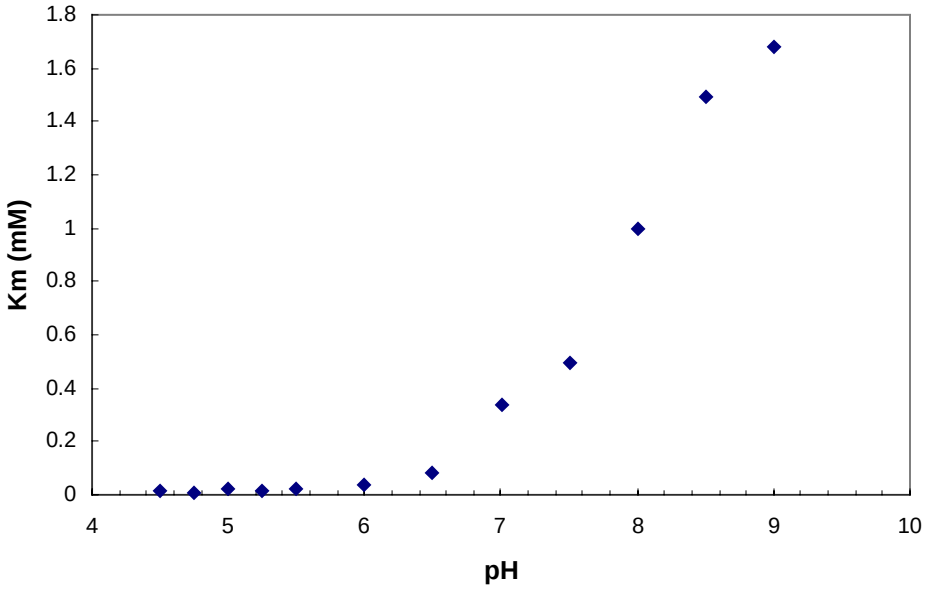

Figure 13. pH effect on the k_{cat} values for Sts-1_{PGM}. Each data set was measured using *p*NPP as the model substrate and fitted to eq [1] (see Materials and Methods, 2.2.8) to obtain k_{cat} values.

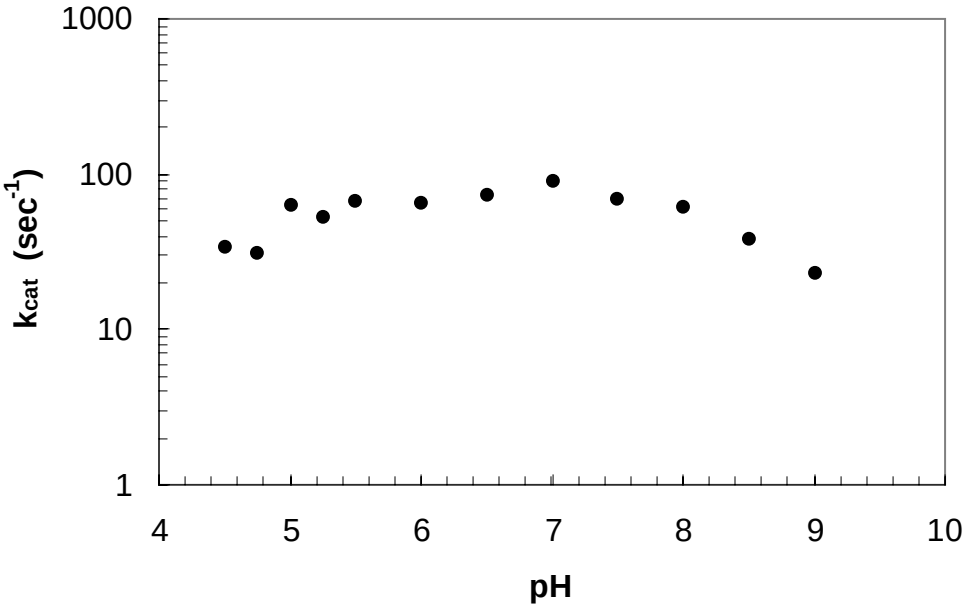

Figure 14. pH dependency of Sts-1 and mutants. The solid triangles represent the wild type enzyme data, open squares represent E490A mutant data, and open circles and diamonds represent mutant H380A and H565A data, respectively.

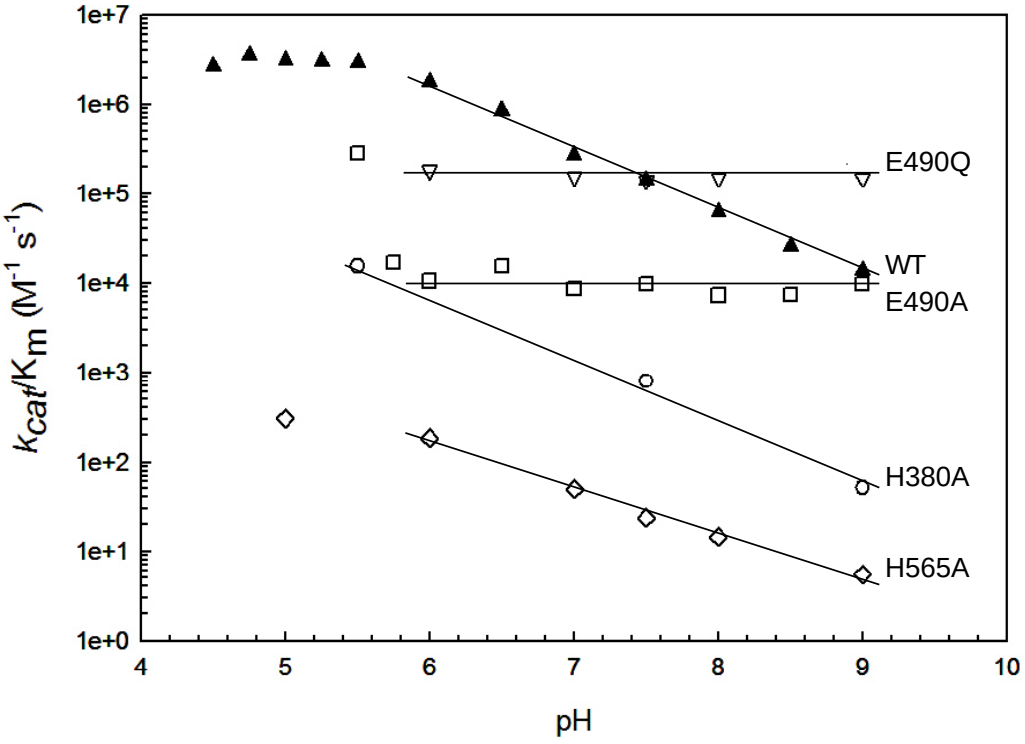

Figure 15. Effect of pH on the k_{cat} value of the E490Q mutant. The solid squares (■) represent wild type Sts-1$_{PGM}$. The solid diamonds (♦) represent E490Q.

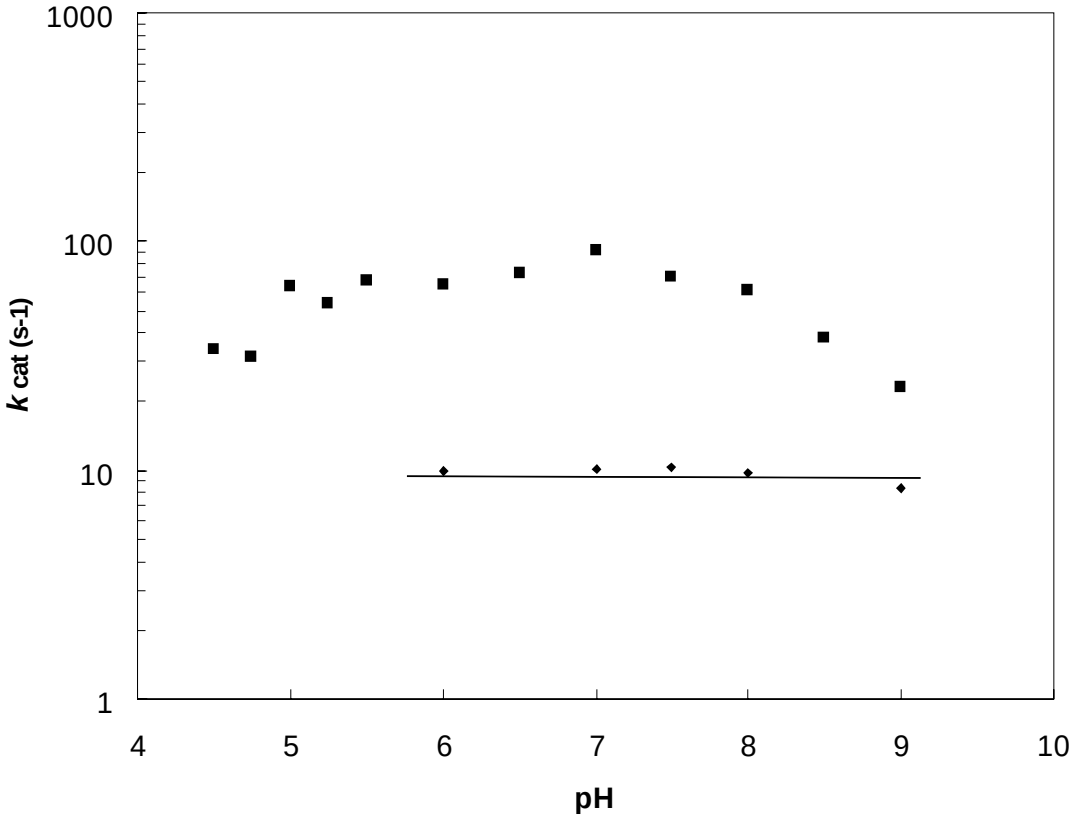

Figure 16. The phosphatase activity of Sts-1_{PGM} is inhibited by sodium tungstate. The protein and substrate concentrations were fixed at 25 nM Sts-1_{PGM} and 1 mM *p*NPP. Each data set was fitted to eq [2] as described in Materials and Methods.

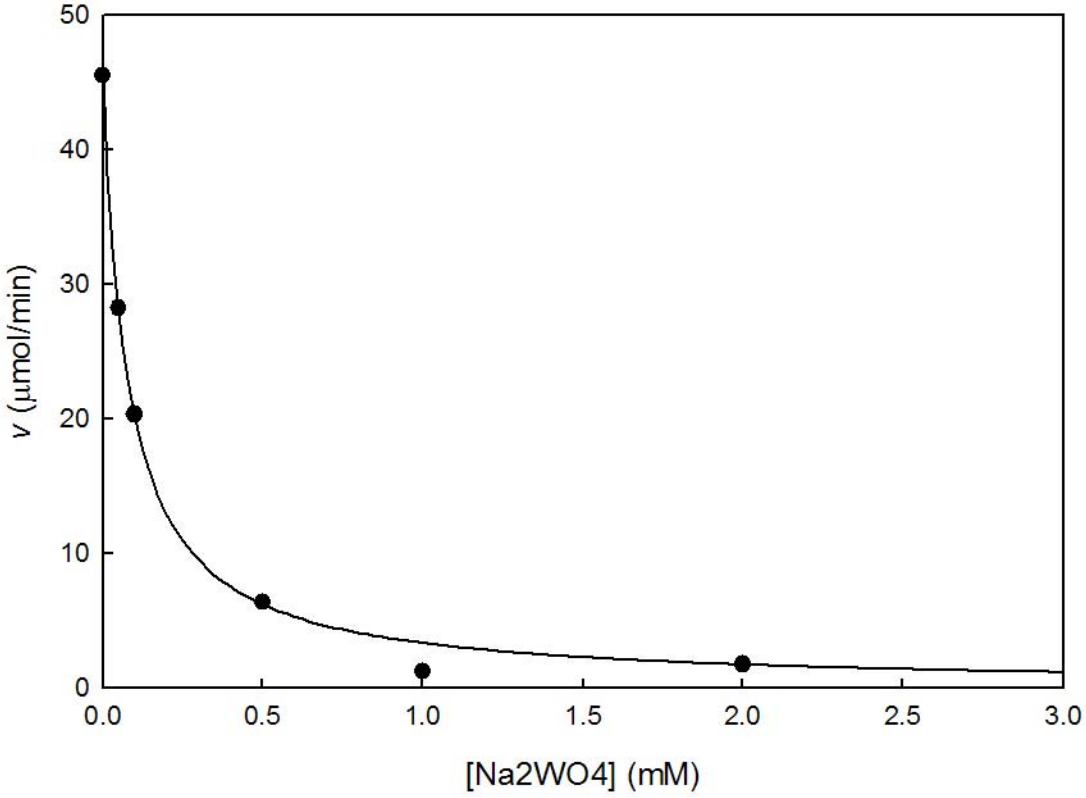

Figure 17. SDS-PAGE analysis for binding assay of pTyr peptide to Sts-1_{PGM} wild type and mutants. Control: half of the amount of protein (14 μg total) used in each reaction and "+" indicates that the molecular weight of the protein is as expected (~ 30 kDa). Peptide: the protein pulled down by peptide-coupled beads and "+" indicates the proteins is pulled down by the beads.

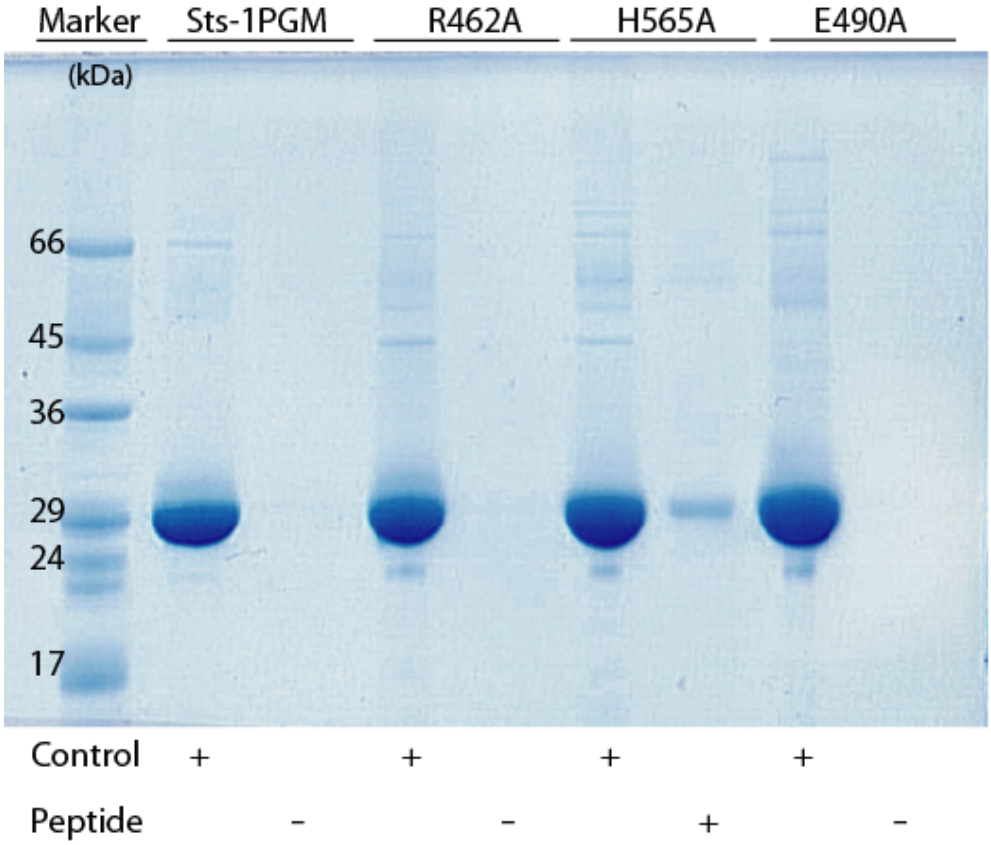

Table 1. Refinement statistics for Sts-1_{PGM}.

	Native	**+ PO_4^{--}**
Resolution Range (Å)	98.05 – 1.82	50.0 - 2.6
Completeness, (%) overall (last shell)	96.3 (94.4)	98.0 (99.5)
Multiplicity, overall (last shell)	5.4 (5.0)	4.1 (4.2)
N° of unique reflections	72,288	25,668
Water molecules	263	13
B factor, (A^2) overall (from Wilson plot)	33.9 (29.5)	40.9 (74.8)
R_{free} †, (%) overall (last resolution shell)	24.2 (32.1)	27.8 (38.1)
R_{cryst} ‡, (%) overall (last resolution shell)	20.3 (27.1)	24.7 (37.1)
Rms deviation in bond length (Å)	0.015	0.013
Rms deviation in bond angle (°)	1.426	1.412
Estimated coordinate error § (Å)	0.138/ 0.093	0.372/ 0.333
Ramachandran plane ¶ (%)	91.9/ 7.7	91.9/7.7

The last resolution shell is the interval 1.86 - 1.82 Å and 2.69 - 2.60 Å for the native and phosphate bound Sts-1.

† $R_{free} = \Sigma_{(hkl)\varepsilon T}||F_{obs}| - |F_{calc}||/\Sigma_{(hkl)\varepsilon T}|F_{obs}|$, where T is the test set (*Brünger 1992*) obtained by randomly selecting 5 % of the data.

‡ $R_{cryst} = \Sigma_{(hkl)}||F_{obs}| - |F_{calc}||/\Sigma_{(hkl)}|F_{obs}|$.

§ Estimated coordinate error based on R_{free}/maximum likelihood.

¶ Most favored/additional allowed regions.

Table 2. Site-directed mutational analysis of Sts-1_{PGM}. Each set of data was fitted to eq [1] as described in Materials and Methods. Activity (%) was carried out by taking the k_{cat}/K_m of native Sts-1_{PGM} as denominator.

Enzyme	k_{cat} s^{-1}	K_m mM	k_{cat}/K_m $s^{-1}M^{-1}$	Activity %
Sts-1	70.10	0.50	1400.0×10^2	100
E490A	1.93	0.20	96.5×10^2	7
E490Q	10.32	0.07	1414.6×10^2	101
H565A	0.04	1.75	0.2×10^2	0.016
H380A	0.40	0.50	7.9×10^2	0.56
R462A	0.02	3.23	0.6×10^1	0.0043

Table 3. List of inhibitors for Sts-1_{PGM}. The ability of inhibitors to suppress pNPP hydrolysis were marked with ++++ to + for various levels, the symbol "-" indicates no or minor effect of inhibition.

Inhibitor	Inhibition	Reference
Inhibitor for PTP1B:		
[1,1-difluoro-1-(2-naphthalenyl)-methyl] phosphonic acid (6)	-	(1) (Ki = 179 μM)
Inhibitor for Acid phosphatase:		
Tartrate	-	(2) (Ki = 10 μM)
Phosphate analogs:		
WO_4^{2-}	++++	
PO_4^{2-}	+	
Na_3VO_4	-	
$NaSeO_4$	-	
$(NH_4)H_2AsO_4$	-	
pNPP analogs:		
4-nitrophenyl sulfate	+	
p-nitrocatechol sulfate	+	
Benzylphosphonic acid	-	
β-naphthyl sulfate	-	
Disodium pyrophosphate	-	

(1) Linqvist et al., 1993.
(2) Burke et al., 1996.

3. STRUCTURAL AND FUNCTIONAL CHARACTERIZATION OF Sts-2_{PGM}

ABSTRACT

Members of the suppressor of T-cell signaling family, Sts-1 and Sts-2, negatively regulate the T cell receptor (TCR) signaling. We have previously demonstrated that the phosphatase activity of Sts-1 is crucial for its signaling, targeting the tyrosine kinase Zap-70 among other proteins (Mikhailik *et al*., 2007). Despite the high sequence homology between Sts-1 and Sts-2 especially within the catalytic residues, the phosphatase activity of the later is orders of magnitude weaker than the former when tested on the non-specific phosphatase substrate, *p*NPP. The X-ray structures of the Sts-2 PGM domain, alone and in complex with tungstate and phosphate were determined to 1.93 Å, 2.25 Å and 2.77 Å, respectively. All structures share homology with Sts-1_{PGM}. The tungstate ion makes tighter interaction with Sts-2 and is closer to the nucleophilic His366 than the phosphate. Catalytic residues lining the active site also show identical configuration between Sts-1_{PGM} and Sts-2_{PGM} and assist in stabilization of bound tungstate or phosphate. Non-conserved residues in the Sts-2_{PGM} active site were mutated to the homologous residues in Sts-1. The generated mutants (E481V, S582Y/Q372V, and A446S/S552A) improved Sts-2_{PGM} phosphatase activity suggesting that Sts-1_{PGM} and Sts-2_{PGM} have different substrate(s), and the mutated residues play a role in substrate specificity.

INTRODUCTION

Within the mammalian immune system, T cells play a central role in the recognition and elimination of invasive microorganisms. However, they also pose a potential danger to their host, in that many of the properties that make them effective mediators of the immune response can be turned inadvertently against host tissue. Not surprisingly, the immune system has evolved a variety of mechanisms to ensure that T cells target foreign microbes with remarkable fidelity and selectivity. When any of these control mechanisms breakdown, varied pathologies ranging from immuno-deficiencies to auto- immune disorders are known to develop. The receptor utilized by T-cells to detect the presence of pathogens is known as the T-cell receptor, or TCR. Activation of the TCR by an antigen turns on an array of intracellular signaling cascades. Src family kinases that are constitutively associated with the receptor complex phosphorylate the TCR (Cheng *et al*., 1997). This allows the tyrosine kinase Zap-70 to be recruited to the receptor complex, where it is phosphorylated and activated. When activated, Zap-70 plays a critical role in propagating downstream signals (Cheng *et al*., 1997). In addition to tyrosine kinases, numerous adaptor and scaffolding proteins as well as lipid kinases, Tec family kinases, and components of both the Ca^{2+}-calcineurin and MAPK signaling cascades (Singer *et al*., 2002; Andreotti *et al*., 1997; Meng *et al*., 1998) participate in TCR signaling.

Signals through the TCR control the extent and duration of the T cell response. To ensure that downstream signaling pathways are appropriately activated, T cells possess a variety of mechanisms to limit the duration and intensity of signals generated by receptor activation (Singer and Koretzky, 2002). For example, after initial engagement of the

TCR, it is rapidly internalized in order to reduce the pool of receptor available for further stimulation. The tyrosine kinases involved in TCR-mediated signaling are also subject to several levels of regulation. These include dephosphorylation by tyrosine phosphatases such as Shp-1, and phosphorylation of inhibitory residues by tyrosine kinases such as Csk. In addition, members of the Cbl family of proteins having ubiquitin ligase activity negatively regulate T cell receptor signaling by targeting selective components of the TCR signaling pathways for degradation (Naramura *et al*., 2002; Kowanetz *et al*., 2004). Recently, a new family of proteins involved in negatively regulating TCR signaling pathways termed the Suppressor of TCR Signaling (Sts) family was identified (Carpino *et al*., 2002; Carpino *et al*., 2004).

Sts-1 and *Sts-2* belong to a gene family whose members can be found in an evolutionarily diverse group of organisms. Most *Sts* family members are characterized by a unique tripartite structure, with an N-terminal UBA (Ubiquitin-association) domain, a central SH3 (Src-homology 3) domain, and a carboxyl region with similarity to the catalytic domain of members of the phosphoglycerate mutase (PGM) family. The PGM motif defines a group of structurally related enzymes that catalyze the transfer of phosphate groups from small molecules such as phospho-glycerate and fructose-2, 6-phosphate (Jedrzejas, 2000). The realization that Sts proteins have a role in regulating TCR signaling pathways emerged from an analysis of mice lacking Sts-1 and -2. Specifically, naïve peripheral T cells isolated from Sts-1/2$^{-/-}$ mice displayed a striking hypersensitivity to *in vitro* T cell receptor stimulation. This was manifested by a pronounced increase in TCR-induced proliferation by mutant T cells relative to wild-type T cells, a phenotype that was accompanied by a marked increase in cytokine production,

and increased susceptibility of mutant mice to autoimmunity in a mouse model of multiple sclerosis. These results argued that Sts-1 and Sts-2 are critical regulators of the signaling pathways that participate in the activation of naïve peripheral T cells.

We have previously demonstrated that Sts-1 has a phosphatase activity localized to its C-terminus PGM domain, Sts-1_{PGM} (Mikhailick *et al*., 2007). This phosphatase activity targets phospho-tyrosine containing proteins including the tyrosine kinase Zap-70. We solved the crystal structure of the Sts-1_{PGM} domain and showed that it has homology to members of the phosphoglycerate mutase/acid phosphatase (PGM/AcP) family of enzymes. Active site residues known to be important for PGM/AcP catalytic activity including the 'RHGE' signature motif and an additional arginine and histidine residues are conserved in nature and position in Sts-1. Point mutations that impair Sts-1 phosphatase activity *in vitro* also impair its ability to regulate TCR signaling in T cells. These observations revealed a novel enzyme activity involved in the control of antigen receptor signaling, and provided the first insights into the mechanism of action of a negative regulator of TCR signaling.

The high similarity between Sts-1 and Sts-2 (35% identity and 65% homology) especially within the catalytic residues of the active site suggests that Sts-2 has also a phosphatase activity with kinetics similar to those of Sts-1. Using a pNPP-based *in vitro* assay, however we showed that Sts-2 has a much weaker phosphatase activity than Sts-1 suggesting that residues besides the ones conserved in PGM family members may play a critical role in catalysis. To shed light on why Sts-2 has a weaker phosphatase activity, we used structural and biochemical approaches to characterize the activity of Sts-2_{PGM} and to compare it to Sts-1_{PGM}'s activity.

MATERIALS AND METHODS

3.2.1 Protein Preparation and Crystallization

The PGM domain of Sts-2 (residues 354-624) was cloned as a His-tagged protein in the pProEX-HTb vector and expressed in the *Escherichia coli* CodonPlus BL21 (DE3) strain as described previously for Sts-1_{PGM} (*Kleinman 2006*). Proteins were purified on a Ni-NTA column (Qiagen) followed by removal of the His-tag by the action of TEV protease and a gel filtration column (Superdex 200, GE Healthcare). Initial crystals were grown at 20°C by mixing 3 µl of 20 mg/ml Sts-2_{PGM} (in 20 mM HEPES, 150 mM NaCl, pH = 7.5) and 3 µl of a reservoir solution. The reservoir consisted of 20% (w/v) Polyethylene Glycol-8000 (PEG8000), 0.2 M Li_2SO_4, 5 to 20 mM $SrCl_2$, and 0.1 M Tris-HCl pH = 8.0. Sts-2_{PGM} crystallized in space group $P2_12_12_1$ (a = 77.9 Å, b = 115.7 Å, c = 121.2 Å) with two dimers in the asymmetric unit corresponding to a V_m value (Matthews 1968) of 2.33 $Å^3$/Da and an estimated solvent content of 47%.

3.2.2 Data Collection, Structure Determination, and Refinement

Native diffraction intensities to 1.95 Å were collected at 100 K on beamline X26C at the National Synchrotron Laboratory Source (NSLS), Brookhaven, on a 2k x 2k CCD detector (ADSC), processed with the HKL2000 package, and scaled with SCALEPACK (*Otwinowski 1997*).

The structure of Sts-2_{PGM} was solved using the single anomalous dispersion (SAD) technique. A run consisting of 270 degrees was collected at a wavelength of 1.0 Å to ensure high anomalous signal on a single Sts-2_{PGM} crystal soaked for one hour in a

solution containing 40 mM sodium tungstate. Bijvoet pairs were scaled and merged separately in HKL2000 (*Otwinowski 1997*). The heavy-atom substructure was solved in the program SHELXD (Sheldrick and Schneider, 1997) with data truncated to 2.7 Å resolution. This resolution cut was based on statistics reported by the program SHELXC. Four tungsten atoms were found using this approach. The coordinates of the heavy atoms were further refined and initial phases calculated with the program SOLVE (Terwilliger and Berendzen, 1999). The electron density map calculated to 2.7 Å resolution after phasing and density modification with RESOLVE (Terwilliger, 2000) proved to be of excellent quality (correlation coefficient of 169). This electron density was used to build an initial model of four Sts-2PGM monomers with the automatic building procedure in RESOLVE. This model was further refined in REFMAC (Murshudov 1997) to 1.95 Å resolution using TLS (Howlin *et al*., 1993) to crystallographic residuals R_{cryst}/R_{free} of 20.0/23.9 % and excellent stereochemistry. The final model has no density for residues A623-A624, B354-B357 and B622-B624, C354-C357 and C621-C624, D354-D357 and D622-D624. There was extra density N-terminus to A354 where the sequence 'AMGS' was built and refined. This extra sequence is likely from the cloning plasmid. Stereochemistry was checked with the program PROCHECK (Laskowski, 1993). Table 1 summarizes statistics on data collection and model refinement.

3.2.3 Phosphatase assay

The Sts-2_{PGM} domain phosphatase activity was measured by following the rate of hydrolysis of para-nitrophenol phosphate (*p*NPP) (Sigma) as a general substrate. *p*NPP is commonly used as a general substrate to study phosphatase activities. For the

measurement of the Sts-2_{PGM} activity, the reaction mixture contained 100 mM TAB (25 mM Tris, 50 mM acetic acid, 25 mM bis-Tris), 150 mM NaCl, 0.1 mM EDTA, and 1 mM DTT. The reaction was initiated by adding the protein (10 μM) to the *p*NPP in the reaction mixture pre-incubated at 37ºC. The reaction was stopped by adding 13% K_2HPO_4 or 0.5 M NaOH and chilled on ice. The amount of para-nitrophenol (*p*NP) converted from *p*NPP was quantified by OD_{405} measurement. OD405 was converted to *p*NP concentration using the following relationship:

$OD_{405} = a \cdot b \cdot c$ ($a = 1.78 \times 10^4\ M^{-1} \cdot cm^{-1}$; b = light path (cm); c = [*p*NP])

3.2.4 k_{cat} and K_m measurements

Initial velocities (v) were measured at various substrate concentrations as the slope of the linear part of the *p*NP concentration plotted function of time. To determine the kinetic parameters k_{cat} and K_m, v was plotted at various substrate concentrations (S) and the data points fitted to equation 2 using the program SigmaPlot 5.05 (SPSS Science Inc., Chicago).

$$v = \frac{k_{cat} \bullet S}{(S + K_m)} \qquad [1]$$

3.2.5 Inhibition of $Sts2_{PGM}$

Tungstate, vanadate, and phosphate at various concentrations were incubated with the *p*NPP (1 mM) containing buffer at 37 °C. $Sts2_{PGM}$ (10 μM) was added to this buffer and the phosphatase activity was measured as previously described. Initial velocities (v) were plotted function of the inhibitor concentration and the data points were fitted to

equation 2 using the program SigmaPlot from which an inhibition constant (K_i) was deduced.

$$\nu = V_{max} / (1 + K_i [I]) \qquad [2]$$

RESULTS AND DISCUSSION

3.3.1 *In vitro* phosphatase activity of Sts-2_{PGM}

In vitro phosphatase activity of Sts-2_{PGM} on the sequence homology between Sts-1 and St-2 PGM domains especially in the active site catalytic residues, one expects Sts-2_{PGM} to efficiently hydrolyze the same phosphorylated substrates with similar kinetics. To test this hypothesis, we purified Sts-2_{PGM} as a recombinant protein and checked its ability to dephosphorylate para-nitrophenylphosphate (*p*NPP). *p*NPP is a general non-specific phosphorylated substrate used to study the activity of many phosphatases. We were unable to detect any significant activity when Sts-2_{PGM} (25 nM) was mixed with 1 mM *p*NPP conditions under which Sts-1_{PGM} was able to efficiently hydrolyze *p*NPP (Mikhailik *et al*., 2007). However, when 10 μM of Sts-2_{PGM} were used in the assay, a phosphatase activity was undoubtedly detected at 405 nm. When tested against increasing concentrations of pNPP, the Sts-2_{PGM} phosphatase activity followed the Michaelis-Menten kinetics with measured k_{cat} and K_m of 0.03 s^{-1} and 2.0 mM (Figure 1 and Table I). This phosphatase activity of Sts-2 is consistent with the conservation of the catalytic core residues with Sts-1. The relatively weaker phosphatase activity of Sts-2 when compared to Sts-1 is mainly due to k_{cat}, which is 1,700 times lower but not to K_m, which is reduced by a factor of four. This result suggests that either slight differences in the three-dimensional structure or non-conserved residues between Sts-1 and Sts-2 in addition to the conserved catalytic residues contribute to the enzymatic activity.

3.3.2 Structure of the Sts-2_{PGM} domain

To shed light on eventual differences between the PGM domains of Sts-1 and Sts-2, we crystallized and solved the crystal structure of Sts-2_{PGM} using the single wavelength anomalous dispersion (SAD) method on a tungstate soaked crystal. The experimental SAD electron density map after phase refinement in RESOLVE (Terwilliger, 1999) was of excellent quality and showed density for four Sts-2_{PGM} monomers arranged in two dimers. The final model was refined against 1.95 Å diffraction data to low crystallographic residuals R_{work}/R_{free} of 19.8/23.7% and good stereochemistry. Tables 2 and 3 summarize statistics on data collection and model refinement. Four Sts-2_{PGM} chains organized in two interacting dimers (AC and BD) occupy the asymmetric unit. The organization of Sts-2_{PGM} into dimers is consistent with size exclusion data (not shown). The two dimers superpose well with an rms deviation of 0.66 Å calculated over all Cα atoms. In addition, all four monomers superpose well. For simplicity, the AC dimer will be considered hereafter when describing the dimer and chain A when describing the Sts-2_{PGM} active site.

As expected, the PGM domains of Sts-1 and Sts-2 superpose well. The calculated rms deviations after superposition of the monomers and dimers of the Sts PGM domains are 1.0 and 1.64 Å, respectively. The Sts-2_{PGM} monomer has an α/β structure similar to that adopted by Sts-1_{PGM} and members of the PGM/AcP superfamily (Jedrzejas 2000). Architecturally, a central 7-stranded β sheet forms the core of the monomer; all β-strands are parallel with the exception of β6 (Figure 2). The core is surrounded by eight α-helices (α1 to α8) and seven 3_{10}-helices. As in Sts-1_{PGM}, residues C-terminal to β7 (the C-terminal extended loop, strand β8, and helix α9 residues 600 to 622) depart from the

core, and project into the second monomer to make strong dimer-interface interactions. This mode of dimerization differentiates Sts proteins from other PGM/AcP family members. The Sts-2_{PGM} dimer interface is larger than the corresponding Sts-1_{PGM} dimer interface. The accessible surface area of the Sts-2_{PGM} dimer interface is 2,350 $Å^2$ compared to 1,640 $Å^2$ for Sts-1_{PGM} (Mikhailic *et al*., 2007).

The loops that are not conserved in sequence and structure between Sts-1 and PGM/AcP family members, inserts 1 and 2, are conserved in structure and sequence between the two Sts isoforms. The '^{365}RHGE^{368}' signature pattern specific of PGM/AcP family members is located at the carboxyl end of the central β sheet structure. As in Sts-1, one additional arginine (Arg448) and one histidine (His551) of Sts-2 also part of the conserved PGM/AcP catalytic residues complement the RHGE signature. Mutating these residues in Sts-1 abolished its phosphatase activity (Mikhailik *et al*., 2007). Our crystallographic results thus predict that like Sts-1_{PGM}, the Sts-2_{PGM} should have a phosphatase activity.

3.3.3 The Sts-2_{PGM} active site

The structural similarity between Sts-2_{PGM}, Sts-1_{PGM}, and PGM family members is very strong in the active site residues within the catalytic pocket. For example, Sts-2 residues (Arg365, His-366, Arg448, Glu-476, and His551) adopt a configuration that is identical to their homologues in Sts-1_{PGM} (Arg379, His380, Arg462, and His565) in PGM family members, suggesting that they are the active site residues of Sts-2_{PGM}. In such a scenario, Sts-2 His-366 would serve as a nucleophile that attacks the phosphorus atom of a phosphorylated substrate and is itself temporarily phosphorylated during the enzyme

reaction. A hydrogen bond between $N^{\delta 1}$ of His-366 with the carbonyl of Gly-367 suggests that $N^{\delta 1}$ is protonated, indicating that $N^{\varepsilon 2}$ of His-366 is deprotonated and able to serve as a nucleophile. To test this hypothesis, we mutated His366 to alanine and checked the activity of the recombinant Sts-2_{PGM}H366A mutant. As expected, Figure 3 shows that this mutant has no detectable activity even when high concentrations of *p*NPP are used.

The three-dimensional structure shows differences in three active site residues between Sts-1_{PGM} and Sts-2_{PGM}. Val386, Val495, and Tyr596 in Sts-1_{PGM}, which surround the nucleophilic histidine from opposite sides of the active site, are found as Gln372, Glu481 and Ser582 in Sts-2_{PGM} (Figure 4). These differences, which change two small hydrophobic side chains into large acidic or hydrogen acceptor/donor ones might explain why Sts-2_{PGM} does not hydrolyze *p*NPP as efficiently as Sts-1_{PGM} and propose that the two Sts isoforms have different substrates (Figure 4). For example, the bulky Glu481, which is making a strong hydrogen bond with Arg448 in Sts-2, introduces a negative charge close to Glu476 and reduces the active site volume. In contrast, the equivalent residue in Sts-1, Val495 is smaller and does not involve in hydrogen bonding with Arg462. To test this hypothesis, we generated and purified the E481V single mutant and the Q372V/S582Y double mutants of Sts-2_{PGM} and assessed the ability of each mutant to hydrolyze *p*NPP by measuring their K_m and k_{cat} values. As shown in Figure 5 and reported in Table 1, the mutations do not significantly affect K_m. The mutations however, increased the k_{cat} values by a factor of 5 for the E481V mutation and 10 for the double mutant. These data clearly show that making the Sts-2 active site more Sts-1-like improves the ability of Sts-2 to hydrolyze *p*NPP. We therefore propose that the trio of residues Gln372, Glu481 and Ser582 are responsible for the difference in activity of the

Sts PGM domains. However, the k_{cat} values for the Sts-2 mutants are still two orders of magnitude smaller than the values we reported for Sts-1. Although we do not know if the Sts-2_{PGM} (Q372V, E481V, S582Y) triple mutant will hydrolyze *p*NPP with kinetics similar to Sts-1 since it is insoluble, it seems that other factors outside the active site influence the phosphatase activity.

Furthermore, two residues, Ser460 and Ala566 that may contribute to the protonation state of Arg462 and His565 in Sts-1 are not conserved in Sts-2. The equivalent residues in Sts-2, Ala446 and Ser552 may agitate Arg448 and His551's role in stabilizing the substrate binding. We generated the A446S and S552A single and double mutants of Sts-2_{PGM} and examined the ability of each mutant towards *p*NPP hydrolysis by measuring their K_m and k_{cat} values. Although the single mutants did not show appreciable effect on Sts-2_{PGM} activity, the A446S/S552A double mutants increased the k_{cat} values by the factor of 9 (Table 1). Consistent with the activity results obtained with Sts-2 Q372V, S582Y and E481V, these data show that the ability of Sts-2 to hydrolyze *p*NPP is improved by making the Sts-2 active site more Sts-1-like. Collectively, the activity difference between Sts-1 and Sts-2 for *p*NPP hydrolysis is not only due to the active site conformational divergence, but also affected by the protonation state of the catalytic residues.

Figure 6 shows a surface representation of Sts-1_{PGM} and Sts-2_{PGM}. The active sites of both proteins revealed an "L-shape" depression with two pockets inside (Figure 6). One pocket is formed by the conserved catalytic residues (Arg365, His366, Arg369 and His552 in Sts-2). The adjacent pocket is formed by less conserved residues. The orientations of the active sites in both Sts proteins are identical. However, the less

conserved pocket in Sts-1_{PGM} is a hydrophobic socket composed of Ser460, Val495, Phe489, Pro501, and Trp503, which is blocked by Glu481 in Sts-2_{PGM}. Besides that, Gln372 was found to protrude right below the catalytic site of Sts-2_{PGM}, which narrows the interacting area for binding substrates. These findings indicate that the changes of the active site surface may be one of the factors that improve the phosphatase activity of Sts-2_{PGM}.

3.3.4 Inhibition of Sts-2 activity by phosphate and phosphate-like molecules

Phosphate and phosphate-like molecules including tungstate and vanadate are commonly used to study the binding and catalytic mechanism involving phospho- and sulfo-groups (Haque *et al*., 1995). To check the ability of these molecules to inhibit the phosphatase activity of Sts-2, we incubated phosphate and tungstate at the concentrations shown on Figure 7 with 1 mM *p*NPP and measured initial velocities of hydrolysis. Fitting of the data points to a hyperbolic equation shows that a tungstate concentration of 0.8 mM decreases the phosphatase activity of Sts-2 by 50% while a 50 mM concentration of phosphate is needed to reach the same inhibition level. This fitting thus shows that tungstate is a potent inhibitor of Sts-2 and that phosphate, which is a product of the hydrolysis reaction, does not inhibit Sts-2. We also checked inhibition effect of vanadate, concentrations as high as 5 mM of vanadate did not inhibit the phosphatase activity of Sts-2_{PGM} suggesting that vanadate is a poor inhibitor for Sts-2_{PGM}. Clearly, although tungstate and vanadate are structurally similar to phosphate, the active sites of Sts-2 and other members of the PGM/AcP family have different preference for phosphate-like inhibitors.

3.3.5 Structure of the tungstate-bound form

To understand the mechanism of action of the phosphate and tungstate ions, we solved the crystal structures of Sts-2_{PGM} in the presence of both anions. The structure of the tungstate complex was refined to 2.0 Å resolution against the absorption-edge data collected at a wavelength of 1.0 Å and used to solve the free Sts-2_{PGM} structure. Superposition of the wild type and tungstate-bound structures shows that both structures are identical. The RMS deviation calculated after superposing all Cαs in the four subunits is 0.5 Å. Specifically, no structural change of the active site residues was observed between the free and tungstate-bound forms.

Sts-2 holds the tungstate ion tightly at the center of the active site where it replaces three water molecules found in the active site of the apo form. The anionic oxygen atoms of the tungstate interact with five basic residues, two histidines (His366 and His551) and three arginines (Arg365, Arg369, and Arg448), the main chain amide group of Ser552, and one acidic residue (Glu476) as shown in Figure 8A. A globular non-protein density was also found within ionic distances (1.8 to 2.0 Å) to an oxygen atom of all four tungstates. A sodium ion was build and refined into this density. The likely role of this solvent exposed sodium ion is to cooperate with the protein basic residues in neutralizing the negative charges of the tungstate ions. In addition to interacting with the tungstate ion, the residues Arg365, Arg369 and Arg448 are involved in hydrogen bond networks with other residues and bridging water molecules, implying that the geometry of the active site is rigid. In all four Sts-2_{PGM} monomers, the deprotonated N^{ε} nitrogen of the active site His366 is within 2.2 to 2.5 Å of the tungsten atom. This geometry implies an in-line nucleophilic attack by His366 with the three

arginines possibly neutralizing the expected negative charge buildup on the transition state during phosphoryl transfer to His366. His551, which contacts the tungstate ion, is a candidate for the general acid.

3.3.6 Structure of the phosphate-bound form

The structure of phosphate-bound Sts-2_{PGM} was refined against 2.8 Å diffraction data collected on a crystal soaked in 0.2 M sodium/potassium phosphate (Table 2). Because of the low resolution of the data, tight non-crystallographic symmetry (NCS) restraints were applied during the refinement. As with the tungstate-bound structure, there is no significant change between the phosphate-bound and apo-Sts-2_{PGM} structures. Comparison of the tungstate- and phosphate-bound Sts-2_{PGM} structures shows two major differences in the active site (Figure 8). First, one phosphate ion is missing from the active site of a monomer; instead, it is replaced by a water molecule that makes a hydrogen bond with His366. Second, the distances between the phosphorous atoms and the Nε nitrogen of His366 are 3.2 Å in one monomer and 4.1 Å in the remaining two. The equivalent W-Nε distances are considerably shorter and vary between 2.2 and 2.5 Å. Both observations are consistent with the low phosphate affinity we observed in our inhibition assays. The interactions of the phosphate ions with Sts-2 depend on how close they are to His366. In the two Sts-2_{PGM} monomers where the P-Nε distance is 4.1 Å, the phosphate ions are within hydrogen bond distances from Arg365 and Arg369 (Figure 8B). In the monomer where the P-Nε distance is 3.2 Å, the phosphate makes additional hydrogen bonds with His366, Arg369, Arg448, Ser552, and His551. Surface representations of tungstate- and phosphate-bound Sts-2_{PGM} structures show that while

tungstate is embedded into the active site, phosphate is more solvent exposed (Figure 9). Because of the proximity of the tungstate ion to His366, we propose that the tungstate-bound structure mimics the structure of the active site before the nucleophilic attack on the phosphorylated substrate by His366. The phosphate-bound structure on the other hand mimics the structure of the active site post hydrolysis of phosphorylated-His366 but before the inorganic phosphate is released to the solvent. The phosphate ion is initially stabilized by Arg365, Arg369, Arg369, His366, Arg448, Ser552 and His551 as in the monomer where the P-Nε distance is 3.2 Å. As the reaction progresses, the phosphate is expelled from the active site into the solvent, its distance to His366 increases and its interactions with Sts-2 are reduced to only Arg365 and Arg369. Combine together, the tungstate and phosphate structures are consistent with a model in which the cluster of basic residues located at the carboxyl end of the central β sheet structure form the active site Sts-2_{PGM}.

CONCLUSION

Our previous studies showed that Sts-1 dephosphorylates tyrosine-phosphorylated proteins, while Sts-2 shows undetectable activity towards dephosphorylation of phosphorylated tyrosine-phosphorylated proteins (Mikhailik *et al*., 2007). In this study, the structures of Sts-2_{PGM} alone or in complex with tungstate and phosphate were determined. These structures show strong structural homology to Sts-1_{PGM}. Both proteins adopt the α/β-fold specific for PGM family members but dimerize through their carboxyl-terminal tails. Our superposition analysis shows that the conserved residues in the active sites of both proteins have identical conformations, suggesting that the Sts-1 and Sts-2 active site employ a similar mechanism for their activity.

Consistent with our structural data, the Sts-2_{PGM} H366A mutant shows no detectable phosphatase activity indicating the important role of His366 as nucleophile during the hydrolysis reaction. Compare the inhibition of phosphate and tungstate to Sts-1_{PGM} (422 mM/μM and 3.2 mM/μM); the activity of Sts-2_{PGM} is inhibited by phosphate and tungstate with stronger effect (5 mM/μM and 0.08 mM/μM). This observation suggests that phosphate and tungstate are bound more stable in Sts-2_{PGM} than in Sts-1_{PGM}. Yet Sts-2_{PGM} displays a significantly lower phosphatase activity when compared to that of Sts-1_{PGM}. We propose two possibilities for the low activity for *p*NPP hydrolysis by Sts-2_{PGM}. First, the amino acids surrounding active site shape the contour to increase specificity towards its substrate(s). Our mutagenesis studies show that by making Sts-2_{PGM} more like Sts-1_{PGM} we increased the ability of Sts-2_{PGM} to hydrolyze *p*NPP, suggesting that residues including Q372V/S582Y and E481V in Sts-2_{PGM} besides the

conserved catalytic amino acids play important roles in substrate recognition. Second, the protonation state of the catalytic residues (His565 in Sts-1_{PGM}) is assisted by the neighboring amino acids (Ser460 and Ala566 in Sts-1_{PGM}) to hydrolyze the substrate. We made both single and double mutations of A446S and S552A in Sts-2_{PGM} for phosphatase activity assays. While single mutations in Sts-2_{PGM} have no effect, Sts-2 double mutant shows a significant increased activity towards *p*NPP hydrolysis, indicating their roles in maintaining protonation state of the catalytic residues in the active site. Moreover, we further confirm that like Sts-1_{PGM}, the Sts-2_{PGM} single and mutants are able to dephosphorylate tyrosine-phosphorylated proteins while wild type shows no detectable effect (data not shown, N. Carpino personal communication). By changing residues other than the conserved active site residues in Sts-2 to more like Sts-1 significantly improved the phosphatase activity of Sts-2_{PGM} suggests that the mutated non-conserved residues have a role to affect the active site activity. It is very likely that unlike Sts-1_{PGM} acts as a phospho-tyrosine phosphatase; Sts-2_{PGM} may act either as a serine/threonine phosphatase or recognize different substrates such as a small molecule. There is also a possibility that Sts-2 requires a condition, such as an intercellular cofactor to activate Sts-2 that we did not provide in our preliminary analysis. Further investigation is required to elucidate the molecular function of Sts-2_{PGM}.

Table 1. Phosphatase activity of Sts wild type and mutants.

Enzyme	k_{cat} s^{-1}	K_m mM	k_{cat}/K_m $s^{-1}M^{-1}$	Activity %
Sts-1$_{PGM}$	70.10	0.50	1400.0×10^2	100
Sts-2$_{PGM}$	0.03	2.05	1.5×10^1	0.01
H366A	ND	ND	ND	ND
E481V	0.17	0.99	1.7×10^2	0.12
S582Y/Q372V	0.41	0.71	5.8×10^2	0.41
A446S/S552A	0.27	0.64	4.2×10^2	0.30

Table 2. Statistics on Data Collection for Sts-2_{PGM}.

	Native	SAD	Phosphate
Wavelength (Å)	0.9	1.0	1.0
Resolution (Å)	83.6 - 1.95	50.0 - 2.25	50.0 - 2.8
Number of Observations	1,303,862	1,398,498	159,957
Number of Unique Reflections	80,016	101,825[#]	28,141
Completeness, overall (last shell)† (%)	99.9 (100.0)	99.4 (97.1)[#]	98.6 (100.0)
Redundancy, overall (last shell)†	7.6 (7.6)	5.5 (4.7)[#]	5.7 (6.0)
$\langle I \rangle / \langle \sigma(I) \rangle$, overall (last shell) †	35.0 (4.5)	18.5 (2.6)[#]	21.1 (2.7)
R_{sym}[*] (%)	8.4 (50.0)	9.8 (56.5)[#]	10.1 (61.7)

† Last shell is 2.02 – 1.95 Å, 2.33 – 2.25 Å , and 2.90 - 2.80 for the native, SAD (tungstate), and phosphate-bound data, respectively.

* $R_{sym} = \Sigma_{i,hkl} | \langle I(hkl) \rangle - I_i(hkl) | / \Sigma_{i,hkl} I_i(hkl)$

[#] The shown statistics are obtained treating I^+ and I^- as independent reflections.

Table 3. Statistics on Model Refinement for Sts-2_{PGM}.

	Native	Tungstate	Phosphate
Resolution (Å)	83.6 – 1.95	84.2 - 2.25	84.2 - 2.77
N° of reflections used	80,219	50,569	26,559
Protein atoms	8,405		
Solvent atoms	291	155	
B factor, (A^2) overall (from Wilson plot)	29.5 (35.9)		
R_{free} †, (%) overall (last resolution shell)	24.1 (26.3)	24.2 (27.6)	27.1 (34.4)
R_{work} ‡, (%) overall (last resolution shell)	20.3 (22.1)	19.4 (22.6)	23.5 (27.7)
R_{cryst} ‡‡, (%)	20.5	19.6	23.7
rms deviation in bond length, (Å)	0.013	0.012	0.014
rms deviation in bond angle, (°)	1.427	1.345	1.523
Estimated standard uncertainties §, (Å)	0.161	0.228	0.434
Ramachandran plane ¶, (%)	91.8/8.1	91.1/8.9	87.1/12.9

† $R_{free} = \Sigma_{(hkl)\varepsilon T}||F_{obs}| - |F_{calc}||/\Sigma_{(hkl)\varepsilon T}|F_{obs}|$, where T is the test set (*Brünger 1992*) obtained by randomly selecting 5% of the data. Last resolution shell is 2.0 – 1.95 Å, 2.3 - 2.25 Å, and 2.85 - 2.77 Å for the native, tungstate- and phosphate-bound structures.

‡ $R_{work} = \Sigma_{(hkl)\varepsilon W}||F_{obs}| - |F_{calc}||/\Sigma_{(hkl)\varepsilon W}|F_{obs}|$, where W is the working set.

‡‡ $R_{cryst} = \Sigma_{(hkl)}||F_{obs}| - |F_{calc}||/\Sigma_{(hkl)}|F_{obs}|$ calculated over the entire set of unique reflections.

§ e.s.u. calculated from R_{free} statistics.

¶ Most favored/additional allowed regions.

Figure 1. Phosphatase activity of Sts-1_{PGM} and Sts-2_{PGM}. 10 mM of Sts-2_{PGM} was required to obtain analyzable data while 25 nM Sts-1_{PGM} was sufficient to catalyze *p*NPP hydrolysis.

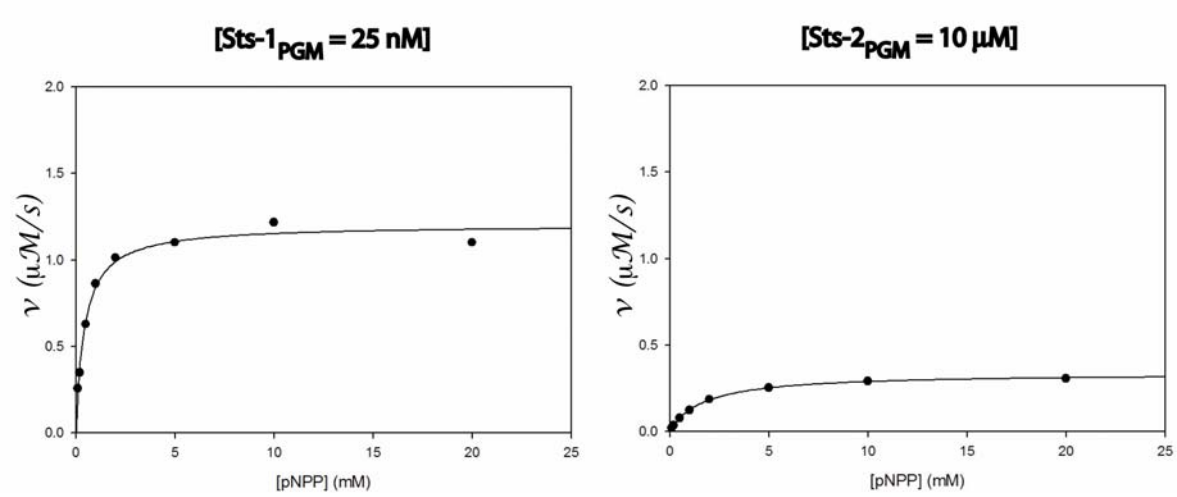

Figure 2. Ribbon diagram of dimeric Sts-2_{PGM}; monomers colored in yellow and blue. This view has the 2-fold axis of the dimer perpendicular to the page. The side chains of His366 and His552 are shown in ball-and-stick representations to indicate the location of the active site.

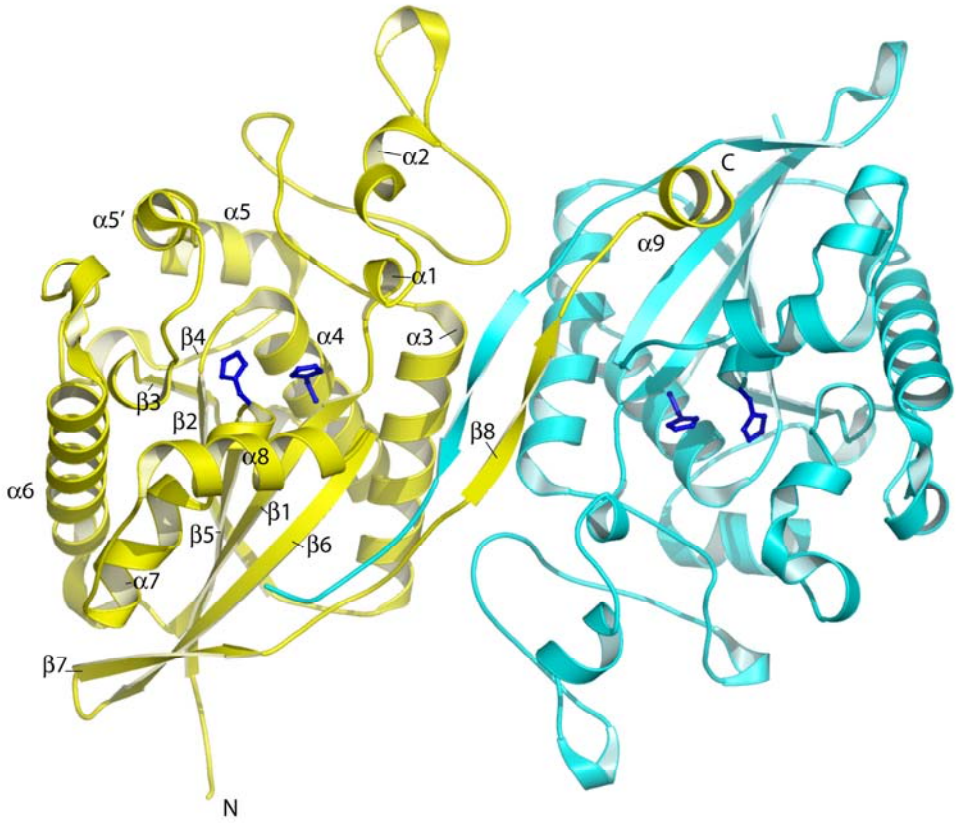

Figure 3. Phosphatase activity of Sts-2_{PGM} H366A mutant. The solid diamond represent the H366A data. 10 μM of protein was used for *p*NPP hydrolysis, see Materials and Methods for details.

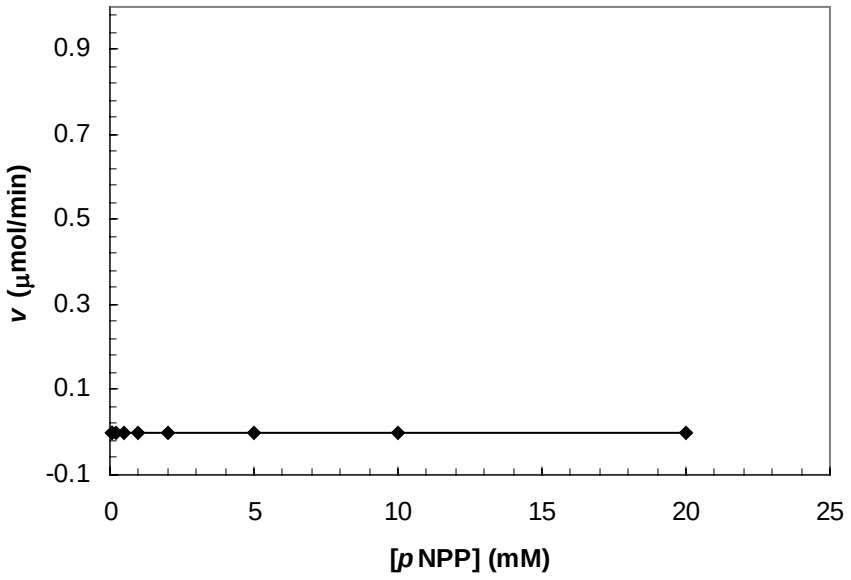

Figure 4. Comparison of the active site residues of Sts-1_{PGM} and Sts-2_{PGM}. The active site residues (Arg379, His380, Arg383, Arg462, and Glu490 in Sts-1) are conserved in sequence and position in Sts-2. However, residues Val386, Val495, and Tyr596 (labeled in red) surrounding the Sts-1 active site are Gln372, Glu481, and Ser582 in Sts-2.

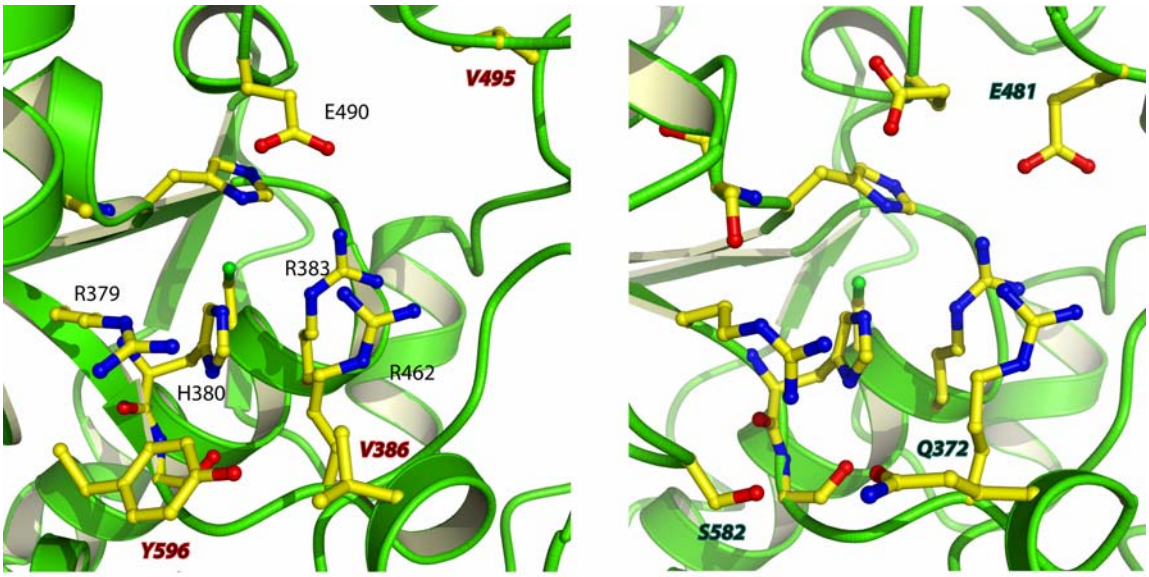

Figure 5. Phosphatase activity of Sts-2_{PGM}. **A**- *p*NPP hydrolyzed by 10 μM Sts-2_{PGM}. **B**- *p*NPP hydrolyzed by 1 μM Sts-2_{PGM} single and double mutants.

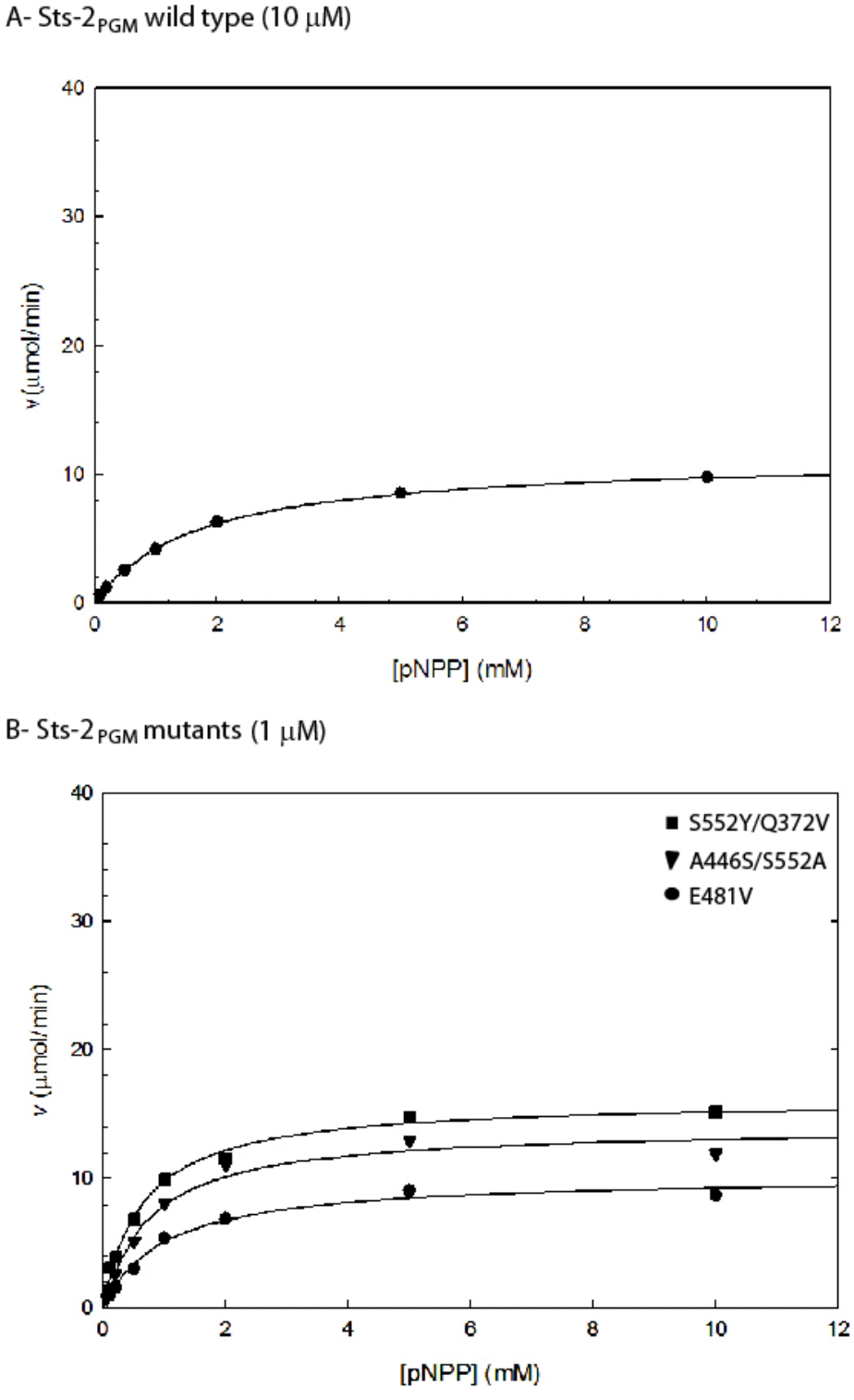

Figure 6. Surface representation of the Sts-1 and Sts-2 active sites. Both active sites form 'L' shape depression. Two catalytic histidines are colored in cyan. The catalytic arginines are in blue, and the general acid glutamate is in red. The yellow socket next to Glu490 of Sts-1_{PGM} is a hydrophobic cavity formed by Ser460, Val495, Phe489, Pro501, and Trp503. This hrydrophobic region is blocked by Glu481 (in red) in Sts-2_{PGM} (bottom). The surface areas in magenta are of residues surrounding the active sites that were mutated in Sts-2_{PGM} (Q372V/S582Y, A446S/S552A) to restore its activity.

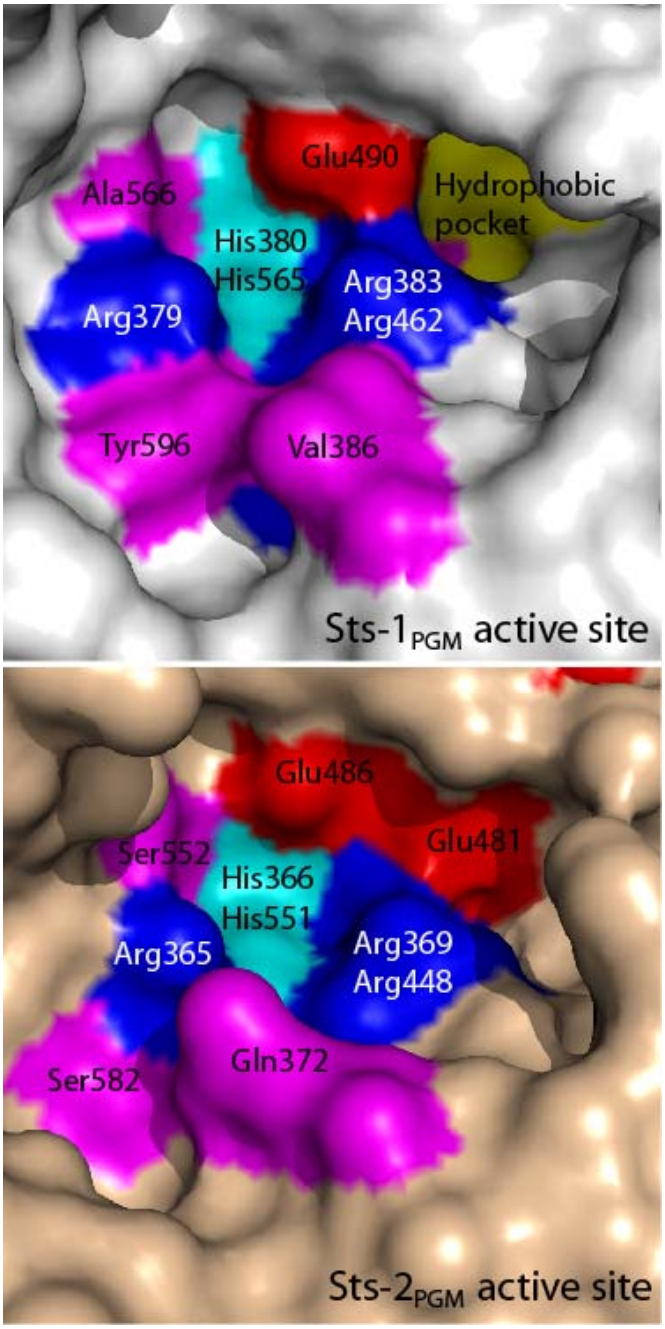

Figure 7. Inhibition of Sts-2_{PGM} activity by phosphate and tungstate. The data was fitted to eq [2]. See Materials and Methods for details.

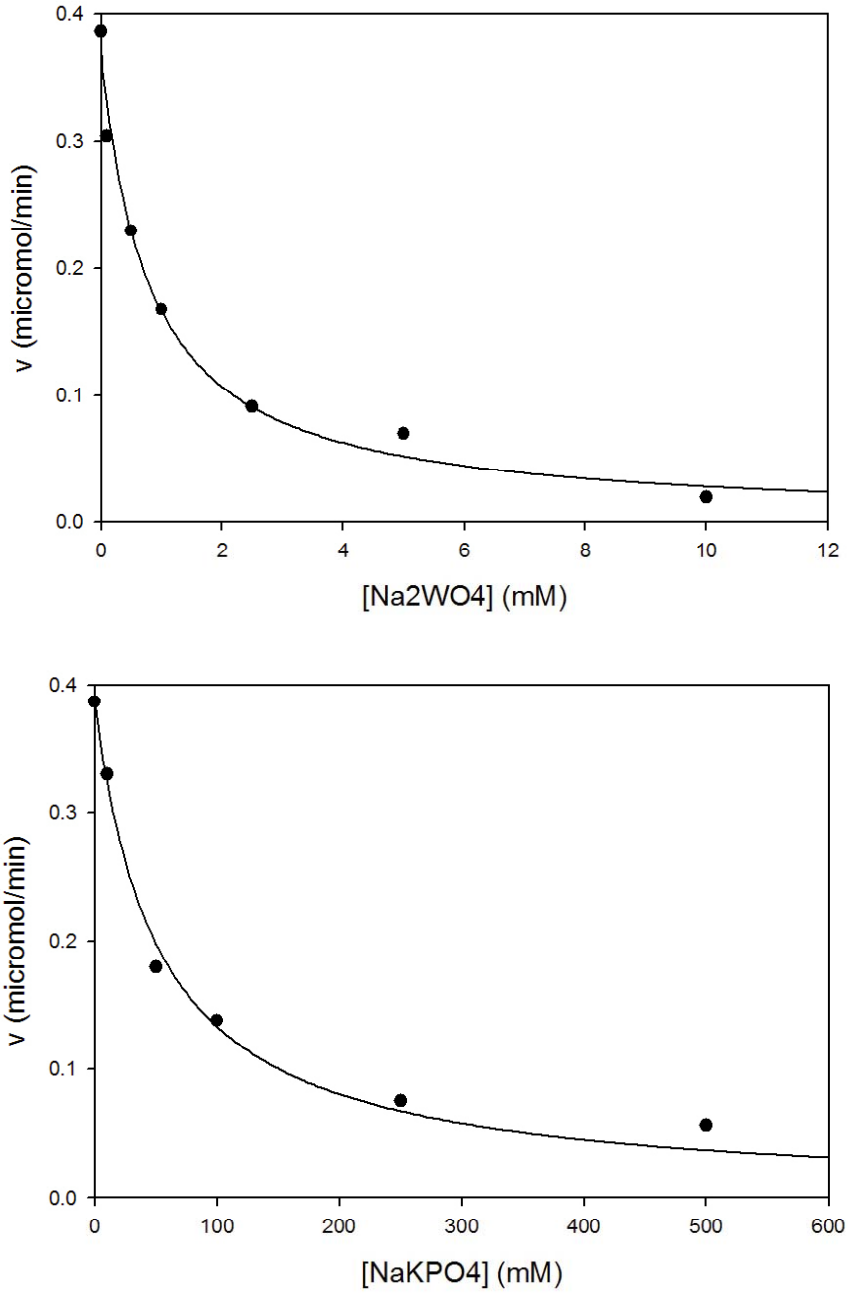

Figure 8. Interactions made by Sts-2_{PGM} active site residues with tungstate and phosphate ions. Both tungstate and phosphate ions are stabilized by the conserved active site residues.

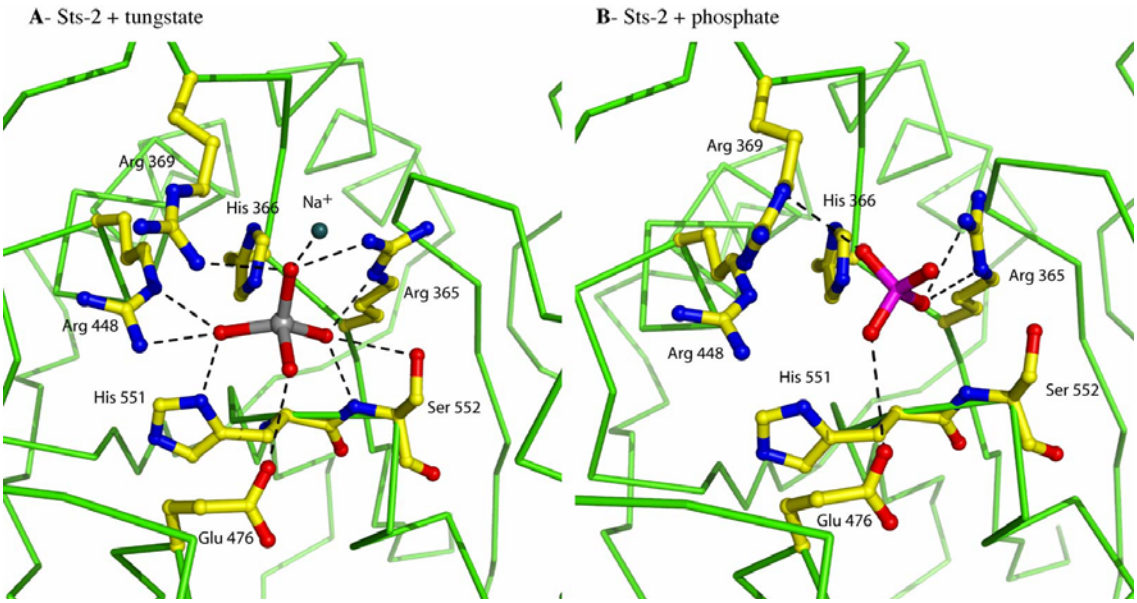

Figure 9. Surface representations of the Sts-2 active sites. The surface area of tungstate is colored by red and phosphate in hot pink. A- the tungstate ion embedded in the active site represents the early stage of the phospho-intermediate formation. B- the phosphate ion on the active site surface represents the stage of phosphate release.

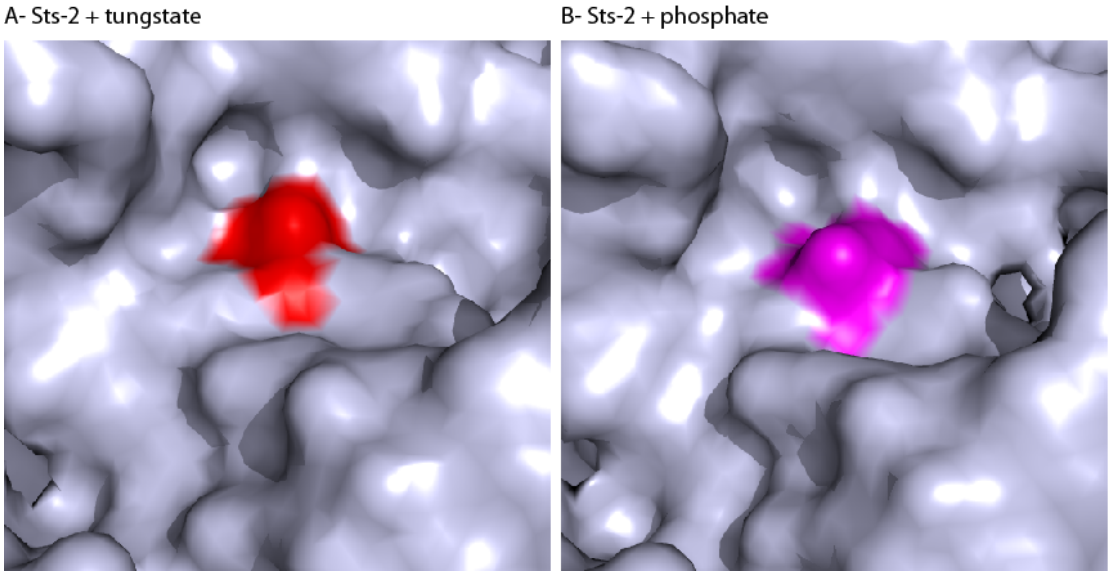

4. CHARACTERIZATION OF A THIRD STS FAMILY MEMBER: EPPase

ABSTRACT

The Silkworm *Bombyx mori* ecdysteroid phosphate phosphatase (EPPase) is involved in the conversion of physiologically inactive conjugated ecdysteroids, including 20-hydroxyecdysone 22-phosphate (20E22P) and ecdysone 22-phosphate (E22P), to active ecdysteroids, such as 20-hydroxyecdysone (20E). 20E is required for insect embryonic development and a deficiency of 20E leads to embryonic diapause. EPPase shares sequence homology with Sts-1, a phosphatase that negatively regulates the TCR signaling. The structure of the EPPase PGM domain in complex with tungstate to 1.76 Å resolution reveals an α/β-type fold that is common to all members of the PGM/AcP superfamily. Superposition of the EPPase and Sts-1 domains shows strong similarity in the catalytic residues lining the active site, consistent with the *in vitro* finding that Sts-1 dephosphorylates E22P. No significant change of the active site was observed between tungstate bound EPPase and Sts-1_{PGM}, indicating the active site does not change conformation upon substrate binding and is relatively rigid. The relatively short distance between tungsten and Nε of the nucleophilic residue His12 (~ 2.45 Å) suggests that the tungstate bound structure mimics an early stage of intermediate formation. Moreover, two residues, Lys224 and Met126 in EPPase, that are not conserved in Sts-1, protrude on the EPPase active site surface implying a role in substrate recognition.

INTRODUCTION

Invertebrates produce hormones to regulate cell reproduction, growth, division, color change, molting and metamorphosis. They do so by controlling the expression of genes involved in ecdysis and metamorphosis. Ecdysone, the prohormone of the major insect molting hormone 20-hydroxyecdysone (20E), which is synthesized from cholesterol in the prothoracic gland (Figure 1), controls the timing of molting (Thummel and Chory, 2002). Juvenile hormone, which is produced by bodies near the brain called the corpora allata, determines the result of molting (Kimball, 2002). In insects, ecdysteroids (ecdysone and its analogues) undergo inactivation by phosphorylation and are stored as physiologically inactive hormones until needed (Webb *et al*., 1995). The predominant phosphorylated steroid form is the 2-phosphate accompanied by small amount of the corresponding 22-phosphate (Webb *et al*., 1995). The important roles of various ecdysteroids for embryonic development in insects have been well demonstrated in the eggs of the silkworm *Bombyx mori* (Makka *et al*., 2002). Insect ecdysteroids such as ecdysone, 20-hydroxyecdysone, and makisterone are steroids that induce growth or molting. Work established from imaginal discs of the Indian meal moth (IAL-PID2) has been reported that the molting hormone, 20-hydroxyecdysone, regulates cell differentiation and was suggested to act in a manner similar to glucocorticoid in mammalian cells (Hatt *et al*., 1994). Analysis of the interaction between the ecdysteroids receptor and various egg ecdysteroids of *B. mori* suggested that the 20-hydroxyecdysone (20E) is responsible for the developmental difference between diapause and non-diapause in *B. mori* embryos (Makka *et al*., 2002). A deficiency of 20E induces embryonic diapause (Yamada and Sonobe, 2003).

Recently, an ecdysteroids-phosphate phosphatase (EPPase) was identified from *B. mori* eggs (Figure 2). EPPase converts inactive ecdysteroids, ecdysone 22-phosphate and 20-hydroxyecdysone 22-phosphate to active phosphate-free ecdysteroids, including 20E, in *B. mori* eggs (Yamada and Sonobe, 2003). The full-length cDNA of EPPase encodes a protein of 331 amino acids was isolated by reverse transcription polymerase chain reaction using degenerate primers on the basis of the partial amino acid sequence obtained from purified EPPase in non-diapause *B. mori* eggs (Yamada and Sonobe, 2003). EPPase is a cytosolic protein that is most active at pH 7.5 and shares ~ 35 % sequence identity to Sts-2, especially in the PGM domain suggesting a potential role of Sts members involved in regulating steroid(s) activation.

B. mori EPPase is a small protein consisting only of a single recognizable PGM domain at its C-terminus (Figure 3). It contains the conserved signature sequence ^{79}RHGE^{82} making it a member of the PGM family. The absence of a UBA and SH3 domains clearly distinguishes it from Sts-1 and -2 despite a high sequence identity in the PGM domain. Using S2 cell line system, Davies *et al*. (2007) showed that three candidate-phosphatases, *B. mori* EPPase, *D. melanogaster* EPPase and Sts-1, hydrolyzed E22P, 3-epiecdysone 22-phosphate (E'22P), and 3-epiecdysone 2-phosphate (E'2P) to varying degrees, with a preference for ecdysteroids with a phosphate at position 22.

Based on sequence and functional similarities between Sts and EPPase, we anticipate that the mechanism of the phosphatase activity in these two proteins is conserved. These similarities make EPPase very appealing since the *in vivo* Sts substrate(s) are still unknown and substrate for EPPase is known. Here we take advantage of the homology of Sts-1 with the silkworm EPPase to study the phosphatase reaction

mechanism and how Sts-1 interacts with its substrate(s). In this study, we used *para*-nitrophenyl phosphate (*p*NPP), a common phosphatase substrate, as our model substrate to study the phosphatase activity of EPPase. X-ray crystallography and site-directed mutagenesis allow us to characterize the roles of residues in the active site during catalytic reaction. This dual approach is in many ways similar to how accumulated knowledge on vaccinia H1-related (VHR), Cdc25, PTP-1B and fructose-2,6-bisphosphatase improved our understanding of Cys-based PTPs (Yuvaniyama *et al*., 1996; Rudolph, 2007; Sarmiento *et al*., 2000; Mizuguchi *et al*., 1999; Zhang *et al*., 1994; Pannifer *et al*., 1998).

MATERIALS AND METHODS

4.2.1 Cell strains and expression system

The PGM domain of ecdysteroid-phosphate phosphatase (EPPase, cDNA provided by Dr. Carpino) was cloned into the pProEx-HTb vector (Life Technologies) and expressed as a His-tagged protein in *E. coli* BL21-CodonPlus strain (Stratagene). The EPPase mutants were generated by the QuikChange XL Site-directed Mutagenesis kit (Stratagene). Cells were cultured in Lurie-Bertani (LB) medium at 37ºC until the absorbance measured at 595 nm reached 0.6. The incubation temperature was reduced to 18ºC and cells were induced for 15 – 20 hours with 0.35 mM IPTG. Cells were harvested and kept at – 80ºC.

4.2.2 Protein purification and crystallization

Cells were lysed by passing through French pressure cell and the lysate was centrifuged at 21,000 rpm for 25 minutes. The supernatant was passed through a Ni-NTA column and washed with buffers containing 5 mM and 20 mM imidazole (pH 8.0). The bound protein was eluted from column with buffer containing 250 mM imidazole and dialyzed against 0.15 M NaCl, 20 mM Tris (pH 8.0), 0.1 mM EDTA, 1 mM DL-dithiothreitol (DTT) (Promega) at 4ºC overnight. Removal of 6x His tag was done by adding rTEV to the dialysis tube and later checked by SDS-PAGE. The EPPase protein was further purified by size exclusion gel filtration (Superdex 200 16/60, GE Healthcare) in buffer containing 0.15 M NaCl, 20 mM Hepes (pH 7.5), 5 mM β-mercaptoenthanol (βME) (Eastman). All the purification steps were carried out at 4ºC.

For crystallization experiments, final concentration of 10 mM DTT was added to EPPase protein at a concentration of 20 mg/ml. To set up crystallization drops, the DTT-treated protein was mixed with reservoir in 1:1 ratio and equilibrated with a reservoir consisting of 0.2 M $MgCl_2$, 0.2 M NaI, 0.1 M Tris pH 7.5, 5 mM Na_2WO_4, and 16% PEG8000 at 4ºC using hanging drop vapor diffusion system. The EPPase crystals appeared after overnight incubation. Crystals were cryo-protected by increasing the PEG8000 (v/v) concentration to 30 % and addition of 10% ethylene glycol before flash freezing them in liquid nitrogen. The addition of tungstate was necessary to obtain good quality of crystals.

4.2.3 Data collection

X-ray diffraction data to 1.76 Å resolution were collected at beamline X6A at the National Synchrotron Light Source (NSLS, Brookhaven National Laboratory) on crystals flash frozen in liquid nitrogen. The structure was solved by the single anomalous dispersion (SAD) technique. A run consisting of 999 frames (300 degrees in total) was collected at the absorption edge of tungsten (E = 12398.5 eV, λ = 1.0 Å) to maximize the anomalous scattering signal. Bijvoet pairs were integrated, scaled and merged separately in HKL2000 (Otwinowski and Minor, 1997). EPPase crystallized in the orthorhombic space group $P2_12_12_1$ with unit-cell dimensions of a = 62.90 Å, b = 134.41 Å, c = 135.19 Å. Diffraction data sets were prepared with the program SHELX-C (Sheldrick and Schneider, 1997). Four tungsten ions were found in the asymmetric unit with the program SHELXD run at a resolution of 2.3 Å and initial phases were calculated with the program

SHELXE (Sheldrick and Schneider, 1997). The initial phases were improved in the density modification program (Cowtan 1994). The model was then built in the program ARP/warp (Morris *et al*., 2002).

The initial model was refined in REFMAC (Murshudov *et al*., 1997) to 1.76 Å resolution and stereochemistry was checked with the program PROCHECK (Laskowski 1993).

4.2.4 Enzyme activity assays

The phosphatase activity of EPPase was measured using *para*-nitrophenyl phosphate (*p*NPP, Sigma) as the substrate. The reaction was initiated by mixing 50 nM enzyme with various concentrations of *p*NPP in a solution containing 0.1M TAB (Tris, acetic acid, and BisTris), 150 mM NaCl, 0.1 mM EDTA, and 1 mM DTT and incubated at 37ºC. At each time interval, the reaction was stopped by addition of 0.1 M NaOH and immediately chilled on ice. The amount of *p*NP converted from *p*NPP was quantified by absorption measurement at 405 nm and carried out using the following relationship:

$OD405 = a \cdot b \cdot c$ ($a = 1.78 \times 10^4\ M^{-1} \cdot cm^{-1}$; b = light path (cm); c = [*p*NP])

4.2.5 Enzyme kinetics analysis

The initial velocities (v) were measured at various substrate concentrations as the slope of the linear part of the *p*NP concentration plotted function of time. To determine the kinetic parameters k_{cat} and K_m, v was plotted at various substrate concentrations (S) and the data points fitted to equation 1 using the program SigmaPlot 5.05 (SPSS Science Inc., Chicago).

$$v = \frac{k_{cat} \bullet S}{(S + K_m)} \qquad [1]$$

4.2.6 Inhibition of EPPase activity

Inhibition of tungstate, phosphate, and vanadate were determined for homogeneous Sts-2_{PGM} in the following manner. Boiling sodium orthovanadate till its color turns clear was required to activate vanadate. The reaction mixture containing sodium tungstate/sodium potassium phosphate/sodium orthovanadate was pre-incubated before adding of protein. At various fixed concentrations of inhibitors (0, 0.1, 0.5, 1, 2.5, and 5 mM), the initial rate at 1 mM *p*NPP was measured as described for phosphatase assay. The data were fit to the equation 2 to obtain the inhibition constant.

$$\nu = V_{max} / (1 + K_i [I]) \qquad (2)$$

RESULTS

4.3.1 Purification of the PGM domain of EPPase

The 6xHis-tagged EPPase PGM domain (261 amino acids, residues 69 – 330) was cloned and first purified on Ni-NTA column, followed by treatment with rTEV for tag cleavage. EPPase was further purified on a size-exclusion gel filtration chromatography (Superdex 200, GE Healthcare). The major peak corresponding to EPPase is consistent with a dimer (Figure 4A). SDS-PAGE analysis revealed that the molecular weight of the purified protein is ~ 30 kDa (Figure 4B). The numbering for $EPPase_{PGM}$ amino acid sequence in this study begins from the N-terminal end of the PGM domain.

4.3.2 Phosphatase activity of EPPase

Yamada and Sonobe (2003) examined the substrate specificity of EPPase. Their data showed that the ability of EPPase to hydrolyze E22P was competitively inhibited by *p*NPP, indicating that *p*NPP binds to the same catalytic site in EPPase as in the case of E22P. In a test of ecdysteroids phosphate phosphatase activity, both Sts-1 and EPPase were shown to hydrolyze ecdysteroids phosphate, E22P, E'22P, and E'2P, with a preference for ecdysteroids with a 22-phosphate (Davies *et al*., 2007). Given that the optimal pH of EPPase-catalyzed E22P hydrolysis was 7.5 (Yamada and Sonobe, 2003), and in order to compare with $Sts\text{-}1_{PGM}$ activity against the same assay system, we used *p*NPP, a general phosphatase substrate, as our model substrate to determine the Michaelis-Menten constant (K_m) and catalytic constant (k_{cat}) of $EPPase_{PGM}$ at pH 7.5. The released product, *p*NP was quantified at OD 405 nm. A linear rate of the product

formation was measured for six or more *p*NPP concentrations and fitted to a Michaelis-Menten equation. The obtained k_{cat} and k_{cat}/K_m of $EPPase_{PGM}$ were 11.67 $sec^{-1}$and $6x10^3$ $M^{-1}s^{-1}$, respectively (Figure 5). In comparison with $Sts\text{-}1_{PGM}$, the k_{cat} and k_{cat}/K_m values of EPP_{PGM} are ~ 6-fold and 20-fold slower than that of $Sts\text{-}1_{PGM}$ (Table 1). Our attempt on generating an $EPPase_{PGM}$ H80A mutant to investigate the catalytic role of His80 was unsuccessful due to the insolubility of the H80A mutant. Instead of replacing His80 with Ala, our next step is to mutate His80 to either serine or asparagine to retain the solubility of EPPase.

4.3.3 Structure determination

The crystal structure of the PGM domain of *B. mori* EPPase was determined by the single anomalous dispersion (SAD) method from data collected at the edge of tungsten (λ = 1.0 Å). The tungstate-derivative crystal produced an interpretable electron density map calculated to 1.76 Å. The crystals contain four molecules (chain A to D) in the asymmetric unit, corresponding to a solvent content of 42%. The molecules are organized into two dimers, A/B and C/D. The current model is refined to a crystallographic R factor of 18.8% and a free R factor of 22.1%. Table 2 and 3 summarize statistics on data collection and model refinement. The stereochemistry of the current model shows that 92.6% of the residues in the most favored regions of the Ramachandran plot (Figure 6), 6.9% fall into the additionally allowed regions.

4.3.4 Overall structure of the PGM domain of EPPase

We superposed all four copies of EPPase and the RMS deviation is 0.324 – 0.402 Å (Table 4) indicating that these chains are identical. Since the electron density of chain A is clearer than other chains, conclusions drawn in this chapter are mainly derived from chain A. The $EPPase_{PGM}$ monomer has an α/β structure similar to that adopted by all members of the PGM/AcP superfamily (Jedrzejas, 2000). The structure has a central seven-stranded β-sheet (β4-β3-β2-β5-β1-β6-β7) that forms the core of the monomer. This central β-sheet is surrounded by seven α-helices. The C-terminal tail (residues 306 – 330) extends outside of the core to interact with the C-terminus of the neighboring monomer (Figure 7). The ^{79}RHGE^{82} signature motif is located at the carboxyl end of the central β sheet, and the two arginines (Arg79 and Arg160) and the two histidines (His80 and His260) of EPPase that are homologous to the Sts-1 catalytic residues (Arg379, His380, Arg462, His565) are also present at this location, forming a semi-barrel-shaped depression. This homology suggests a conservation of the catalytic mechanism between the two proteins.

4.3.5 Structural comparison to $Sts\text{-}1_{PGM}$ and other known PGMs

Structure superposition of the Cα coordinates of the PGM domains of EPPase and $Sts\text{-}1_{PGM}$ were made with the program SSM (Krissinel and Henrick, 2004) in the CCP4 suite (1994) and visualized by the program PyMOL (DeLano, 2002). The RMS deviation for structurally equivalent Cα atoms is 1.315 Å. The structures reveal a closer resemblance between $EPPase_{PGM}$ and $Sts\text{-}1_{PGM}$ than that between $Sts\text{-}1_{PGM}$ and ecPGM (Figure 8). The regions (insert 1 and 2) that are topologically different between $Sts\text{-}1_{PGM}$

and ecPGM superimpose well between Sts-1_{PGM} and $EPPase_{PGM}$. The C-terminus of both proteins (EPPase residues 315 – 330; Sts-1 residues 614 – 629) are involved in dimerization, while ecPGM dimerizes through one of its α-helix from the opposite side. A region (residues 275 – 293) close to one side of the proposed catalytic pocket of EPPase appeared to be a less structured loop while it is an α-helix in Sts-1 (residues 578 – 594).

4.3.6 The $EPPase_{PGM}$ active site

The structure similarity between $EPPase_{PGM}$ and Sts-1_{PGM} is particularly strong in the active site residues within the catalytic pocket. In Sts-1_{PGM}, His380 was proposed as the nucleophile in the dephosphorylation reaction, and five other residues (residues Arg379, Arg383, Arg462, Glu490, and His565) coordinate to the negatively charged phosphate that is being hydrolyzed (Mikhailik *et al*., 2007). The homologous residues within EPPase (Arg79, His80, Arg83, Arg160, Glu188, and His260) adopt an identical configuration (Figure 9), suggesting they are involved in the dephosphorylation reaction in EPPase.

Figure 10 shows surface electrostatic potential representation of $EPPase_{PGM}$, Sts-1_{PGM} and Sts-2_{PGM} dimers, visualized by the program PyMOL. As shown on the left panel, the regions with positive charges (in blue) formed by the side chains of the conserved arginines (Arg79, Arg83 and Arg160 in EPPase) are the active sites for the substrates. Although the positive charge distribution on the Sts-2_{PGM} active site surface is less pronounced, both active sites of these three protein dimers face the same side suggesting a similar mechanism for substrate binding is employed. The back views of

these three proteins (180º rotation along horizontal axis) reveal a deep, long groove (~ 55 Å) between dimerization areas (Figure 10 in the right). The center of the groove of Sts-1_{PGM} is formed by a group of proton donors (Arg439, Gln465, Asn469, and Lys472), which are scattered in $EPPase_{PGM}$ and Sts-2_{PGM}. This groove may play a role in receiving other ligands or to fit the N-terminal portion of Sts-1 and Sts-2.

The EPPase PGM domain could only be crystallized in the presence of tungstate. The electron density of the tungstate molecule was very clear in the electron density map. The side chains of residues Arg79, His80, Arg83, Arg160, His260, and Lys292 stabilize the tungstate ion through a network of tight H-bonds (Figure 11). In addition, Glu188 mediates two water molecules to coordinate the tungstate ion. A network of hydrogen bonds is also found between these residues and other residues, implying that the geometry of the active site is rigid. The tungstate ion is trapped at the center of the active site where the residue His80 points to the tungsten atom with the ring Nε nitrogen atom (2.43 to 2.49 Å in all four copies). Three water molecules were found in the active site (Figure 11). Residues Arg79, Arg83, and Arg160 and these water molecules coordinates the anionic oxygen atoms of tungstate through hydrogen bonds. Lys292, which has no equivalent in Sts-1, was also found to make hydrogen bond to the oxygen of tungstate. Besides, the carboxyl oxygen of Glu188 makes strong interaction with Lys196 (3.33 Å), suggesting that Lys196 mediates the protonation state of Glu188. This geometry implies an in-line nucleophilic attack by His80, with Glu188 likely to be the general acid to deprotonate the water molecule to attack the tungstate.

The surface presentations of the $EPPase_{PGM}$ and Sts-1_{PGM} active sites show an "L-shape" depression containing two small pockets (Figure 12). One pocket is formed by the

catalytic residues, the second pocket is formed by less conserved residues (residues Val495, Phe489, Pro501, and Trp503 in Sts-1; Phe187, His193, Ile198, and Phe200 in EPPase). The first pocket is where the phosphate and tungstate sit in Sts-1_{PGM} and $EPPase_{PGM}$. However, unlike Sts-1_{PGM} active site that has an open accessible binding pocket, the active site of $EPPase_{PGM}$ seems to be governed by a residue, Lys292 to form a branch on top of two catalytic histidines (His80 and His260), leaving a limited space for substrate binding.

4.3.7 Phosphatase activity of EPPase is inhibited by Tungstate and Phosphate

The phosphotyrosyl-protein phosphatase activity is sensitive to several classical inhibitors of prostatic acid phosphatase including L(+)-tartrate, molybdate and vanadate (Li *et al*., 1984). Potent inhibitors such as tungstate were used to mimic phosphate meioty for the phosphatases (e.g. SixA) has been published in the literature (Hamada *et al*., 2005). It was found that the activity of EPPase was scarcely affected by L(+)-tartrate (Yamada and Sonobe, 2003), we tested the inhibition effect of other phosphate analogs on EPPase. Like many other histidine phosphatases and Sts proteins, both tungstate and phosphate are inhibitors for EPPase for *p*NPP hydrolysis. Fitting the data to a hyperbolic equation shows that a tungstate concentration of 52 μM decreases the phosphatase activity of EPPase by 50% while a 39 mM concentration of phosphate is needed to reach the same inhibition level (Figure 13). In comparison, the inhibition of tungstate to EPPase (1 μM/nM) is stronger than it is to Sts-1_{PGM} (3.2 μM/nM), while inhibition of phosphate to EPPase (780 μM/nM) is weaker than it is to Sts-1_{PGM} (420 μM/nM).

DISCUSSION

The aim of this research was to determine the crystal structure of $EPPase_{PGM}$ and use the obtained information to understand how Sts-1 interacts with its substrate. Previously, the silkworm *B. mori* EPPase was shown to be involved in the conversion of E22P and 20E22P to active ecdysteroids, which are molting hormones required for insect embryonic development (Yamada and Sonobe, 2003). This ecdysteroid-phosphate phosphatase activity was later observed in Sts-1 with an EPPase-like preference of substrates in the order of E22P > E'22P > E'2P (Davies *et al*., 2007). Herein, the first crystal structure of recombinant silkworm *B. mori* EPPase PGM domain in complex with tungstate ion was determined by single wavelength anomalous dispersion method, phased and refined to 1.76 Å resolution.

The overall structure of the $EPPase_{PGM}$ monomer reveals an α/β-type structure with strong homology to Sts-1 and superposition analysis showed strong conformational similarities of the conserved active site residues, His80, Arg83, Arg160, Glu188, and His260, in $EPPase_{PGM}$ with their homologues in $Sts\text{-}1_{PGM}$. Moreover, $EPPase_{PGM}$ dimerizes through its extended C-terminal region like $Sts\text{-}1_{PGM}$ does suggesting that EPPase shares closer conservation to Sts-1 than to other PGM/AcP family members. The tungstate ion, which mimics phosphate moiety, is located at the predicted active site and stabilized by conserved catalytic residues. The short distance between tungsten and the Nε of His80, the nucleophilic residue (2.4 – 2.5 Å in the four copies), is consistent with the structure of an early attack on the substrate. Superposition analysis of the active site residues of the PGM domain of EPPase (Arg79, Arg83, Arg160, Glu188, and His260)

and apo-structure of Sts-1 (Arg379, Arg383, His565, Arg462, and Glu490) showed identical conformation. This structural conservation indicating both proteins must employ a similar catalytic mechanism and the active site does not substantially change its structure upon substrate binding. Based on the structural similarity, could the PGM domain of Sts-1 have steroid-like substrate(s)?

In general, steroids are derived from a common precursor, cholesterol, and can be divided into four major types: progestins, androgens, estrogens, and corticoids (Ashwell *et al*., 2000). It has been shown that estrone, a subtype of estrogens, is stored as estrone sulfate (Figure 14) in human tissue and can be converted to biologically active form by steroid sulfatase (STS) (Reed *et al*., 2005). Estrogens contribute to the growth of breast cancers (Suzuki *et al*., 2005), and an increased expression of STS has been observed in breast carcinoma tissues (Reed *et al*., 2005). It will not be surprising that Sts-1 may function like STS to regulate the activation of steroid-like substrate(s) in human tissue.

Although structures that have similar features are likely to share closer evolutionary relationship, the work we presented was done with the PGM domains of EPPase and Sts proteins. While EPPase is a one-domain protein exists in insects, Sts proteins contain three domains and exist in mammalian cells. The importance of two other domains UBA and SH3 in Sts-1 was shown that domain-inactivating mutations impair the ability of Sts-1 to reduce the hyperproliferative response of Sts-1/2$^{-/-}$ (Mikhailik *et al*., 2007). This observation indicates the UBA and SH3 domains may be involved in the intracellular localization of Sts-1 or may contribute to substrate specificity. Moreover, the known EPPase substrate, ecdysteroid phosphate is so far discovered only from insects, no study has shown any ecdysteroid phosphate is existed in

human. Whether there is an “ecdysteroid phosphate-like” analog in human that is recognized by Sts proteins requires further studies for understanding the structural evolution and expanding the category of the phosphatase superfamily.

Figure 1. The ecdysteroid biosynthesis pathway in *Drosophila*. (Taken from Thummel and Chory, 2002; original diagram from Warren *et al*., 2002)

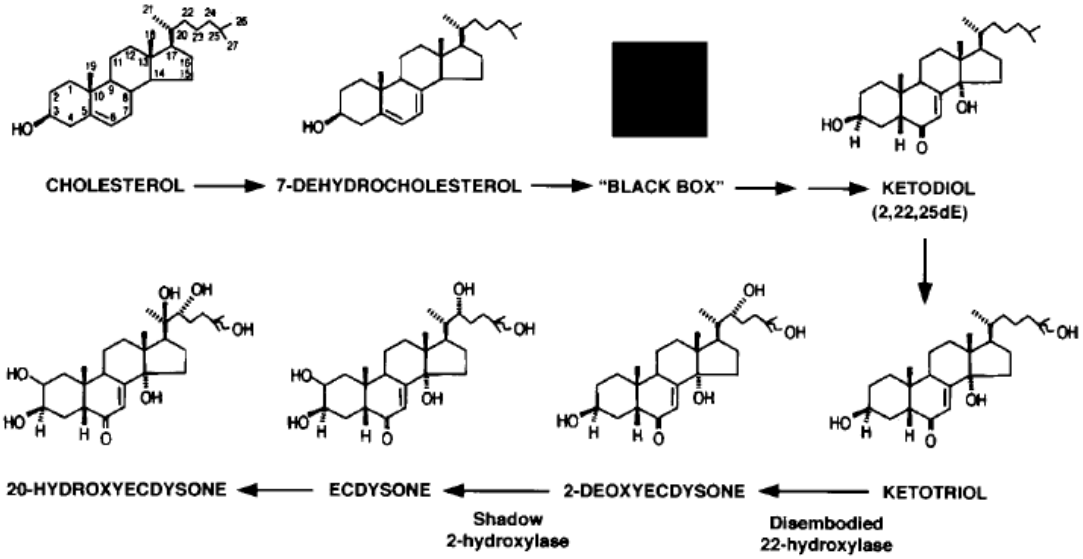

Figure 2. Reversible conversion of ecdysone 22-phosphate to ecdysone by two enzymes: ecdysteroids-phosphate phosphatase and ecdysteroids kinase (Yamada and Sonobe, 2003). Ecdysone is a prohormone of the insect molting hormone 20-hydroxyecdysone.

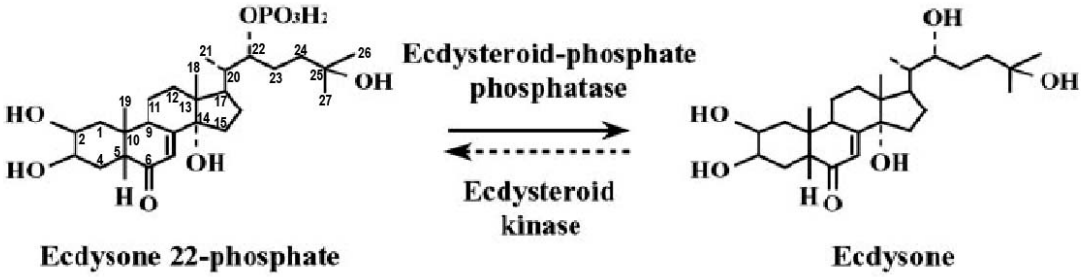

Ecdysone 22-phosphate

Ecdysone

Figure 3. Domain structures of *B. mori* EPP and three closely related proteins. UBA (blue): ubiquitin association domain. SH3 (yellow): Src-homology domain. PGM (pink): phosphoglycerate mutase homology region.

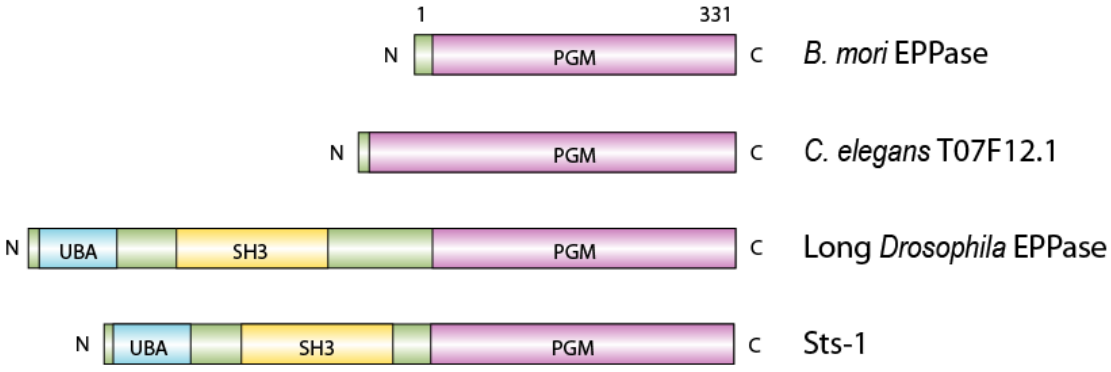

Figure 4. Purification of EPPase PGM domain. (A) Gel filtration profile of $EPPase_{PGM}$ on Superdex 200 16/60 (GE Healthcare). The y-axis indicates the absorption at 280 nm for the eluted sample. The x-axis indicates the elution time and the numbers in red indicates the eluted fractions. (B) SDS-PAGE analysis of the purified $EPPase_{PGM}$ from gel filtration. The fraction numbers on the gel correspond to the fractions from the peak of 76.99 mAu in (A).

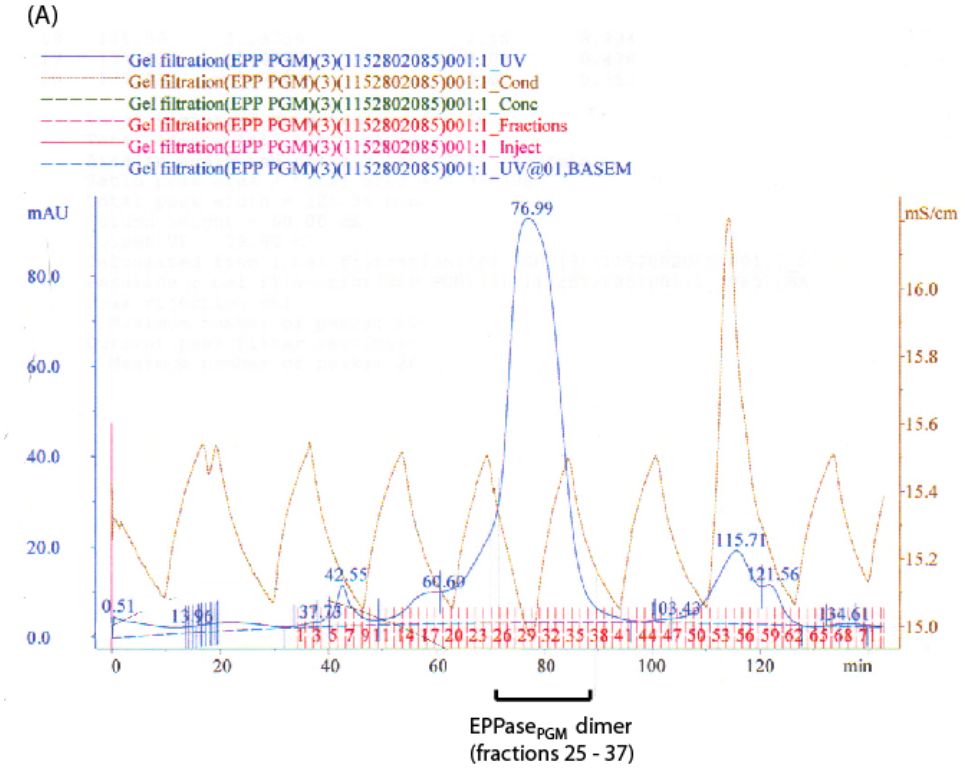

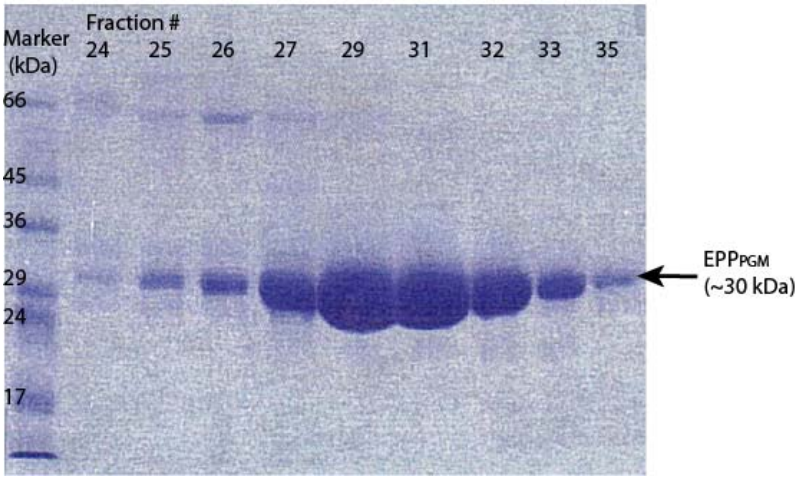

Figure 5. Phosphatase activity of the *B. mori* EPPase PGM domain. Assay was carried out with 50 nM protein at pH 7.5 and 37ºC. The data set was fitted to eq [1] to obtain K_m and k_{cat}.

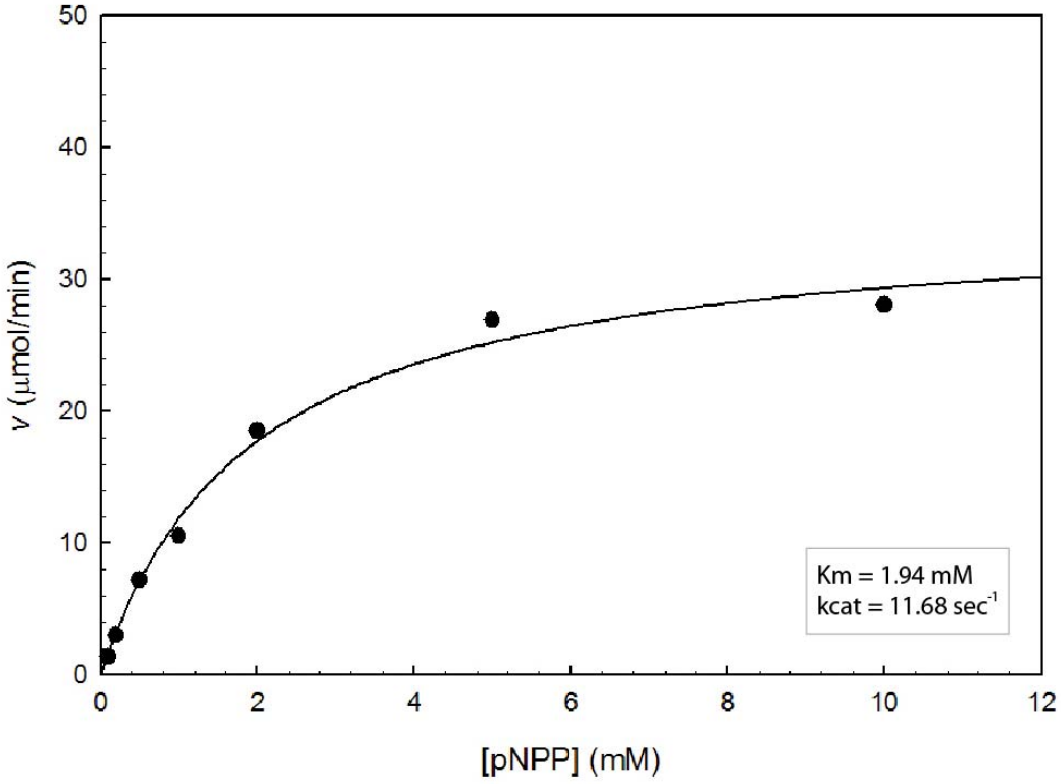

Figure 6. Ramachandran plot of $EPPase_{PGM}$ structure refinement produced by PROCHECK.

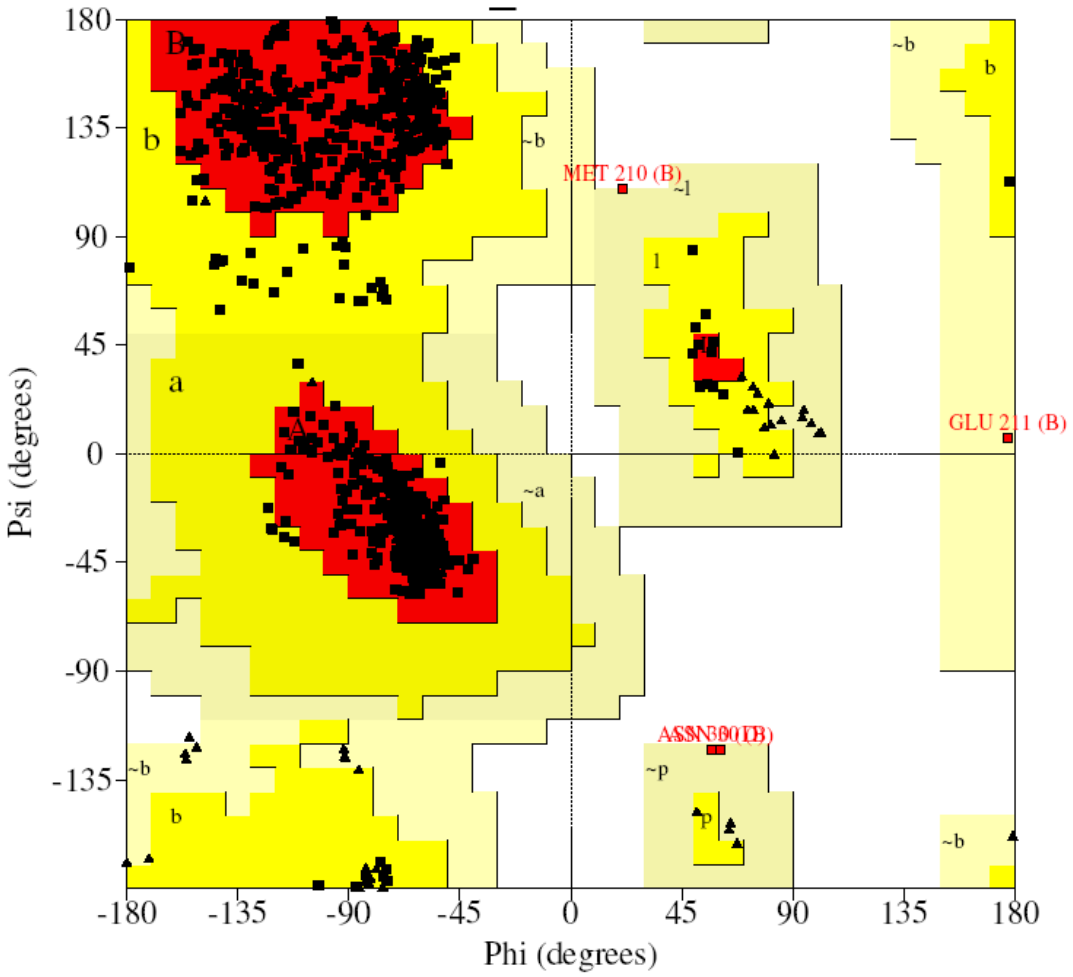

Plot statistics

Residues in most favoured regions [A,B,L]	801	92.8%
Residues in additional allowed regions [a,b,l,p]	58	6.7%
Residues in generously allowed regions [~a,~b,~l,~p]	4	0.5%
Residues in disallowed regions	0	0.0%
Number of non-glycine and non-proline residues	863	100.0%
Number of end-residues (excl. Gly and Pro)	423	
Number of glycine residues (shown as triangles)	96	
Number of proline residues	68	
Total number of residues	1450	

Based on an analysis of 118 structures of resolution of at least 2.0 Angstroms and R-factor no greater than 20%, a good quality model would be expected to have over 90% in the most favoured regions.

Figure 7. Ribbon diagram of $EPPase_{PGM}$ dimer structure. The top view has the 2-fold axis of the dimer perpendicular to the page. In the bottom view, the 2-fold axis is parallel to the page. The side chains of His80 and His260 are shown as ball-and-stick representations to indicate the location of the active site. Prepared by PYMOL (http://pymol.sourceforge.net/).

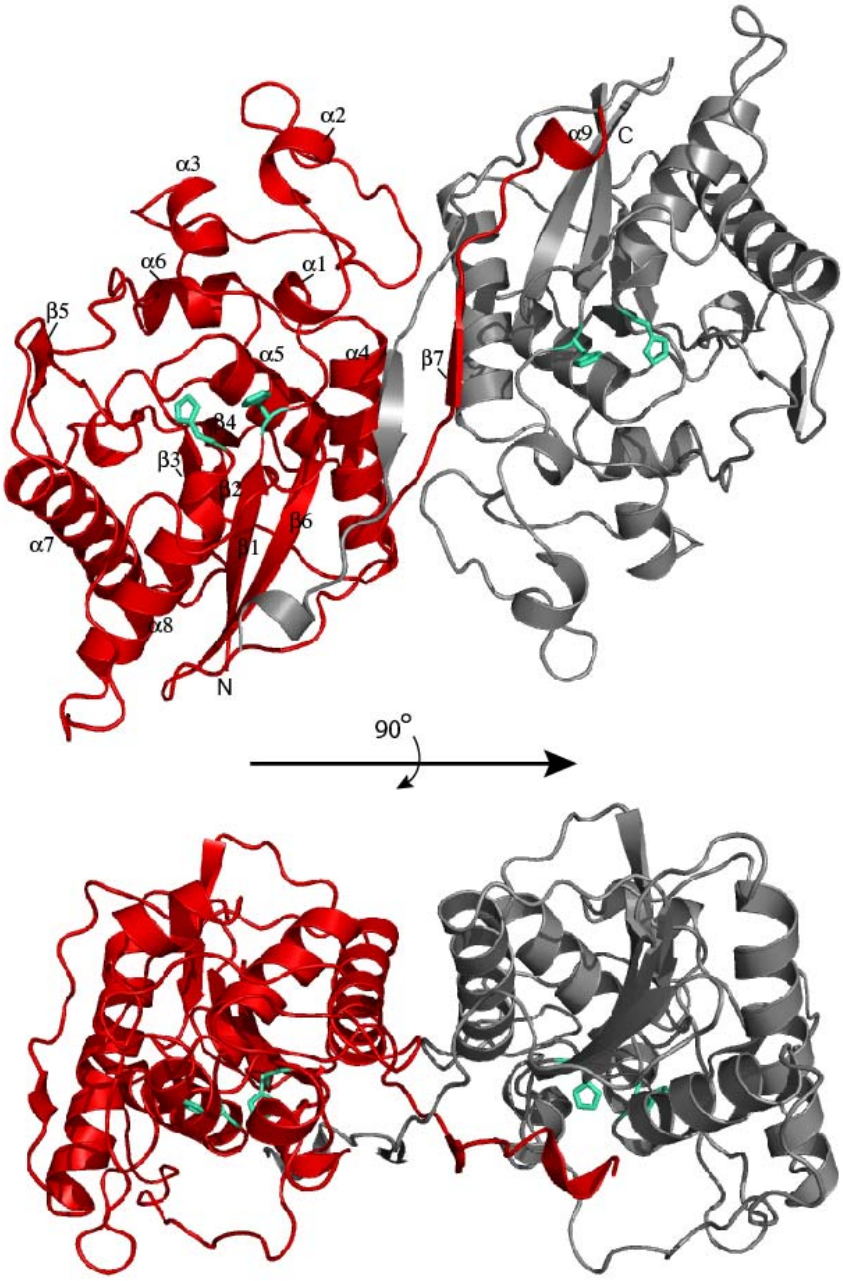

Figure 8. Comparison of EPP_{PGM} with Sts-1_{PGM}. (A) Critical catalytic residues of mSts-1_{PGM}, and the homologous residues of $EPPase_{PGM}$, are shown in gold ball-and-stick representation. The region that deviate between the two structures, insert H (EPPase residues 275 – 293), is in violet. The two regions that are different in ecPGM and Sts-1, insert 1 and 2, are in red and blue, respectively. The C termini are shown in green. (B) Cα superposition of Sts-1_{PGM} and $EPPase_{PGM}$ made by the program SSM (RMSD=1.315 Å). The loop between two arrows (residues 275 – 293) in EPPase is deviated in same region of Sts-1 (residues 578 – 594).

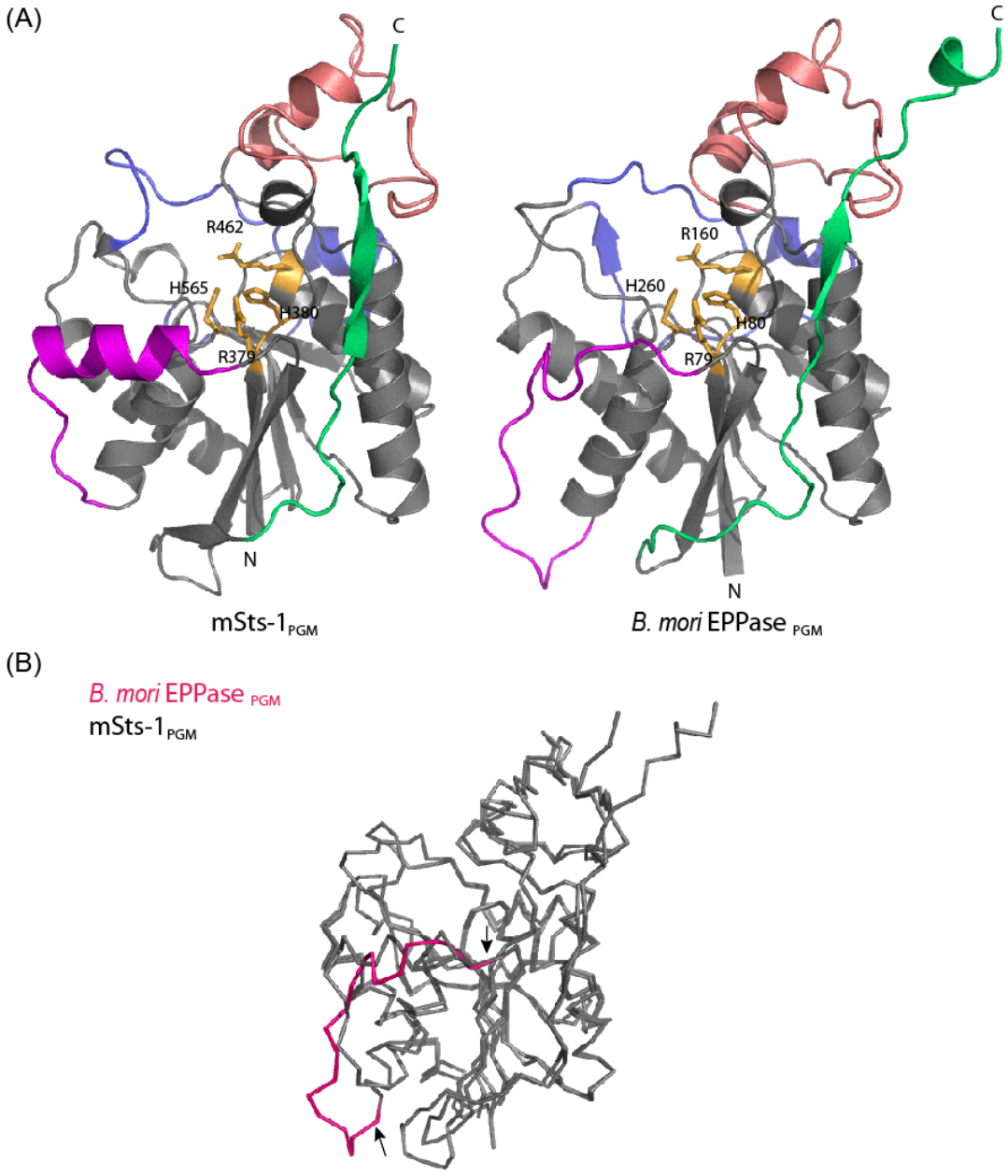

Figure 9. Superposition of the active site residues of Sts-1_{PGM} (pale yellow) with the homologous residues of $EPPase_{PGM}$.

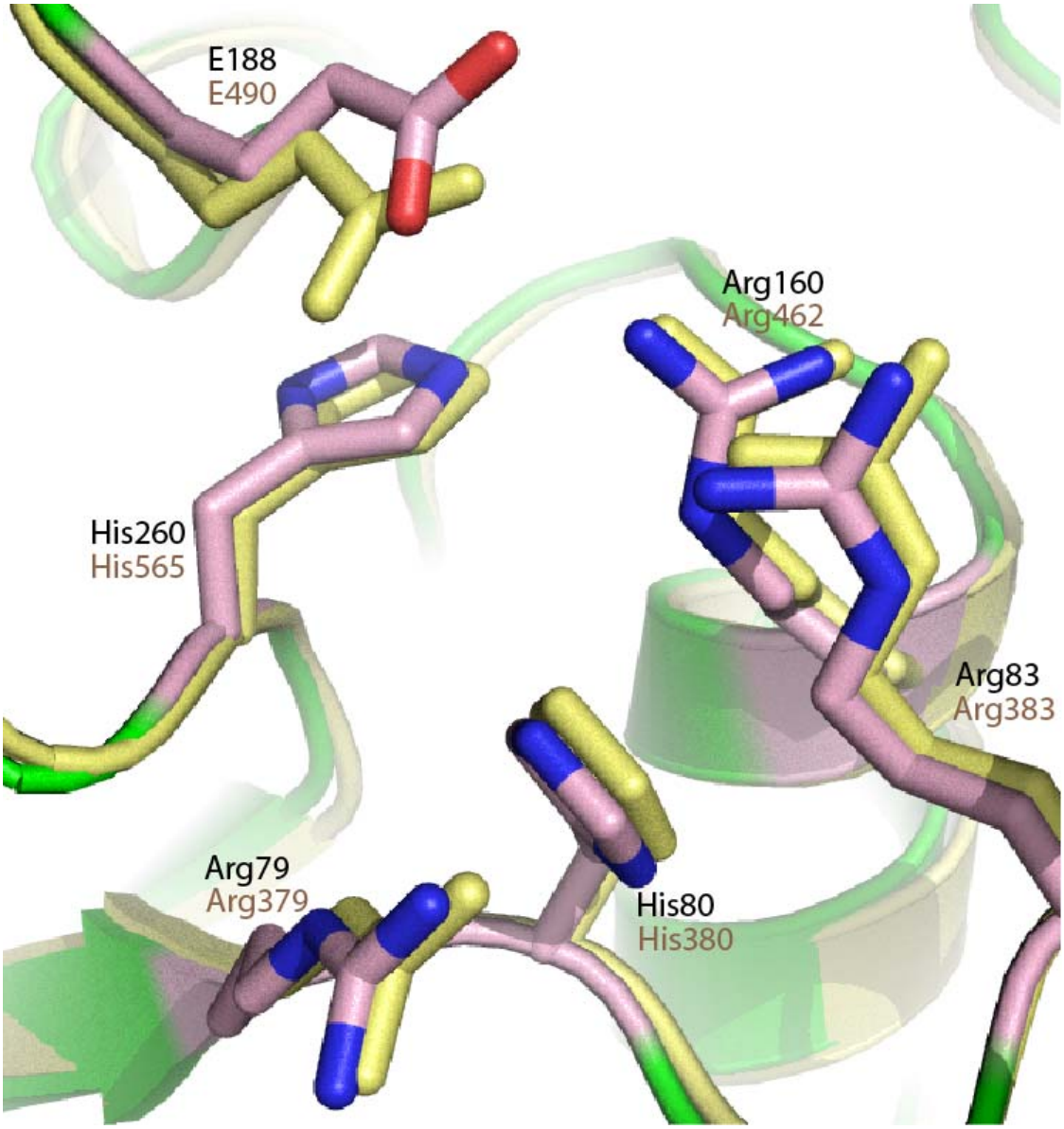

Figure 10. Electrostatic potential representation of $EPPase_{PGM}$, $Sts\text{-}1_{PGM}$, and $Sts\text{-}2_{PGM}$ dimers superimposed on the backbone. The electrostatic potentials are contoured from –60 (intense red) to 60 k_BT/e (intense blue).

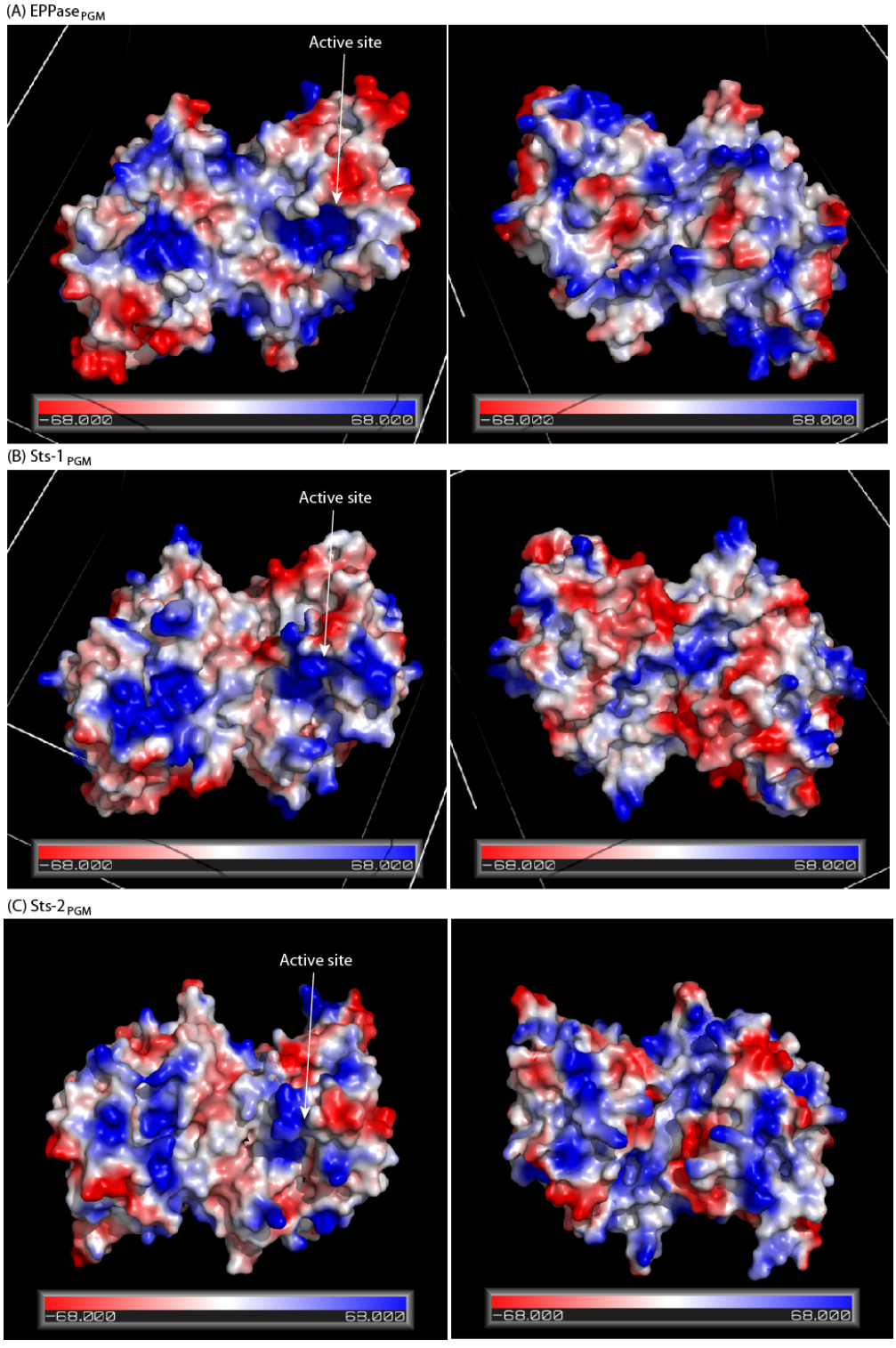

Figure 11. Interactions made by $EPPase_{PGM}$ active site residues with a tungstate ion. The $EPPase_{PGM}$ active site residues interacting with the tungstate molecule are shown in ball-and-stick representation. Dash lines represent hydrogen bond interactions. Secondary structure elements are displayed in pale green.

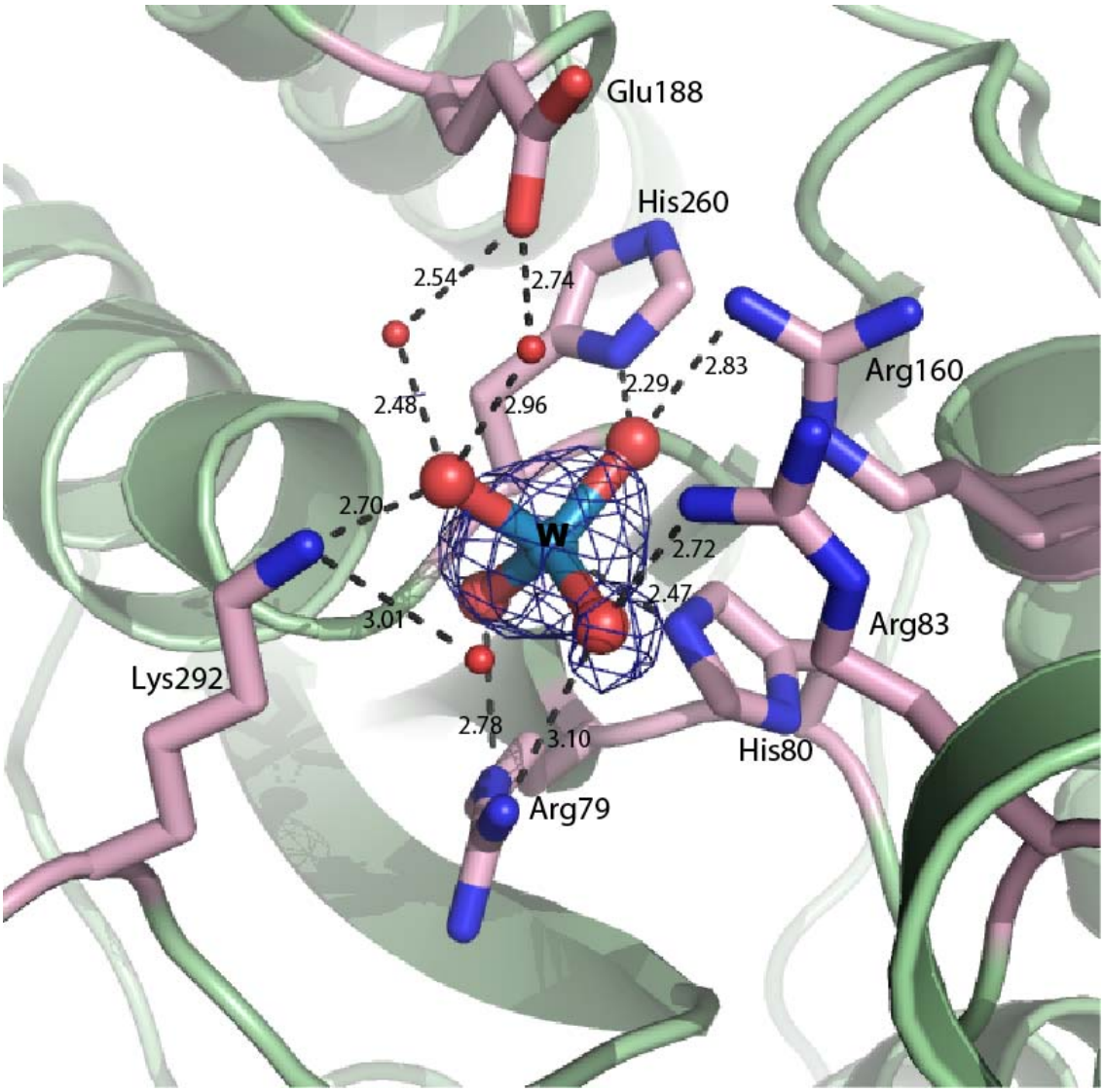

Figure 12. Surface representation of the active sites of the EPPase and Sts-1 PGM domain. The conserved catalytic histidines (His80 and His260 in EPPase, His380 and His565 in Sts-1) (cyan) are shown in the center of active sites of both proteins (top and bottom), surrounded by a glutamic acid (red) and two arginines (blue). Two residues, Lys292 (violet) and Met194 are on top of the catalytic pocket of $EPPase_{PGM}$.

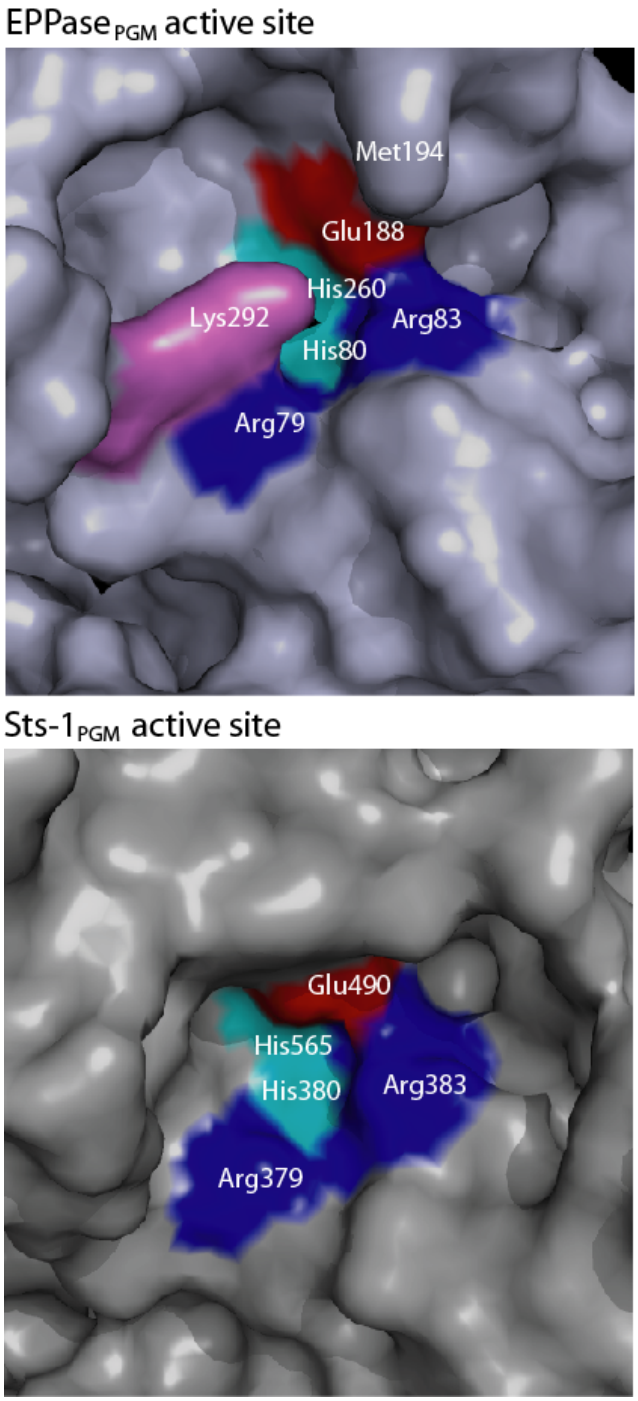

Figure 13. Inhibition effect of tungstate and phosphate on $EPPase_{PGM}$ activity for *p*NPP hydrolysis.

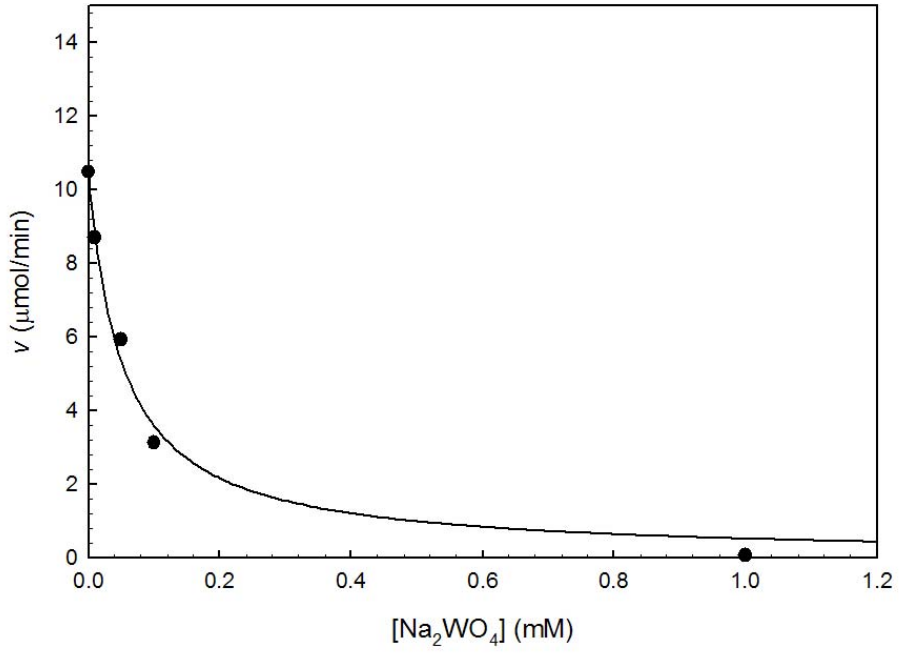

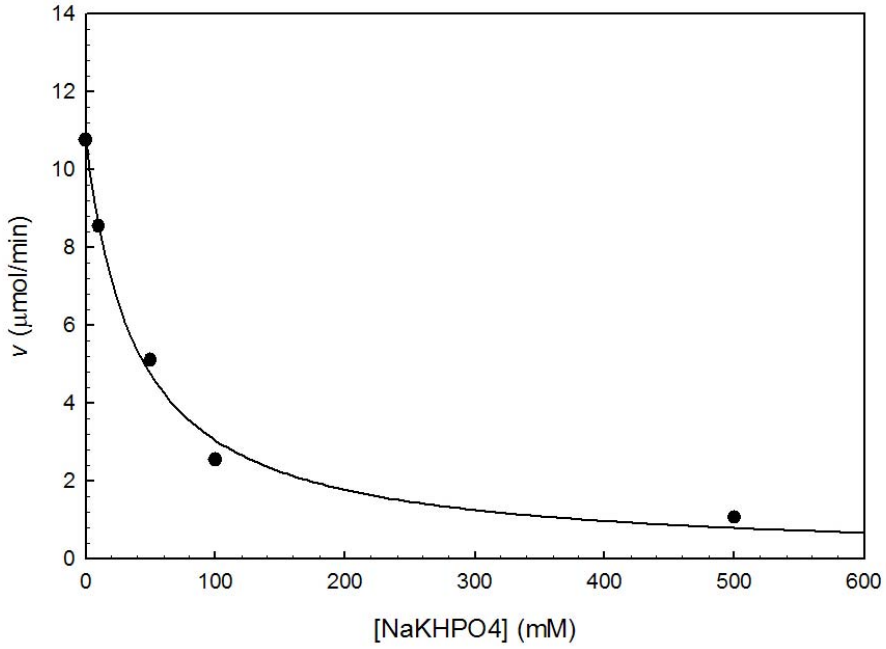

Figure 14. The scheme diagram of estrone sulfate (E1S) converting to estrone (Reed et al., 2005). SULT: sulfotransferase.

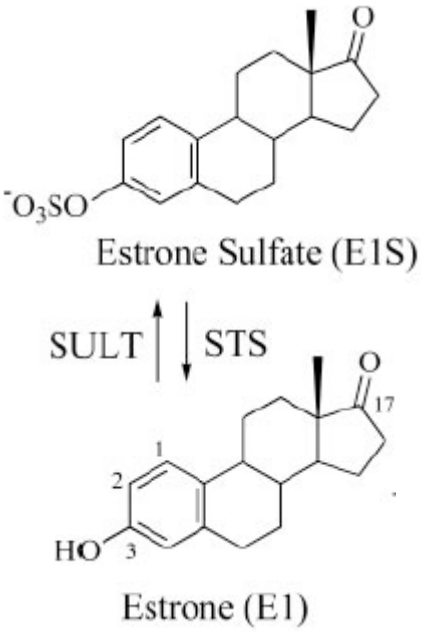

Table 1. Kinetic analysis. Phosphatase activity of the PGM domain of Sts-1, Sts-2, and EPPase was determined at pH 7.5, using *p*NPP as substrate.

Enzyme	k_{cat} s^{-1}	K_m mM	k_{cat}/K_m $s^{-1}M^{-1}$	Activity %
Sts-1	70.10	0.50	14000.0×10^1	100
Sts-2	0.03	2.05	1.5×10^1	0.01
EPPase	11.68	1.94	600.0×10^1	4.28

Table 2. Statistics on data collection for $EPPase_{PGM}$.

	SAD
Wavelength (Å)	1.0
Resolution (%)	95.35 – 1.76
Completeness, (%) overall (last shell)	99.17 (91.96)
Redundancy, overall (last shell)	6.9 (6.3)
Number of reflections	104,620
$\langle I \rangle / \langle \sigma(I) \rangle$, overall (last shell)	29.6 (2.6)
R_{sym} *, (%)	9.9

The last resolution shell is the interval 1.80 - 1.76 Å for the tungstate bound EPPase.

* R_{sym} =* $R_{sym} = \Sigma_{i,hkl} |\langle I(hkl) \rangle - I_i(hkl)| / \Sigma_{i,hkl} I_i(hkl)$

Table 3. Statistics on model refinement for $EPPase_{PGM}$.

Refinement statistics	+ $\mathbf{WO_4^{--}}$
Resolution Range (Å)	95.35 – 1.76
N° of unique reflections	108,260
Water molecules	559
B factor, (A^2) overall (from Wilson plot)	25.18 (19.23)
R_{free} †, (%) overall (last resolution shell)	22.1 (24.7)
R_{cryst} ‡, (%) overall (last resolution shell)	18.8 (21.1)
Rms deviation in bond length (Å)	0.013
Rms deviation in bond angle (°)	1.423
Estimated coordinate error § (Å)	0.117/ 0.073
Ramachandran plane ¶ (%)	92.6/6.9

The last resolution shell is the interval 1.80 - 1.76 Å for the tungstate bound EPPase.

† $R_{free} = \Sigma_{(hkl)\varepsilon T}||F_{obs}| - |F_{calc}||/\Sigma_{(hkl)\varepsilon T}|F_{obs}|$, where T is the test set (*Brünger 1992*) obtained by randomly selecting 5 % of the data.

‡ $R_{cryst} = \Sigma_{(hkl)}||F_{obs}| - |F_{calc}||/\Sigma_{(hkl)}|F_{obs}|$.

§ Estimated coordinate error based on R_{free}/maximum likelihood.

¶ Most favored/additional allowed regions.

Table 4. RMS deviation between four copies of EPPase PGM domain. Superposition done with the program SSM (Krissinel and Henrick, 2004) of the CCP4 suite (1994).

	RMSD (Å)			
Chain	A	B	C	D
A	—	0.402	0.331	0.349
B		—	0.390	0.358
C			—	0.324
D				—

CONCLUSION REMARKS AND FUTURE PERSPECTIVES

The presented work has focused on the structural and functional characterization of two newly discovered mammalian proteins, Sts-1 and Sts-2. The important roles of Sts-1/-2 in negative regulation of TCR signaling have been described (Carpino *et al*., 2004). Because of their multi-domain structure, the Sts proteins are likely to have multiple binding partners linking many signaling pathways. Sts-1 was first identified as a Jak2 interacting protein (Carpino *et al*., 2002) and Sts-2 was found to interact and inhibit c-Cbl through its SH3 domain (Feshchenko *et al*., 2004). Both proteins can be ubiquitinated via their UBA domain (Kowanetz *et al*., 2004; Feshchenko *et al*., 2004). The fact that the *in vivo* targets of Sts-1 and Sts-2 remain unknown hinders the detailed study of their molecular functions. However, the recently identified homologous phosphatase, EPPase, from silkworm seems to fill this gap since its substrate is known. Therefore, we used *B. mori* EPPase as a model to improve our understanding of the phosphatase activity of Sts-1/-2 and how they interact with substrates.

The Sts-1_{PGM} crystal structure was determined in our lab and showed structural homology to members of PGM/AcP superfamily (Mikhailik *et al*., 2007). We have determined the crystal structures of Sts-1, Sts-2, and EPPase in complex with phosphate or tungstate to high resolution. Residues important for the PGM/AcP catalytic activity are conserved in nature and position in all three proteins. Superposition of Sts-1_{PGM}, Sts-2_{PGM} and $EPPase_{PGM}$ dimers reveals a striking similarity in the overall structure. These three proteins all dimerize through their C-terminal tails. This mode of dimerization differs from that of *E. coli* PGM (Mikhailik *et al*., 2007). The important question here is whether

this dimer-form of Sts-1/-2 and EPPase are required for their activity. It is of the essence to generate the Sts-1/-2_{PGM} monomers to understand the purpose of the dimerization in these proteins.

The surface electrostatics potential of Sts-1_{PGM}, Sts-2_{PGM} and EPPase$_{PGM}$ showed that these proteins have a positive charge distribution in the active site (Figure 10 in Chapter 4). This positive potential stabilizes the binding of a negatively charged molecule like phosphate to the active site. The conformations of the active site residues are identical in these proteins. In this active site, the tight distance between the tungsten atom and the Nε of His366 in Sts-2_{PGM} (His380 in Sts-1_{PGM}, and His80 in EPPase$_{PGM}$) indicates the critical role of this histidine in the formation of a transient phosphorylated intermediate. This is confirmed by the MALDI-TOF and NMR data although these experiments do not definitely show that His380 was phosphorylated. Ultimately, trypsin digestion of phosphorylated Sts-1 followed by mass spectroscopy sequencing of the peptide fragments should demonstrate whether His380 is phosphorylated. Unfortunately, these experiments were not successful in the case of Sts-1 despite several attempts. Whether the phosphate was covalently bound to His380 awaits further experiments.

As mentioned previously, Sts-1_{PGM} has a protein tyrosine phosphatase activity that can target the tyrosine kinase Zap-70 among other proteins (Mikhailik *et al.*, 2007). We have studied the catalytic mechanism of Sts-1_{PGM} by investigating the pH dependence of k_{cat} and k_{cat}/K_m using *p*NPP as a model substrate. We demonstrated that at least one active site group acts as the general acid in Sts-1 during hydrolysis. By generating site-directed mutants, we have shown that the pH dependency is lost in the k_{cat}/K_m profile when Glu490 was mutated. This observation strongly suggests that Glu490 is the general

acid to protonate the phenolate ion during the formation of the phospho-intermediate. The success of identifying important catalytic residues using this method has been described in literature (Porvari *et al*., 1994; Denu *et al*., 1995; Denu and Dixon, 1995; Denu *et al*., 1996).

Despite ~ 40% sequence identity to Sts-1, Sts-2 showed a weaker activity towards *p*NPP hydrolysis. Moreover, the activity of Sts-2_{PGM} was significantly reduced when His366 (the equivalent of His380 in Sts-1) was mutated to Ala implying that the catalytic mechanism employed by Sts-1_{PGM} must be conserved in Sts-2_{PGM}. We generated several site-directed mutants of the residues that differ in the active sites to make of Sts-2_{PGM} more like Sts-1_{PGM}. The increased activity of Sts-2_{PGM} single and double mutants (E481V, S582Y/Q372V, and A446S/S552A) suggests that Sts-1_{PGM} and Sts-2_{PGM} might have different substrate(s) and the residues mutated are involved in substrate recognition.

One point should be addressed is that the expression system we used to generate full-length Sts proteins in *E. coli* yielded insoluble proteins. All tests were performed with the homogeneously purified PGM domains of Sts-1, Sts-2, and EPPase, and the biochemical assay conditions in this study were carried out *in vitro*. One of the remaining questions is whether Sts-1 itself is regulated by inter- or intra-molecular interactions. Reminiscent of kinases, phosphatases need a mechanism to regulate their activity. It can be imagined that a constant active/inactive phosphatase over/under regulate the signaling pathways it is involved, which may lead to severe disastrous consequences. Therefore, highly activated Sts-1_{PGM} may require a regulator or an autoinhibitory region to control its action level. Since the Sts-1 UBA domain can be ubiquitinated, it is possible that Sts-1 can be degraded upon Ub-binding and therefore down-regulate its activity. Besides, the

SH3 domain is known to recognize the proline-rich motif of its binding partner and also important for subcellular localization. Sts-1 may be directed to its target by its SH3 domain.

To summarize, the structural and biochemical data presented in this study of Sts proteins provide the foundation to further investigate the molecular roles of Sts members in TCR signaling. Although the striking structural similarity between the PGM domains of Sts proteins and EPPase suggests a close evolutionary relationship, Sts proteins contain three domains and exist in mammalian cells while EPPase is a one-domain protein exists in insects. In addition, the known EPPase substrate, ecdysteroid phosphate is present in insects and does not exist in humans. Currently, we have shown that the Sts-1_{PGM} H565A mutant binds to a synthesized pTyr-peptide. Determining the crystal structure of the H565A/peptide complex and investigate EPPase' ability to dephosphorylate the tyrosine phosphorylated proteins will provide us more detailed information regarding substrate recognition. In future, we sought to provide a framework for understanding the structural evolution and expanding the category of PTP/PGM/AcP superfamily.

REFERENCES

Ahmad, F., Li, P.M., meyerovitch, J., and Goldstein, B.J. 1995. Osmotic loading of neutralizing antibodies demonstrates a role for protein-tyrosine phosphatase 1B in negative regulation of the insulin action pathway. *J Biol Chem* 270(35): 20503 – 20508.

Andreotti, A.H., Bunnell, S.C., Feng, S., Berg, L.J., and Schreber, S.L. 1997. *Nature* 385, 93 – 97. *Letter*.

Ashwell, J.D., Lu, F.W., and Vacchio, M.S. 2000. Glucocorticoids in T cell development and function. *Annu Rev Immuno* 18, 309 – 345.

Bazan, J.F., Fletterick, R.J., and Pilkis, S.J. 1989. Evolution of a bifunctional enzyme: 6-phospho-fructo-2-kinase/fructose-2,6-bisphosphatase. *Proc Natl Acad Sci USA* 86, 9642 – 9646.

Bond, C.S., White, M.F., and Hunter, W.N. 2002. Mechanistic implications for *Escherichia coli* cofactor-dependent phosphoglycerate mutase based on the high-resolution crystal structure of a vanadate complex. *J Mol Biol* 316(5), 1071 – 1081.

Bonne-Tamir, B., DeStefano, A.L., Briggs, C.E., Adair, R., Franklyn, B., Weiss, S., Korostishevsky, M., Fryman, M., Baldwin, C.T., and Farrer, L.A. 1996. Linkage of congenital recessive deafness (gene DFNB 10) to chromosome 21q22.3. *Am J Hum Genet* 58(16): 1254 – 1259.

Burke, T.R., Ye, B., Yan, X., Wang, S., Jia, Z., Chen, Zhang, Z., and Barford, D. 1996. Small molecule interactions with protein-tyrosine phosphatase PTP1B and their use in inhibitor design. *Biochemistry* 35, 15989 – 15996.

Carpino, N., Kobayashi, R., Zang, H., Takahashi, Y., Jou, S., Feng, J., Nakajima, H., and Ihle, J.N. 2002. Identification, cDNA cloning, and targeted deletion of p70, a novel,

ubiquitously expressed SH3 domain-containing protein. *Mol cell Biol* 22(21), 7491 – 7500.

Carpino, N., Turner, S., Mekala, D., Takahashi, Y., Zang, H., Geiger, T.L., Doherty, and Ihle, J.N. 2004. Regulation of ZAP-70 activation and TCR signaling by two related proteins, Sts-1 and Sts-2. *Immunity* 20, 37 – 46.

Chen, S.H., Anderson, J., Giblett, E.R., and Lewis, M. 1974. Phosphoglyceric acid mutase: rare genetic variants and tissue distribution. *Am J Hum Genet* 26(1): 73 – 77.

Cheng, A.M., Negishi, I., Anderson, S.J., Chan, A.C., Bolen, J., Loh, D.Y., and Pawson, T. 1997. The Syk and Zap-70 SH2-containing tyrosine kinases are implicated in pre-T cell receptor signaling. *Proc Natl Acad Sci USA* 94, 9797 – 9801.

Clements, J.L., Boerth, N.J., Lee, J.R., and Koretzky, G.A. 1999. Integration of T cell receptor-dependent signaling pathways by adapter proteins. *Immunol* 17, 89 –108.

Collaborative computational project, Number 4. 1994. The CCP4 suite: programs for protein crystallography. *Acta Cryst* D50, 760 – 763.

Cowtan, K. 1994. DM: an automated procedure for phase improvement by density modification. Joint CCP4 and ESF-EA CBM newsletter on *Prot Cryst* 31, 34 – 38.

Crowhurst, G.S., Dalby, A.R., Isupov, M.N., Campbell, J.W. and Littlechild, J.A. 1999. Structure of a phosphoglycerate mutase: 3-phosphoglyceric acid complex at 1.7 Å. *Acta Crystallogr Sect D* (55), 1822 – 1826.

Cui, X., De Vivo, I., Slany, R., Miyamoto, A., Firestein, R., and Cleary, M.L. 1998. Association of SET domain and myotubularin-related proteins modulates growth control. *Nat Gent* 18, 331 – 337.

Davies, L., Anderson, I.P., Turner, P., Shirras, A.D., Rees, H.H., and Rigden D.J. 2007. An unsuspected ecdysteroid/steroid phosphatase activity in the key T-cell regulator, Sts-1: surprising relationship to insect ecdysteroid phosphate phasphatase. *Proteins* 67: 720 – 731.

DeLano, W.L. 2002. The PyMOL molecular graphics system. (http://www.pymol.org/)

Denu, J.M., Zhou, G., Guo, Y., and Dixon, J.E. 1995. The catalytic role of aspartic acid-92 in a human dual-specific protein-tyrosine-phosphatase. *Biochemistry* 34, 3396 – 3403.

Denny, M.F., Patai, B., and Straus, D.B. 1999. Differential T-cell antigen receptor signaling mediated by the Src family kinases Lck and Fyn. *Mol Cell Biol* 20(4), 1426 – 1435.

Denu, J.M., Lohse, D.J., Vijayalakshmi, J., Saper, M.A., and Dixon, J.E. 1996. Visualization of intermediate and transition-state structures in protein-tyrosine phosphatase catalysis. *Proc Natl Acad Sci USA* 93, 2493 – 2498.

Di Fiore, P.P., Polo, S., and Hofmann, K. 2003. When ubiquitin meets ubiquitin receptors: a signaling connection. *Nature Rev Mol Cell Biol* 4, 491 – 497.

Dikic, I. And Giodano, S. 2003. Negative receptor signaling. *Curr Opin Cell Biol* 15: 128 – 135.

Elder, M.E. 1998. ZAP-70 and defects of T-cell receptor signaling. *Semin Mematol* 35(4): 310 –320.

Ellis, K.J. and Morrison, J.F. 1982. Buffers of constant ionic strength for. studying pH-dependent processes. *Methods Enzymol* 87, 405 – 426.

Feng, J., Witthuhn, B.A., Matsuda, T., Kohlhuber, F., Kerr., I.M., and Ihle, J.N. 1997. Activation of Jak2 catalytic activity requires phosphorylation of Y1007 in the kinase activation loop. Mol Cell Biol 17(5): 2497 – 2501.

Feshchenko, E.A., Smirnova, E.V., Swminathan, G., Teckchandani, A.M., Agrawal, R., Band, H., Zhang, X., Annan, R.S., Carr, S.A., and Tsygankov, A.Y. 2004. TULA: an SH3- and UBA- containing protein that binds to c-Cbl and ubiquitin. Oncogene 23, 4690 – 4706.

Fothergill-Gilmore, L.A. and Watson, H.C. 1989. The phosphoglycerate mutases. *Adv Enzymol* 62, 227 – 313.

Fraser, M.M., Zhu, X., Kwon, C., Uhlmann, E.J., Gutmann, D.H., and Baker, S.J. 2004. Pten loss causes hypertrophy and increased proliferation of astrocytes *in vivo*. *Cancer Res* 64, 7773 – 7779.

Hamada, K., Kato, M., Shimizu, T., Ihara, K., Mizumo, T., and Hakoshima, T. 2005. Crystal structure of the protein histidine phosphatase SixA in the multistep His-Asp phosphorelay. *Genes to Cells* 10, 1 – 11.

Haque, S.J., Flati, V., Deb, A., and Willaims, B.R.G. 1995. Roles of Protein-tyrosine phosphatases in Stat1α-mediated cell signaling. *J Biol Chem* 270(43), 25707 – 25714.

Hatt, P.J., Moriniere, M., Oberlander, H., and Porcheron, P. 1994. Roles for insulin and ecdysteroids in differentiation of an insect cell line of epidermal origin. *In Vitro Cell Dev Biol Anim* 30A(10): 717 – 720.

Hicke, L., Schubert, H.L., and Hill, C.P. 2005. Ubiquitin-binding domains. Nature Rev Mol Cell Biol 6, 610 – 621.

Howlin, B., Butler, S.A., Moss, D.S., Harris, G.W., and Driessen, H.P.C. 1993. TLSANL: TLS parameter analysis program for segmented anisotropic refinement of macromolecular structures. *J Appl Cryst* 26, 622 – 624.

Jameson, S.C., Hogquist, K.A., and Bevan, M.J. 1995. Positive selection of Thymocytes. *Annu Rev Immunol* 13: 93 – 126.

Jedrzejas, M.J., Chander, M., Setlow, P., and Krishnasamy, G. 2000. Mechanism of catalysis of the cofactor-independent phosphoglycerate mutase from *Bacillus stearothermophilus*. Crystal structure of the complex with 2-phosphoglycerate. *J Biol Chem* 275(30), 23146 – 23153.

Jedrzejas, M.J. 2000. Structure, function, and evolution of phosphoglycerate mutases: comparison with fructose-2,6-bisphosphatase, acid phosphatase, and alkaline phosphatase. *Prog Biophys Mol Biol* 73, 263 – 287.

Kilsheimer, G.S. and Axelrod, B. 1957. Inhibition of prostatic acid phosphatase by alpha-hydroxycarboxylic acids. *J Biol Chem* 227(2): 879 – 890.

Kimball, J.W. 2002. Biology (http://home.comcast.net/~john.kimball1/BiologyPages/)

Kleinman, H., Ford, B., Keller, J., Carpino, N., and Nassar, N. 2006. Crystallization and initial crystal characterization of the C-terminal phosphoglycerate mutase homology domain of Sts-1. *Acta Crystallograph Sect F Struct Biol Cryst Commun* 62(Pt 3): 218 – 220.

Koretzky, G.A. and Myung, P.S. 2001. Positive and negative regulation of T-cell activation by adaptor proteins. *Nat Rev Immunol* 1, 95 – 107.

Kowanetz, K., Crosetto, N., Haglund, K., Schmidt, M.H.H., Heldin, C., and Dikic, I. 2004. Suppressors of T-cell receptor signaling Sts-1 and Sts-2 bind to Cbl and inhibit endocytosis of receptor tyrosine kinases. *J Biol Chem* 279(31), 32786 – 32795.

Krissinel, E. and Henrick, K. 2004. Secondary structure matching (SSM), a new tool for fast protein structure alignment in three dimensions. *Acta Cryst* D60, 2256 – 2268.

Mustelin, T., Vang, T., and Bottini, N. 2005. Protein tyrosine phosphatases and the immune response. *Nat Rev Immunol*. 5(1): 43 – 57.

Lawrence, P.O. 1991. Hormonal effects on insects and other endoparasites in vitro. *In Vitro Cell Dev Biol* 27A(6): 487 – 496.

Lee, Y.H., Li, Y., Uyeda, K., and Hasemann, C.A. 2003. Tissue-specific structure/function differentiation of the liver isoforms of 6-phosphofructo-2-kinase/fructose-2,6-bisphosphatase. *J Biol Chem* 278, 523 – 530.

Li, H.C., Chernoff, J., Chen, L.B., and Kirschonbaum, A. 1984. A phosphotyrosyl-protein phosphatase activity associated with acid phosphatase from human protate gland. *Eur J Biochem* 138(1), 45 – 51.

Makka, T., Seino, A., Tomita, S., Fujiwara, H., and Sonobe, H. 2002. A possible role of 20-hydroxyecdysone in embryonic development of the silkworm *Bombyx mori*. *Arch Insect Biochem Physiol* 51(3), 111 – 120.

McCain, D.F., Catrina, I.E., Hengge, A.C., and Zhang, Z-Y. 2002. The catalytic mechanism of Cdc25A phosphatase. *J Biol Chem* 277(13), 11190 – 11200.

Meng, T.C., and Lin, M.F. 1998. Tyrosine phosphorylation of c-Erb-2 is regulated by the cellular form of prostatic acid phosphatase in human prostate cancer cells. *J Biol Chem* 273, 22096 – 22104.

Mizuguchi, H., Cook, P.F., Tai, C., Hasemann, C.A., and Uyeda, K 1999. Reaction mechanism of fructose-2,6-bisphosphatase. *J Biol Chem* 274(4), 2166 – 2175.

Morris, R.J., Perrakis, A., and Lamzin, V.S. 2002. ARP/wARP's model-building algorithms. I. The main chain. *Acta Cryst* D58, 968 – 975.

Nairn, J., Krell, T., Coggins, J.R., Pitt, A.R., Fothergill-Gilmore, L.A., Walter, R., and Price, N.C. 1995. The use of mass spectrometry to examine the formation and hydrolysis of the phosphorylated form of phosphoglycerate mutase. *FEBS Lett* 359(2-3): 192 – 194.

Naramura, M., Jang, I.K., Kole, H., Huang, F., Haines, D., and Gu, H. 2002. C-Cbl and Cbl-b regulate T cell responsiveness by promoting ligand-induced TCR down-modulation. *Nat Immunol* 5, 43 – 57.

Negishi, I., Motoyama, N., Nakayama, K., Nakayama, K., Senju, S., Hatakeyama, S., Zhang, Q., Chan, A.C., and Loh, D.Y. 1995. Essential role for ZAP-70 in both positive and negative selection of thymocytes. *Nature* 376(6539): 435 – 438.

Nielsen, J.E. and McCammon, J.A. 2003. Calculating pKa values in enzyme active sites. *Protein Sci* 12(9), 1894 – 1901.

Pawson, T. 1995. Protein molecules and signaling networks. *Nature* 373, 573 – 580.

Pickart, C.M. 2001. Mechanisms underlying ubiquitination. *Annu Rev Biochem* 70, 503 – 533.

Porvari, K.S., Herrala, A.M., Kurkela, R.M., Taavitsainen, P.A., Lindqvist, Y., Schneider, G., and Vihko, P.T. 1994. Site-directed mutagenesis of prostatic acid phosphatase. *J Biol Chem* 269(36), 22642 – 22646.

Reed, M.J., Purohit, A., Woo, L.W.L., Newman, S.P., and Potter, B.V.L. 2005. Steroid Sulfatase: Molecular biology, regulation and inhibition. *Endocrine Rev* 26(2): 171 – 202.

Rigden, D.J., Bagyan, I., Lamani, E., Setlow, P., and Jedrzejas, M.J. 2001. A cofactor-dependent phosphoglycerate mutase homolog from *Bacillus stearothermophilus* is actually a broad specificity phosphatase. *Protein Sci* 10(9): 1835 –1846.

Rogden, D.L., Littlejohn, J.E., Henderson, K., and Jedrzejas. M.J. 2003. Structures of phosphate and trivanadate complexes of Bacillus stearothermophilus phosphatase PhoE: structural and functional analysis in the cofactor-dependent phosphoglycerate mutase superfamily. *J Mol Biol* 325, 411 – 420.

Roit, 2001. Immunology.

Rose, Z.B. 1970. Evidence for a phosphohistidine protein intermediate in the phosphoglycerate mutase reaction. *Arch Biochem Biophys* 140(2): 508 – 513.

Rose, Z.B. 1971. The phosphorylation of yeast phosphoglycerate mutase. *Arch Biochem Biophys* 146(1): 359 – 360.

Rudolph, J. 2007. Cdc25 phosphatase: Structure, specificity, and mechanism. *Biochemistry* 46(12), 3595 – 3604.

Sarmiento, M., Puius, Y.A., Vetter, S.W., Keng, Y., Wu, L., Zhao, Y., Lawrence, D.S., Almo, S.C., and Zhang, Z. 2000. Structural basis of plasticity in protein tyrosine phosphatase 1B substrate recognition. *Biochemistry* 39, 8171 – 8179.

Sheldrick, G. and Schneider, T. 1997. SHELX: high-resolution refinement. *Methods Enzymol*. 277, 319 – 343.

Singer, A.L., and Koretzky, G.A. 2002. Control of T cell function by positive and negative regulators. *Science* 296, 1639 – 1640.

Sparks, A.B., Rider, J.E., Hoffman, N.G., Fowlkes, D.M., Quilliam, L.A., and Kay, B.K. 1996. Distinct ligand preferences of Src homology 3 domains from Src, Yes, Abl, Cortactin, p53bp2, PLCγ, Crk, and Grb2. *Proc Natl Acad USA* 93, 1540 – 1544.

T. C. Terwilliger 1999. Reciprocal-space solvent flattening. *Acta Cryst* D55, 1863 – 1871.

Terwilliger, T.C. and Berendzen, J. 1999. Automated MAD and MIR structure solution. *Acta Cryst* D55, 849 – 861.

Terwilliger, T.C. 2000. Maximum likelihood density modification. *Acta Cryst* D56, 965 – 972.

Thien, C.B. and Langdon, W.Y. 2001. Cbl: many adaptations to regulate protein tyrosine kinase. *Nat Rev Mol Cell Biol* 2(4): 294 – 307.

Thummel, C.S. and Chory, J. 2002. Steroid signaling in plants and insects – common themes, different pathways. *Gene Develop* 16: 3113 – 3129.

Vincent, J.B., Crowder, M.W., and Averill, B.A. 1992. Hydrolysis of phosphate monoesters: a biological problem with multiple chemical solutions. *Trends Biochem Sci* 17(3): 105 – 110.

Watanabe, S., Itoh, T., and Arai, K. 1997. Roles of Jak Kinase in human GM-CSF receptor signals. *Leukemia* 3, 76 – 78.

Warren, J.T., Petryk, A., Marques, G., Jarcho, M., Parvy, J.P., Dauphin-Villemant, C., O'Connor, M.B., and Gilbert, L.I. 2002. Molecular and biochemical characterization of two P450 enzymes in the ecdysteroidogenic pathway of *Drosophila melanogaster*. *Proc Natl Acad Sci* 99: 11043 – 11048.

Wattenhofer, M., Shibuya, K., Kudoh, J., Lyle, R., Michaud, J., Rossier, C., Kawasaki, K., Asakawa, S., Minoshima, S., Berry, A., Bonne-Tamir, B., Shimizu, N., Antonarakis, S.E., and Scott, H.S. 2001. Isolation and characterization of the UBASH3A genen on 21q22.3 encoding a potential nuclear protein with a novel combination of domains. *Hum Genet* 108: 140 –147.

Webb, T.J., Powls, R., and Rees, H.H. 1995. Enzymes of ecdysteroid transformation and inactivation in the midgut of the cotton leafworm, *Spodoptera littoralis*: properties and developmental profiles. *Biochem J* 312, 561 – 568.

Weiss, A. and Littman, D.R. 1994. Signal transduction by lymphocyte antigen receptors. *Cell* 76(2): 263 – 274.

Winn, S.I., Watson, H.C., Harkins, R.N., and Fothergill, L.A. 1981. Structure and activity of phosphoglycerate mutase. *Philos Trans R Soc Lond Ser* B 293, 121 – 130.

Winoto, A. and Littman, D.R. 2002. Nuclear hormone receptors in T lymphocytes. *Cell* 109, S57 – 66.

Witthuhn, B.A., Quelle, F.W., Silvennoinen, O., Yi, T., Tang, B., Miura, O., and Ihle, J.N. 1993. JAK2 associates with the erythropoietin receptor and is tyrosine phosphorylated and activated following stimulation with erythropoietin. *Cell* 74(2): 227 – 236.

Yamada, R. and Sonobe, H. 2003. Purification, kinetic characterization, and molecular cloning of a novel enzyme ecdysteroid-phosphate phosphatase. *J Biol Chem* 278(29), 26365 – 26373.

Yamasaki, S., Nishida, K., Hibi, M., Sakuma, M., Shiina, R., Takeuchi, A., Ohnishi, H., Hirano, T., and Saito, T. 2001. Docking protein Gab2 is phosphorylated by ZAP-70 and negatively regulates T cell receptor signaling by recruitment of inhibitory molecules. *J Biol Chem* 276(48), 45175 – 45183.

Yin, V.P. and Thummel, C.S. 2005. Mechanisms of steroid-triggered programmed cell death in Drosophila. *Semin Cell Dev Biol* 16, 237 – 243.

Yuvaniyama, J., Denu, J.M., Dixon, J.E., and Saper, M.A. 1996. Crystal structure of the dual specificity protein phosphatase VHR. Science 272, 1328 – 1331.

Zhang, W., Sloan-Lancaster, J., Kitchen, J., Tribe, R.P., and Samelson, L.E. 1998. LAT: the ZAP-70 tyrosine kinase substrate that links T cell receptor to cellular activation. *Cell* 92, 83 – 92.

Zhou, G., Denu, J.M.,Wu, L., and Dixon, J.E. 1994. The catalytic role of Cys124 in the dual specificity phosphatase VHR. *J Biol Chem* 269, 28084 – 28090.